NONUNIFORM ELECTRICAL CONDUCTION IN MAGNETOHYDRODYNAMIC CHANNELS

by

D. A. Oliver

May 1967

SU-IPR Report No. 163

Prepared under

Air Force Office of Scientific Research
Contract AF 49(638)1695
National Aeronautics and Space Administration
Contract NAS 3-6261

Institute for Plasma Research
Stanford University, Stanford, California

ACKNOWLEDGMENTS

The author gratefully acknowledges the support and assistance of M. Mitchner, C. H. Kruger, R. H. Eustis, and S. Schechter with this work. This research was supported by the Air Force Office of Scientific Research under contract AF 49(638)1695 and by the National Aeronautics and Space Administration under contract NAS 3-6261. Some of the numerical computations were supported by a grant from the Stanford Computation Center.

ABSTRACT

Methods of describing steady electrical conduction in a partially ionized gas with Hall effect, strong applied or magnetically induced electric fields, and a nonuniform electrical conductivity are proposed. One of these methods is based on model conductivity distributions, and the other is based on a nonequilibrium conductivity and incorporates the electron energy and ionization equations. The occurrence of a nonequilibrium conductivity leads to the development of an ionization instability. It is shown that the steady equations with a nonequilibrium conductivity are of mixed elliptic-hyperbolic type and that the condition for the uniform ellipticity of these equations is identical to the condition for the prevention of the ionization instability.

These methods are applied to flowing gases in two-dimensional linear magnetohydrodynamic channels with segmented electrode structures. Detailed numerical solutions for current and potential are obtained. In general, it is found that conductivity nonuniformities lead to a degradation of performance as reflected in increased internal impedance of the conducting gas and depressed Hall voltage. Theoretically obtained distributions of current on electrodes in contact with a nonuniformly conducting gas are found to be in accord with experimental measurements.

TABLE OF CONTENTS

LIST OF FIGURES

LIST OF TABLES

NOMENCLATURE

Where appropriate, the equation in which the symbol characteristically appears is specified in parentheses following the meaning. Symbols defined and used locally are not listed in this table.

Upper-Case Latin Symbols

A, B, C	Coefficients of quadratic forms (4-34)
A_{T_e}, B_{T_e}, C_{T_e}	Coefficients of quadratic forms (4-25)
A_{n_e}, B_{n_e}, C_{n_e}	Coefficients of quadratic forms (4-26)
A_{ij}, B_{ij}, C_i	Matrix coefficients (4-49)
A_E, B_E, C_E	Coefficients in the quasi-linear second-order operator L_E (4-69)
A_J, B_J, C_J	Coefficients in the quasi-linear second-order operator L_J (4-74)
$\vec{B}$	Magnetic field intensity
D	Discriminant (4-76)
D_E, E_E	Coefficients in the second-order operator L_E (4-69)
D_J, E_J	Coefficients in the second-order operator L_J (4-74)
$\vec{E}$	Electric field intensity (2-1)
$\vec{E}'$	Electric field intensity in moving gas frame (2-2)
$\vec{E}_n$	Effective field due to electron-pressure gradient (2-3)
F_E, F_J	Nonuniform conductivity functions (2-23), (2-24)
G_E, G_J	Nonuniform conductivity functions (2-23), (2-24)

G, G_β, G^*	One-dimensional nonuniformity functions (3-9), (3-12), (3-15)
$I(x)$	Cumulative current on electrode
I_x,I_y	Net current per unit channel depth in axial and transverse directions (2-36), (2-38)
$\vec{J}$	Current density (2-1)
$K(T_e)$	Equilibrium constant in Saha equation (2-29)
$\vec{K}$	Wave number
L_E	Nonequilibrium conductivity operator in field representation (4-68)
L_J	Nonequilibrium conductivity operator in current representation (4-73)
M_E	Nonuniform conductivity operator in field representation (2-18)
M_J	Nonuniform conductivity operator in current representation (2-18)
Q	Quadratic form (4-33)
Q_{T_e}	Quadratic form (4-23)
Q_{n_e}	Quadratic form (4-23)
Q_E	Electron-pressure gradient contribution to the combined current conservation equation and Maxwell Faraday equation in the field representation (2-13)
Q_J	Electron-pressure gradient contribution to the combined current conservation equation and Maxwell Faraday equation in the current representation (2-16)
$\overleftrightarrow{R}$	Resistance tensor (2-40)
$\overline{R}_T$	Nondimensional transverse impedance (2-47)
$\overleftrightarrow{S}$	Conductance tensor (2-39)
T	Gas temperature (2-31)

T_e	Electron temperature (2-31)
V'_x	Voltage in moving gas frame between adjacent electrodes (2-36)
V'_y	Voltage in moving gas frame across electrodes (2-37)
$\overline{V}_H$	Nondimensional Hall voltage (2-46)

Lower-Case Latin Symbols

a	Length of electrode (2-37)
e	Electron charge
f	Degree of ionization
f_E	Nonequipartition parameter (4-18)
h	Height of channel (2-37); Planck's constant
k	Boltzmann's constant
ℓ	Period length of channel (2-37)
ℓ_q	Effective length for heat conduction due to a temperature gradient (4-17)
ℓ_d	Effective length for diffusion due to electron-pressure gradients (4-16)
m_e	Mass of electron
n_e	Electron-number density (2-27)
$\dot{n}_e$	Net production of electrons due to ionization and recombination (2-28)
$n_e^*(T_e)$	Equilibrium electron-number density (2-29)
n_{s_o}	Ionizable species number density before ionization occurs
$\vec{q}_e$	Electron heat-flux vector (2-32)
q_E	Coefficient in the operator M_E (2-11)

I. INTRODUCTION

I.1 Background

In recent years considerable effort has been devoted to the development of closed cycle magnetohydrodynamic (MHD) generators utilizing a noble gas as a working fluid with slight additions of an easily ionized alkali metal vapor, such as potassium or cesium. Particular attention has been given to the possible operation of MHD generators of this type, such that nonequipartition of electron and gas temperatures occurs as a result of Joulean heating of the electrons by the current flowing in the gas.[1] Simple theoretical considerations indicate that the enhanced electron temperature will result in a higher electron number density and thus a conducting gas of lower internal impedance than would exist if the electrons were at the same temperature as the gas.[1,2] These theoretical predictions have been experimentally verified for noble gas plasmas described above, when an electric field is applied and there is no magnetic field present.[1,2,3,4]

The conditions necessary for nonequipartition heating such that the electrons gain large amounts of energy from the field and lose it ineffectively to the heavy particles in the gas require infrequent electron-heavy particle collisions and large electric fields. If the electric field is to be magnetically induced by the motion of the plasma through the magnetic field, then the induced electric field will be proportional to the magnetic field strength. If ν_e denotes the electron-heavy particle collision frequency and B denotes the magnetic field intensity, a condition for nonequipartition heating is that the parameter B/ν_e be large. The Hall parameter β is defined as the ratio of the electron

gyro frequency in a magnetic field to its heavy particle collision frequency and is given by $\beta = eB/m_e\nu_e$, where e/m_e is the electron charge to mass ratio. It can be seen, therefore, that the condition for the occurrence of nonequipartition heating is that the Hall parameter β be large. Thus, significant nonequipartition heating in an alkali metal seeded noble gas MHD generator will invariably be accompanied by Hall effects. Physically, the Hall effect refers to the conduction process within a plasma in which an electric field in the presence of a magnetic field produces a component of current flow in the direction mutually perpendicular to the electric and magnetic fields as well as a component parallel to the electric field. The component of current which is perpendicular to the electric and magnetic fields is called the Hall current.

To this date, the experimental duplication of the performance predicted by simple theory[2] with magnetically induced electric fields has not been obtained. Instead, the actual performance of experimental generators as reflected in measured values of the internal impedance has been considerably below the performance predicted by the simple theories.[5] Whereas the simple theoretical predictions of performance have been based upon the existence of a uniform plasma with uniform properties, experiment indicates the presence of large fluctuations of the electric current in time and space and concentrations of the current in the conducting gas, particularly near electrodes.[5]

Nonuniformities in the electrically conducting fluid may arise from a variety of causes. Electrode segmentation is required with strong Hall effects to prevent the flow of axial (Hall) current in the channel.

Since such segmentation cannot be infinitely fine, nonuniformities in the potential and current exist in the vicinity of the electrode segments even if the electrical conductivity of the gas is uniform. Spatial nonuniformities in the electrical conductivity may arise from inhomogeneous mixing of ionizable species in the gas or from fluctuations of the form discussed by Velikhov[6] and McCune[7,8] The electrical conductivity may also exhibit nonuniformities if variable fluid properties exist near surfaces which are heated or cooled or where finite electrode segments induce nonuniformities in the current distribution, which in turn produce nonuniform Joulean heating of the electrons.

The results of experiment and the existence of several mechanisms for the introduction of nonuniformities in a gas therefore suggest the desirability of extending the simple theories predicting performance. Such a development of theory to include nonuniformities would provide improved predictions of generator performance; in addition, the inclusion of nonuniformity effects would aid in the understanding of mechanisms which might explain the performance results of experimental generators now available. In what follows, uniform conductivity work and the limited amount of nonuniform conductivity work available are reviewed. The scope of the present study is then presented.

1.2 Review of Uniform Conductivity Work

When the electrical conductivity of the plasma in an MHD channel is uniform, the governing steady-state electromagnetic and diffusion equations reduce to the Laplace equation for the electric potential or current stream function within the gas.[9] The boundary conditions of inter-

est in finitely segmented electrode channels are mixed, however, since electrodes and insulators exist adjacent to one another along the same boundary. In addition, the vanishing of the normal component of the current on an insulating boundary leads to a condition of the form

$$\frac{\partial \Phi}{\partial n} \pm \beta \frac{\partial \Phi}{\partial t} = 0$$

where Φ is the electric potential and n and t are the coordinates normal and tangential to the boundary, respectively. In the absence of the Hall effect ($\beta = 0$), the above condition reduces to a simple Neumann condition on Φ on the insulating boundary. When Hall effects are present, the condition is an *oblique* Neumann condition. Both the mixed and oblique Neumann nature of the boundary conditions prohibit the solution of the Laplace equation by the standard techniques.

The first significant solution to the finitely segmented MHD channel with uniform electrical conductivity was obtained in 1961 by Hurwitz, Sutton, and Kilb.[9] These investigators obtained solutions to the mixed boundary value problem using conformal transformations under the assumption that in the center of the channel the axial component of the current density was negligibly small. It was shown that the finite length of the electrode segments increases the internal impedance of the channel relative to the case where the electrode segmentation is infinitely fine. In addition, the axial voltage gradient which develops due to the Hall effect is depressed below that obtained with infinitely fine segmentation. A significant result of the work of Hurwitz, Sutton, and Kilb was the prediction of concentrations of current at the electrode edges due to the Hall effect. These concentrations were found to become

more intense as the Hall parameter β was increased. The work of Hurwitz, Sutton, and Kilb was immediately followed by a large number of published solutions concerned with various kinds of electrode arrangements and geometrical arrangements including the problem of end effects.[10,11,12,13] Conformal mapping methods were utilized in most of these studies as a means of dealing with the mixed boundary conditions. A slightly different approach to the end effect problem was given by Dzung[14] who used a series solution technique.

An attempt was made to relax the assumption of a vanishing axial current in the Hurwitz, Sutton, Kilb calculation by Schultz-Grunow and Denzel.[13] These investigators, however, introduced additional approximations concerned with the shape and location of the dividing current line between electrode segments. Even with these slightly different assumptions, the results of these calculations for a large range of geometries were in substantial agreement with those of Hurwitz, Sutton, and Kilb.

A numerical relaxation technique was employed by Crown[15] in examining the infinitely long segmented electrode channel which was the problem originally posed by Hurwitz, Sutton, and Kilb. The assumption of negligible axial current was relaxed by Crown and numerical results were obtained in substantial agreement with Hurwitz, Sutton, and Kilb. Crown's work was confined to Hall parameters less than two because of numerical instabilities which developed for larger Hall parameters.

Celinski and Fischer[16] developed numerical solutions to the problem considered by Crown. By utilizing difference formulas for the boundary conditions on the insulator which were numerically stable for

large Hall parameters, the difficulty encountered by Crown was circumvented. An extensive parameter study was completed by Celinski and Fischer for Hall parameters as large as ten. In general, the results show increases in the internal impedance of the channel with finite electrode segments and decreasing Hall potential. The effects of variable electrode to insulator segment length ratios was also examined by Celinski and Fischer. Such effects were also considered earlier by Witalis.[17] Both studies showed that for uniform conductivity the minimum internal impedance is obtained for electrode segments of the same length as the insulator segments, when the Hall parameter is large.

1.3 Review of Nonuniform Conductivity Work

The first published examination of conductivity nonuniformities in magnetohydrodynamic generators was that of Rosa[18] who considered the effects of conductivity nonuniformities confined to one space dimension. Rosa showed that the impedance of the current carrying gas is markedly increased by even slight nonuniformities if strong Hall effects are present. In particular, Rosa considered the effects of random nonuniformities which might be due to inhomogeneous mixing of the ionizable species in the gas.

The occurrence of a nonuniform conductivity due to Joulean heating induced nonequipartition of electron and gas temperature with subsequent ionization in the high electron temperature regions was first examined by Kerrebrock.[19,20] Kerrebrock assumed that the effects of nonuniform Joulean heating of the electrons resulting from the finite size of electrode segments could be approximated by assuming that such non-

uniformities generate a layer of high electrical conductivity over the conductors, but that the resulting current is uniformly distributed over the conductor. This assumption circumvented the difficulty of the mixed boundary value problem. By further assuming that the conductivity varied only in the direction transverse to the electrodes in the form

$$\frac{\sigma}{\sigma_o} = e^{-\nu y} \qquad (1\text{-}1)$$

where y is the distance from the electrode in the transverse direction, Kerrebrock was able to develop series solutions to the nonuniform conduction problem. The parameters σ_o and ν in the conductivity expression (1-1) were fixed by requiring that the conductivity distribution be such that the electron energy equation be satisfied for the gas layer near the electrodes. An important result of Kerrebrock's analysis was the prediction of a "shorting" effect in which a layer of high conductivity would be generated over the electrode segments, thereby destroying the effect of the segmentation. This shorting effect led to the existence of two modes of operation: one in which the segmentation was fine enough to achieve large electron temperature elevation in the core, and the other in which the coarse segmentation led to a shorting of the Hall field and very little electron temperature rise in the core of the channel.

Sherman[21] has analyzed the effect of an electrical conductivity σ dependent upon the local current density $\vec{J}$ in the gas of the form

$$\sigma = \sigma_o + C|\vec{J}|$$

where σ_o and C are constants. The resulting nonlinear boundary value problem for the finitely segmented electrode channel was solved by an expansion technique for small C. Each inhomogeneous linear problem in

the expansion was solved using numerical relaxation. Sherman's work was restricted to small values of C and Hall parameters of the order unity or less. The major result of this study was the calculation of decreases in Hall potential which occurred due to the current dependent conductivity.

1.4 The Scope of the Present Study

In the present study an examination of a variety of mechanisms and consequences of two dimensional nonuniformities in MHD channels attributable to some of the causes discussed above will be undertaken. The principal tool for this study will be a numerical solution technique for solving the equations governing nonuniform electrical conduction.

In chapter 2 a formulation of the equations governing electrical conduction with a nonuniform electrical conductivity and methods for closing the system of equations are presented. One of these methods introduces model conductivity distributions and the other considers a nonuniform nonequilibrium conductivity which consistently incorporates the effects of electron ionization and recombination and energy transfer to the electron fluid.

In chapter 3 electrical conduction in an MHD channel with model conductivity distributions is examined. One dimensional conductivity nonuniformities are first examined in the presence of the Hall effect. Numerical solutions are then obtained to two dimensional nonuniformity situations which arise with finite electrode segments. It will be shown that in general the existence of nonuniformities leads to a degradation of performance as reflected in increased internal impedance of the con-

ducting gas and depressed Hall voltage.

In chapter 4 several theoretical questions concerning instabilities and the steady state characteristics of the conducting gas are considered. These instabilities arise when nonequipartition heating of the electrons occurs in a magnetic field. It will be shown that there exists an important correspondence between the conditions for stability of the non-steady equations and the condition for uniform ellipticity of the steady equations.

In chapter 5 the finitely segmented electrode MHD channel is examined with a nonequilibrium conductivity and nonuniform Joulean heating arising from the finite size of electrode segments. For these calculations, the electrons are assumed to be in ionization equilibrium at the local (nonuniform) electron temperature. It will be shown that the nonuniform Joulean heating, like other nonuniformities, leads to an increase in internal impedance and a reduction of the Hall voltage.

Consideration of the conditions under which the electrons may be driven out of ionization equilibrium by gas dynamic connection is presented in chapter 6. A model periodic temperature field corresponding to the periodic high temperature zones in a finitely segmented MHD channel is utilized to study the response of the electron number density to temperature disturbances in the presence of a convective nonequilibrium.

In chapter 7 the problem of a finitely segmented electrode MHD channel with Joulean heating induced nonequipartition of electron and gas temperature is again reconsidered. The electrons are now allowed to experience an ionization nonequilibrium due to gas dynamic convection. It will be shown that the existence of finite rates of ionization and

recombination lead to an antisymmetry between the upper electrode wall and the lower electrode wall. These results will be shown to be in qualitative agreement with experimental measurement.

2. FORMULATION

In this chapter the basic principles governing electrical conduction in a quasi-neutral gas are presented. The electromagnetic and diffusion equations are shown to contain unknown transport property gradients and hence are not closed. Two methods of closure are presented: one method introduces model conductivity distributions obtained either heuristically or from experimental data; the second method is based on a non-equilibrium conductivity resulting from Joulean-heating induced non-equipartition of electron and gas temperature. Consideration is given to the boundary conditions and magnetohydrodynamic channel geometry to which the basic principles are to be applied. Global resistance and conductance tensors are described which reflect the overall electrical behavior of the channel based upon the detailed distribution of current and potential within the conducting gas.

2.1 Electromagnetic and Diffusion Equations

Consider an orthogonal right-handed coordinate system with axes denoted x, y, z, as shown in Fig. 2-1. A strong imposed magnetic field $\vec{B}$ is oriented parallel to and in the direction of the positive z axis. In the x,y plane normal to $\vec{B}$ a fluid flows with mass velocity $\vec{u}$ and a conduction current density $\vec{J}$ is established. The changes in time which occur in this medium are assumed to be slow enough so that the time dependent terms in the Maxwell-Faraday equation and the current conservation equation are negligably small. If the imposed field $\vec{B}$ is unperturbed by the current $\vec{J}$ which flows in the gas (i.e., the magnetic Reynolds Number of the flow is small), the appropriate equations for the electric field

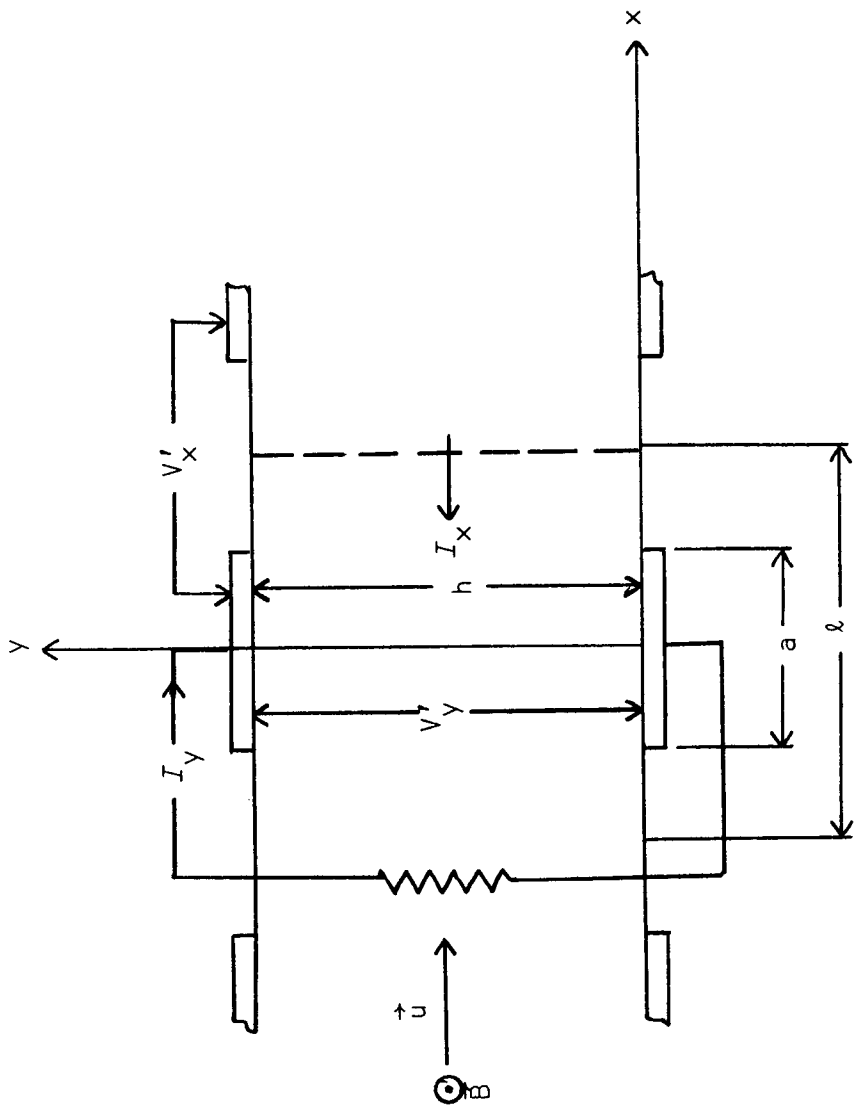

Fig. 2-1 Coordinate system and channel geometry

$\vec{E} = (E_x, E_y)$ and the current density $\vec{J} = (J_x, J_y)$ are the Maxwell- Faraday equation and the current conservation equation for an electrically neutral fluid:

$$\text{curl } \vec{E} = 0 \qquad \text{div } \vec{J} = 0 \tag{2-1}$$

The electrical conduction current density $\vec{J}$ is assumed to be dominated by the electron conduction current. The generalized Ohm's Law is then[22,23]

$$\vec{J} = \overleftrightarrow{\sigma} \cdot (\vec{E}' + \vec{E}_n), \quad \text{or} \quad \vec{E}' = \overleftrightarrow{\rho} \cdot \vec{J} - \vec{E}_n. \tag{2-2}$$

In Eq. (2-2) $\vec{E}_n$ represents the effective field acting on the electrons due to electron pressure gradients and is given by[23]

$$\vec{E}_n = \frac{k}{en_e} \text{ grad } (n_e T_e) \tag{2-3}$$

The field $\vec{E}' = \vec{E} + \vec{u} \times \vec{B}$ represents the electric field in the moving fluid frame of reference. The conductivity tensor $\overleftrightarrow{\sigma}$ and resistivity tensor $\overleftrightarrow{\rho}$ are given by

$$\overleftrightarrow{\sigma} = \sigma_\beta \begin{pmatrix} 1 & -\beta \\ \beta & 1 \end{pmatrix}, \qquad \overleftrightarrow{\rho} = \frac{1}{\sigma} \begin{pmatrix} 1 & \beta \\ -\beta & 1 \end{pmatrix}. \tag{2-4}$$

The scalar conductivity σ, Hall parameter β, and coefficient σ_β may be expressed as

$$\sigma = en_e\mu, \qquad \beta = \mu B, \qquad \sigma_\beta = \frac{\sigma}{1 + \beta^2}$$

The electron mobility is $\mu = e\left(m_e \sum_j \nu_{ej}\right)^{-1}$, where ν_{ej} is the average electron momentum transfer collision frequency with species j and m_e is the electron mass.

From equation (2-1) the electric field $\vec{E}$ may be represented as the gradient of a potential Φ. For those cases in which curl $(\vec{u} \times \vec{B}) = 0$, the

electric field $\vec{E}'$ may also be represented as the gradient of a potential Φ':

$$\vec{E}' = -\nabla\Phi'. \tag{2-5}$$

For this case, Φ and Φ' are related by the line integral of $\vec{u}\times\vec{B}$. We shall assume in what follows that $\vec{u}$ is always prescribed such that the above is true. Equations (2-1) also permit the representation of $\vec{J}$ in terms of the flux function ψ:

$$J_x = \frac{\partial\psi}{\partial y}, \qquad J_y = -\frac{\partial\psi}{\partial x}. \tag{2-6}$$

Substituting from Eqs. (2-2) into Eqs. (2-1), two equivalent sets of equations for $\vec{E}'$ and $\vec{J}$ may be developed where each set contains only $\vec{E}'$ or $\vec{J}$. The set containing $\vec{E}'$ is termed the *field representation:*

$$\frac{\partial E'_x}{\partial x} + \frac{\partial E'_y}{\partial y} + q_E E'_x + r_E E'_y + Q_E(n_e,T_e) = 0, \tag{2-7}$$

$$\frac{\partial E'_x}{\partial y} - \frac{\partial E'_y}{\partial x} = 0. \tag{2-8}$$

The set containing only $\vec{J}$ is termed the *current representation:*

$$\frac{\partial J_x}{\partial y} - \frac{\partial J_y}{\partial x} - q_J J_y + r_J J_x + Q_J(n_e,T_e) = 0, \tag{2-9}$$

$$\frac{\partial J_x}{\partial x} + \frac{\partial J_y}{\partial y} = 0. \tag{2-10}$$

The functions appearing in Eqs. (2-7) through (2-10) are defined as follows:

$$q_E = \frac{\partial\, \ell n(\sigma_\beta)}{\partial x} + \beta\left[\frac{\partial\, \ell n(\sigma_\beta)}{\partial y} + \frac{\partial\, \ell n(\beta)}{\partial y}\right], \tag{2-11}$$

$$r_E = \frac{\partial\, \ell n(\sigma_\beta)}{\partial y} - \beta\left[\frac{\partial\, \ell n(\sigma_\beta)}{\partial x} + \frac{\partial\, \ell n(\beta)}{\partial x}\right], \tag{2-12}$$

$$Q_E(n_e,T_e) = \frac{\partial E_{nx}}{\partial x} + \frac{\partial E_{ny}}{\partial y} + \beta\left(\frac{\partial E_{nx}}{\partial y} - \frac{\partial E_{ny}}{\partial x}\right) + q_E E_{nx} + r_E E_{ny}, \quad (2\text{-}13)$$

$$q_J = -\frac{\partial\, \ell n(\sigma)}{\partial x} + \beta\left(\frac{\partial\, \ell n(\sigma)}{\partial y} - \frac{\partial\, \ell n(\beta)}{\partial y}\right), \quad (2\text{-}14)$$

$$r_J = -\frac{\partial\, \ell n(\sigma)}{\partial y} - \beta\left(\frac{\partial\, \ell n(\sigma)}{\partial x} - \frac{\partial\, \ell n(\beta)}{\partial x}\right), \quad (2\text{-}15)$$

$$Q_J(n_e,T_e) = \sigma\left(\frac{\partial E_{nx}}{\partial y} - \frac{\partial E_{ny}}{\partial x}\right). \quad (2\text{-}16)$$

Under those circumstances where the "field" $\vec{E}_n$ is much smaller than the field $\vec{E}'$, the terms $Q_E(n_e,T_e)$ and $Q_J(n_e,T_e)$ in Eqs. (2-7) and (2-9) become negligible. If the potential change is of order $\Delta\Phi$ over a region in which the electron number density changes significantly, it follows from Eq. (2-3) that

$$\frac{E_n}{E'} \sim \frac{kT_e/e}{\Delta\Phi}. \quad (2\text{-}17)$$

From (2-17) it can be seen that, with strong applied potentials, E_n will in general be much smaller than E'; exceptions occur for such cases as the region of a plasma in contact with a cold catalytic surface in the absence of a strong applied field. If $Q_E(n_e,T_e)$ and $Q_J(n_e,T_e)$ are neglected, the system of equations in either the field or the current representation may then be combined by introducing the potential Φ' and flux function ψ. In terms of the second-order operator

$$M_{E,J} \equiv \frac{\partial^2}{\partial x^2} + \frac{\partial^2}{\partial y^2} + q_{E,J}\frac{\partial}{\partial x} + r_{E,J}\frac{\partial}{\partial y}, \quad (2\text{-}18)$$

the foregoing equations may be written as

$$M_E(\Phi') = 0, \qquad M_J(\psi) = 0. \tag{2-19}$$

The functions $q_{E,J}$ and $r_{E,J}$ assume the forms q_E, r_E and q_J, r_J, respectively, for the operators M_E and M_J. The functions $q_{E,J}$ and $r_{E,J}$ vanish if the conductivity is uniform.

Either the field representation or the current representation may be utilized in the description of the electric conduction. In much of the development which follows, the field representation will be used. The parallel development in the current representation is similar. In the work which is to be described, numerical calculations have been performed using both representations to check for consistency of the numerical results. Once a solution for either Φ' or ψ has been obtained by solving either of Eqs. (2-19), the other function may be obtained by a straightforward integration using the Ohm's Law, Eqs. (2-2) and the definitions (2-5) and (2-6).

2.2 Model Conductivity

The transport properties which appear in Eqs. (2-7) through (2-10) through the functions $q_{E,J}$ and $r_{E,J}$ are as yet unspecified; hence, the electrical equations are not closed. In the present analysis, we shall consider two methods of closure. In the first, we may directly introduce heuristic *model* distributions of σ, β, μ, and n_e (or $\vec{E}_n$) into Eqs. (2-7) and (2-9) and examine the effects of such distributions on the resulting current and potential fields. These property distributions may be constructed to reflect actual Joule heating effects in the energy

equation of the gas; or in the case where the dynamic and thermal state of the gas is dominated by viscous and heat-conduction effects of the heavy species of the gas, they may be calculated from the temperature and density fields of existing solutions for channel flows.

The model distributions might also simulate the effect of high conductivity regions near current concentrations in segmented electrode magnetohydrodynamic channels; or when ionization and recombination effects are important, the effects of frozen ionization could be modeled by layers of uniform conductivity near the conducting and insulating surfaces in the channel as Kerrebrock[19] has suggested.

2.3 Nonequilibrium Conductivity

The second method to be considered for the determination of the electrical transport property distributions required in Eqs. (2-7) and (2-9) incorporates the electron energy and ionization equations. For this method σ, σ_β, and β are regarded as functions of the local thermodynamic state of the gas, which is fixed by the mass density ρ, temperature T, and neutral species composition. This dependence is symbolized as ρ, T, ... In the event that the electron temperature T_e deviates from the gas temperature and/or the electron number density deviates from its Saha Equilibrium value, this set of state variables must also include the electron temperature T_e and the electron number density n_e. The transport properties σ, σ_β, and β are thus in general functions of the state variables ρ, T, ... , T_e, n_e.

With this point of view, the terms $q_E E_x'$, $r_E E_y'$, $q_J J_x$, $r_J J_y$ in Eqs. (2-7) through (2-10) may now be expressed to reveal explicitly their

dependence upon the state functions ρ, T, ... , T_e, n_e. Thus if $\eta = \eta(\rho, T, \ldots, T_e, n_e)$ represents σ, σ_β, or β, and ξ represents either x or y, the generalized gradient $\partial\, \ell n(\eta)/\partial\xi$ may be expressed as

$$\frac{\partial\, \ell n(\eta)}{\partial \xi} = \frac{\partial\, \ell n(\eta)}{\partial \rho}\frac{\partial \rho}{\partial \xi} + \frac{\partial\, \ell n(\eta)}{\partial T}\frac{\partial T}{\partial \xi} + \ldots +$$

$$+ \frac{\partial\, \ell n(\eta)}{\partial T_e}\frac{\partial T_e}{\partial \xi} + \frac{\partial\, \ell n(\eta)}{\partial n_e}\frac{\partial n_e}{\partial \xi} . \qquad (2\text{-}20)$$

If the gradients of σ, σ_β, and β appearing in q_E, r_E, q_J, and r_J are expressed according to Eq. (2-20), there results for Eqs. (2-7) and (2-9)

$$\frac{\partial E'_x}{\partial x} + \frac{\partial E'_y}{\partial y} + F_E(T_e)\frac{\partial T_e}{\partial x} + G_E(T_e)\frac{\partial T_e}{\partial y} +$$

$$+ F_E(n_e)\frac{\partial n_e}{\partial x} + G_E(n_e)\frac{\partial n_e}{\partial y} + \Gamma_E = 0, \qquad (2\text{-}21)$$

$$\frac{\partial J_x}{\partial y} - \frac{\partial J_y}{\partial x} + F_J(T_e)\frac{\partial T_e}{\partial x} + G_J(T_e)\frac{\partial T_e}{\partial y} +$$

$$+ F_J(n_e)\frac{\partial n_e}{\partial x} + G_J(n_e)\frac{\partial n_e}{\partial y} + \Gamma_J = 0, \qquad (2\text{-}22)$$

where

$$F_E(\eta) \equiv E'_x \frac{\partial\, \ell n(\sigma_\beta)}{\partial \eta} - \beta\, E'_y\left[\frac{\partial\, \ell n(\sigma_\beta)}{\partial \eta} + \frac{\partial\, \ell n(\beta)}{\partial \eta}\right],$$

$$G_E(\eta) \equiv E'_y \frac{\partial\, \ell n(\sigma_\beta)}{\partial \eta} + \beta\, E'_x\left[\frac{\partial\, \ell n(\sigma_\beta)}{\partial \eta} + \frac{\partial\, \ell n(\beta)}{\partial \eta}\right], \qquad (2\text{-}23)$$

$$F_J(\eta) \equiv -\beta\left[\frac{\partial\, \ell n(\sigma)}{\partial \eta} - \frac{\partial\, \ell n(\beta)}{\partial \eta}\right] J_x + \frac{\partial\, \ell n(\sigma)}{\partial \eta} J_y,$$

$$G_J(\eta) \equiv -\frac{\partial\, \ell n(\sigma)}{\partial \eta} J_x - \beta\left[\frac{\partial\, \ell n(\sigma)}{\partial \eta} - \frac{\partial\, \ell n(\beta)}{\partial \eta}\right] J_y. \qquad (2\text{-}24)$$

The functions Γ_E, Γ_J contain the effects of gradients in the heavy species properties of the gas:

$$\Gamma_E = (q_E)_{T_e,n_e} E_x' + (r_E)_{T_e,n_e} E_y' + Q_E, \qquad (2\text{-}25)$$

$$\Gamma_J = -(q_J)_{T_e,n_e} J_y + (r_J)_{T_e,n_e} J_x + Q_J. \qquad (2\text{-}26)$$

The subscripts on q_E, r_E, q_J, and r_J indicate that T_e and n_e are to be held constant while the derivatives of σ, σ_β, and β are calculated.

In what follows, the distributions of the gas state variables ρ, T, ... are assumed to be given (hence the functions Γ_E, Γ_J are prescribed); the electron temperature and number density however are determined by appropriate electron continuity and energy equations, which are now described.

The electron number density n_e is governed by the electron continuity equation[22]

$$\frac{\partial n_e}{\partial t} + \nabla\cdot(n_e \vec{u}) - \frac{1}{e}\nabla\cdot\vec{J} = \dot{n}_e . \qquad (2\text{-}27)$$

For the plasma of interest in the present study, the particle production and recombination term $\dot{n}_e$ is due principally to electron neutral impact and three body recombination, so that

$$\dot{n}_e = \alpha n_e (n_e^{*2} - n_e^2) , \tag{2-28}$$

where $\alpha(T_e)$ is the recombination coefficient and $n_e^*(T_e)$ is the equilibrium number density. A theory for the dependence of α on T_e is given by Hinnov and Hirschberg[24] (see also appendix C). The equilibrium number density $n_e^*(T_e)$ is given by Saha's relation:

$$n_e^{*2}(T_e) = n_s K(T_e), \tag{2-29}$$

where the equilibrium constant $K(T_e)$ is

$$K(T_e) = G\left(\frac{2\pi m_e k T_e}{h^2}\right)^{\frac{3}{2}} \exp\left(\frac{-\varepsilon_i}{kT_e}\right) ,$$

and G is a factor involving statistical weights. The ionizable species number density is n_s and ε_i is the energy required to singly ionize an s species atom. Using Eq. (2-1), Eq. (2-27) may be expressed as

$$\frac{\partial n_e}{\partial t} + \nabla\cdot(n_e\vec{u}) = \alpha n_e (n_e^{*2} - n_e^2). \tag{2-30}$$

The electron fluid energy equation in a form suitable for the plasma under consideration is[40]

$$\frac{\partial}{\partial t}\left[n_e(\tfrac{3}{2}kT_e + \varepsilon_i)\right] + \nabla\cdot\left[n_e\vec{u}(\tfrac{3}{2}kT_e + \varepsilon_i)\right] + p_e\nabla\cdot\vec{u} +$$

$$+ \nabla\cdot\vec{q}_e - \vec{J}\cdot\vec{E}' + \theta n_e(T_e - T) = 0, \tag{2-31}$$

where $\vec{q}_e$ is the electronic heat flux vector and is given by[22]

$$\vec{q}_e = -\left[\left(\frac{5}{2} kT_e + \varepsilon_i\right)\frac{\vec{J}}{e} + \lambda_e \frac{\overleftrightarrow{\sigma}}{\sigma} \cdot \nabla T_e\right], \tag{2-32}$$

and λ_e is the electron fluid thermal conductivity. The coefficient θ is proportional to the rate at which energy is transfered between the electron fluid and the heavy species in the gas. For purely elastic collisional transfer from the electron fluid to heavy monatomic species, θ is given by[25]

$$\theta = 3k \sum_j \left(\frac{m_e}{m_j}\right) \nu_{ej} , \tag{2-33}$$

where m_j is the mass of a heavy species particle. In developing the energy equation (2-31) it has been assumed that in the volume of the gas, the stress work and inelastic collisional energy transfer terms which result in a loss of energy from the gas are small compared to the Joulean heating of the diffusing electrons and that the heavy species temperatures differ negligibly from the gas temperature. Thermal diffusion effects have been neglected in both the electron heat flux and the current density.

It is to be noted that if the heavy species property distributions ρ, $\vec{u}$, T, ... are given, Eqs. (2-21) and (2-8) [or (2-22) and (2-10)] with Eqs. (2-30) and (2-31) form a closed system for E_x', E_y', (or J_x, J_y) n_e, and T_e.

2.4 Boundary Conditions and Channel Geometry

2.4.1 The gas-solid interface

The application of the differential equations (2-7) through (2-10) to a gas in contact with conducting and insulating surfaces will be considered. Lyubimov[26] has suggested that the gas-surface electrical interface which embodies the effects of electrode emission and absorption extends over a thin region near these surfaces of the order of collisional free paths. Some investigators[27] have proposed boundary conditions which may in some sense model the interface phenomena; however, in the interest of explicitly revealing the role of volume effects, the effect of the interface will be neglected entirely and the conducting surfaces in contact with the gas will be assumed infinitely conducting, and the potential of the gas and the conducting surface will be assumed identical at the conducting surface. Insulating surfaces in contact with the gas are assumed infinitely nonconducting. The boundary conditions on the gas are then the condition of constant potential Φ on conducting surfaces and the vanishing of the normal component of current $\vec{J}$ on insulating surfaces.

2.4.2 The infinitely long periodic channel

The geometry of interest for the application of the foregoing equations is a two-dimensional channel with conductors and insulators arranged in an infinitely long periodic structure as shown in Fig. 2-1. The fluid mass velocity is assumed to be in the positive x direction and to be a function of y only: $u_x = u_x(y)$. It is readily verified that

the condition curl$(\vec{u}\times\vec{B}) = 0$ is satisfied and that Φ' and Φ are related by

$$\Phi'(x,y) - \Phi'(x,0) = \Phi(x,y) - \Phi(x,0) + B\int_0^y u(\xi)d\xi. \qquad (2\text{-}34)$$

For such a configuration, the boundary conditions may be specified as follows. The existence of periodic solutions for $\vec{E}'$, J requires that the fluid properties also be periodic. While this will in general not be the case, the nonperiodic variation in the important parameters for the determination of the electrical transport properties can, in many cases, be neglected over the region consisting of several pairs of electrodes. Under such circumstances the periodicity conditions imposed on the gas properties are (for period of length ℓ)

$$\begin{aligned} T(x+\ell) &= T(x), \\ \rho(x+\ell) &= \rho(x), \\ &\vdots \quad\quad \vdots \\ T_e(x+\ell) &= T_e(x), \\ n_e(x+\ell) &= n_e(x). \end{aligned} \qquad (2\text{-}35)$$

The periodicity of the conductors and insulators requires

$$\begin{aligned} \Phi'(x+\ell,y) &= \Phi'(x,y) + V_x', \\ \psi(x+\ell,y) &= \psi(x,y) + I_y, \end{aligned} \qquad (2\text{-}36)$$

where V_x' is the axial voltage difference in period ℓ and I_y is the

transverse current flowing through the electrodes. The remaining boundary conditions on Φ' on the conducting and insulating surfaces are

for $|x| < a/2$,

$$\Phi'(x,0) = 0, \qquad \Phi'(x,h) = V_y' ,$$

and for $y = 0$ or h, and either $-\ell/2 < x < -a/2$ (2-37)

or $a/2 < x < \ell/2$, $J_y = 0$ implies that

$$\frac{\partial \Phi'}{\partial y} + \beta \frac{\partial \Phi'}{\partial x} = 0.$$

The electrode length is a, the period length is ℓ, and the channel height is h. The boundary conditions on ψ on the conducting and insulating surfaces are

for $-\ell/2 < x < -a/2$;

$$\psi(x,0) = 0, \qquad \psi(x,h) = -I_x,$$

for $a/2 < x < \ell/2$,

$$\psi(x,0) = I_y, \qquad \psi(x,h) = I_y - I_x, \tag{2-38}$$

and for $y = 0$ or h, and $|x| < a/2$, $E_x' = 0$ implies that

$$\frac{\partial \psi}{\partial y} - \beta \frac{\partial \psi}{\partial x} = 0.$$

The potential V_y' is the transverse voltage across opposed electrodes in the period length ℓ, and the current I_x is the total axial current flowing in the channel, assumed positive in the negative x direction.

It can be shown (appendix B) that the specification of a pair from the four "global" voltages and currents V'_x, V'_y, I_x, I_y, such as (V'_y,V'_x), (I_y,I_x), (V'_y,I_x), (V'_x,I_y) determines a unique distribution of electric field and current within the gas.

2.5 The Resistance and Conductance Tensors

Let the vectors $\vec{V}'$, $\vec{I}$ have components $\vec{V}' = (V'_x,V'_y)$, $\vec{I} = (I_x,I_y)$. A resistance tensor $\overleftrightarrow{R}$ and conductance tensor $\overleftrightarrow{S} = (\overleftrightarrow{R})^{-1}$ based upon these quantities may be defined as

$$\vec{V}' = \overleftrightarrow{R} \cdot \vec{I}, \qquad \vec{I} = \overleftrightarrow{S} \cdot \vec{V}', \tag{2-39}$$

where

$$\overleftrightarrow{R} = \begin{pmatrix} R_{xx} & R_{xy} \\ R_{yx} & R_{yy} \end{pmatrix}. \tag{2-40}$$

The resistance tensor $\overleftrightarrow{R}$ depends upon the distribution of the electrical transport properties within the gas, the geometrical parameters of the channel a, ℓ, h, and, when nonequipartition electron heating is possible, the potential vector $\vec{V}'$. It is readily shown (appendix B) that the electrical power dissipated in the gas in a channel of length ℓ is given by

$$P_d = I_x^2 R_{xx} + I_y^2 R_{yy} + I_x I_y (R_{xy} + R_{yx}). \tag{2-41}$$

The elements of $\overleftrightarrow{R}$ therefore represent the internal impedance of the channel.

Several special cases are of interest. In the idealized case when the conducting gas has uniform electrical transport properties and the electrode segmentation is infinitely fine, it follows from Eq. (2-2) that

$$\overleftrightarrow{R} = \overleftrightarrow{R^{\circ}} = \begin{pmatrix} R^{\circ}_{xx} & R^{\circ}_{xy} \\ R^{\circ}_{yx} & R^{\circ}_{yy} \end{pmatrix}, \tag{2-42}$$

where

$$R^{\circ}_{xx} = \sigma_{\circ}^{-1}\left(\frac{\ell}{h}\right), \quad R^{\circ}_{xy} = \sigma_{\circ}{}^{-1}\beta_{\circ}, \quad R^{\circ}_{yx} = -\sigma_{\circ}{}^{-1}\beta_{\circ}, \quad R^{\circ}_{yy} = \sigma_{\circ}{}^{-1}\left(\frac{h}{\ell}\right). \tag{2-43}$$

The uniform conductivity and Hall parameter for such cases are denoted $\sigma_{\circ}$, $\beta_{\circ}$.

A second special case is that in which the gas properties may be nonuniform; however, the Hall parameter β is identically zero. In that event, the principal impedances R_{xx}, R_{yy} will be denoted $R_{xx}(0)$, $R_{yy}(0)$.

An important mode of operation of the channel is that in which $I_x \equiv 0$ and power is transferred into or out of the gas through the transverse circuit. This mode of operation is called the "Faraday Mode". In that event, the internal impedance of the channel to such power transfer is R_{yy}. The voltage which develops in the axial direction under such circumstances can be shown from Eqs. (2-39) to be given by

$$V'_x = \left(\frac{R_{xy}}{R_{yy}} V'_y\right)_{I_x=0} \tag{2-44}$$

The voltage V'_x given by Eq. (2-44) is called the Hall voltage. The Hall voltage for uniform properties is denoted V'_{x0}. From Eq. (2-43),

$$V'_{x0} = \beta_o \left(\frac{\ell}{h}\right) V'_y \,. \tag{2-45}$$

A non-dimensional Hall voltage for a general nonuniform gas may be defined as

$$\overline{V}_H \equiv \frac{V'_x}{V'_{x0}} \,, \tag{2-46}$$

and a non-dimensional transverse impedance may be defined as

$$\overline{R}_T \equiv \frac{R_{yy}}{R_{yy}(0)} \,. \tag{2-47}$$

These non-dimensional quantities will be useful in describing the overall electrical performance to be discussed in chapters 3, 5, and 7. By virtue of the normalization of R_{yy} on the impedance which occurs with uniformities but no Hall effect, the parameter $\overline{R}_T$ reflects those effects on performance which the Hall effect introduces over and above those introduced by the conductivity nonuniformities alone.

3. NONUNIFORM ELECTRICAL CONDUCTION WITH MODEL CONDUCTIVITY DISTRIBUTIONS

In this chapter solutions to the electrical equations (2-19) with model conductivity distributions discussed in section 2.2 are presented. Consideration is first given to nonuniform distributions in one dimension for which simple analytical results are obtainable. Two-dimensional nonuniformities with finite electrode segments are then considered and detailed numerical solutions for potential and current within the gas are obtained. The effects of layered conductivity variations consisting of high and low conductivity layers over the electrodes are examined. The distribution of current on a finite electrode segment with a nonuniform layered conductivity is compared with experimental measurements.

3.1 One-Dimensional Nonuniformities

3.1.1 One-dimensional nonuniformity solutions

In the limit in which the electrode structure of a linear magnetohydrodynamic channel becomes either infinitely finely segmented or continuous, nonuniformities resulting from the finite size of electrode segments vanish. If in addition property variations occur in only one of the coordinate directions, then both the fluid variables and geometrical variables are uniform in one of the coordinate directions. Solutions of the electrical equations (2-7) and (2-8) or (2-9) and (2-10) are now developed for this case when the electron pressure gradient field $\vec{E}_n$ is negligible.

Consider that all variables are independent of the x coordinate so that

$$\frac{\partial}{\partial x}\,(E_x', E_y', J_x, J_y, \sigma, \beta) \;=\; 0.$$

Using the above condition, the Maxwell Equation curl $\vec{E}' = 0$ and the current conservation equation $\nabla \cdot \vec{J} = 0$ become

$$\frac{\partial E_x'}{\partial y} \;=\; 0, \qquad\qquad \frac{\partial J_y}{\partial y} \;=\; 0.$$

It thus follows that E_x' and J_y are constants, but that E_y' and J_x may be functions of y. If the average operation <> for any function f(y) is defined as

$$\langle f(y) \rangle \;=\; \frac{1}{h} \int_0^h f(y)\,dy, \tag{3-1}$$

then Eqs.(2-2) of chapter 2, with $E_n' = 0$, may be solved for E_y' and J_x in terms of E_x' and J_y and then averaged according to Eq. (3-1). The result is

$$\langle E_y' \rangle \;=\; \left\langle \frac{1 + \beta^2}{\sigma} \right\rangle J_y \;-\; \langle \beta \rangle E_x', \qquad \langle J_x \rangle \;=\; \langle \sigma \rangle E_x' \;-\; \langle \beta \rangle J_y. \tag{3-2}$$

These equations were first obtained by Rosa[18], who used them to examine the effects of random one-dimensional nonuniformities in a conducting gas. Rosa's Eqs. (3-2) may be cast in a useful and compact form which may be regarded as a "global Ohm's Law" for a nonuniform gas. This form is achieved by solving Eqs. (3-2) explicitly for $\langle J_x \rangle$, J_y in terms of E_x', $\langle E_y' \rangle$:

$$\begin{pmatrix} \langle J_x \rangle \\ J_y \end{pmatrix} = \frac{1}{\left\langle \frac{1+\beta^2}{\sigma} \right\rangle} \begin{pmatrix} \langle\sigma\rangle\left\langle \frac{1+\beta^2}{\sigma} \right\rangle - \langle\beta\rangle^2 & -\langle\beta\rangle \\ \langle\beta\rangle & 1 \end{pmatrix} \begin{pmatrix} E'_x \\ \langle E'_y \rangle \end{pmatrix}. \tag{3-3}$$

The inverse of Eqs. (3-3) is

$$\begin{pmatrix} E'_x \\ \langle E'_y \rangle \end{pmatrix} = \frac{1}{\langle\sigma\rangle} \begin{pmatrix} 1 & \langle\beta\rangle \\ -\langle\beta\rangle & \langle\sigma\rangle\left\langle \frac{1+\beta^2}{\sigma} \right\rangle - \langle\beta\rangle^2 \end{pmatrix} \begin{pmatrix} \langle J_x \rangle \\ J_y \end{pmatrix}. \tag{3-4}$$

The resistance tensor $\overleftrightarrow{R}$ may be extracted from Eqs. (3-3) and (3-4) for the case of one-dimensional nonuniformities.

3.1.2 The resistance tensor

The global voltages and currents V'_x, V'_y, I_x, I_y, may be introduced by noting that by definition

$$\begin{aligned} E'_x &= -\frac{V'_x}{\ell}, \\ \langle E'_y \rangle &= -\frac{V'_y}{h}, \\ \langle J_x \rangle &= -\frac{I_x}{h}, \\ J_y &= -\frac{I_y}{\ell}. \end{aligned} \tag{3-5}$$

In terms of the vectors $\vec{V}'$ (V'_x, V'_y) and $\vec{I}$ (I_x, I_y), Eqs. (3-3) and (3-4) are

$$\vec{V}' = \overleftrightarrow{R} \cdot \vec{I}, \qquad \vec{I} = \overleftrightarrow{S} \cdot \vec{V}', \tag{3-6}$$

where the global resistance and conductance tensors are defined as

$$\overleftrightarrow{R} = \frac{R_{yy}(0)}{\langle\sigma\rangle\langle\sigma^{-1}\rangle} \begin{pmatrix} (\frac{\ell}{h})^2 & \langle\beta\rangle\frac{\ell}{h} \\ -\langle\beta\rangle\frac{\ell}{h} & G \end{pmatrix}, \tag{3-7}$$

$$\overleftrightarrow{S} = \frac{R_{yy}^{-1}(0)\langle\sigma^{-1}\rangle}{\langle\frac{1+\beta^2}{\sigma}\rangle} \begin{pmatrix} G\,(\frac{h}{\ell})^2 & -\langle\beta\rangle\frac{h}{\ell} \\ \langle\beta\rangle\frac{h}{\ell} & 1 \end{pmatrix}. \tag{3-8}$$

The factor

$$G = \langle\sigma\rangle\langle\sigma^{-1}\rangle\,[1 + \langle\sigma^{-1}\rangle^{-1}\,(\langle\beta^2\sigma^{-1}\rangle - \langle\beta^2\rangle\langle\sigma\rangle^{-1})] \tag{3-9}$$

contains the coupling of nonuniformities and the Hall effect and is equal to unity in a uniform gas. Based upon the definitions given in chapter 2, the non-dimensional transverse impedance $\overline{R}_T$ and Hall voltage $\overline{V}_H$ for Faraday operation (I_x=0) are

$$\overline{R}_T = \frac{R_{yy}}{R_{yy}(0)} = 1 + G_\beta\,, \tag{3-10}$$

$$\overline{V}_H = \frac{V'_x}{V'_{x0}} = \frac{1}{G}\,, \tag{3-11}$$

where

$$G_\beta \equiv \langle\sigma^{-1}\rangle^{-1}\,(\langle\beta^2\sigma^{-1}\rangle - \langle\beta^2\rangle\langle\sigma^{-1}\rangle). \tag{3-12}$$

In those cases where β is uniform, the above results reduce to

$$G = 1 + G^*(1 + \beta^2), \tag{3-13}$$

$$G_\beta = \left(\frac{G^*}{1 + G^*} \right) \beta^2 , \tag{3-14}$$

where

$$G^* \equiv \langle\sigma\rangle\langle\sigma^{-1}\rangle - 1. \tag{3-15}$$

Thus for uniform β, the non-dimensional impedance and Hall voltage become

$$\overline{R}_T = 1 + \left(\frac{G^*}{1 + G^*} \right) \beta^2 , \tag{3-16}$$

$$\overline{V}_H = \frac{1}{1 + G^*(1+\beta^2)} . \tag{3-17}$$

It may be observed that when $G^* \to 0$, the uniform conductivity results are obtained:

$$\overline{R}_T \to 1 \quad \text{and} \quad \overline{V}_H \to 1, \quad \text{as } G^* \to 0.$$

For very strong nonuniformities, $G^* \to \infty$, and there results the limit

$$\overline{R}_T \to (1 + \beta^2) \quad \text{and} \quad \overline{V}_H \to 0, \quad \text{as } G^* \to \infty.$$

It may be noted that these limiting values for strong nonuniformities are precisely the same as the results for continuous electrodes ($E'_x \equiv 0$). Thus, strong conductivity nonuniformities may destroy the effect of electrode segmentation, even if such segmentation is infinitely fine.

3.1.3 Potential and current distributions

The potential $\Phi'(x,y)$ and current flux function $\psi(x,y)$ may be obtained by integrating Eqs. (2-2) with $\vec{E}_n = 0$ and using the condition for one-dimensional nonuniformities in the y direction that E'_x and J_y are constants. The results in terms of V'_x, I_y are

$$\Phi'(x,y) - \Phi'(0,0) = [\tilde{\rho}_\beta(y)\, I_y - (\tilde{\beta}(y) - \tfrac{x}{h})V'_x]\,\frac{h}{\ell}\,, \qquad (3\text{-}18)$$

$$\psi(x,y) - \psi(0,0) = [(\tilde{\beta}(y) + \tfrac{x}{h})I_y - \tilde{\sigma}(y)V'_x]\,\frac{h}{\ell}\,. \qquad (3\text{-}19)$$

The functions $\tilde{\sigma}(y)$, $\tilde{\beta}(y)$, and $\tilde{\rho}_\beta(y)$ are defined as

$$\tilde{\sigma}(y) \equiv \frac{1}{h}\int_0^y \sigma(\xi)d\xi\,, \qquad (3\text{-}20)$$

$$\tilde{\beta}(y) \equiv \frac{1}{h}\int_0^y \beta(\xi)d\xi\,, \qquad (3\text{-}21)$$

$$\tilde{\rho}_\beta(y) \equiv \frac{1}{h}\int_0^y \frac{1+\beta^2(\xi)}{\sigma(\xi)}\,d\xi\,. \qquad (3\text{-}22)$$

3.1.4 Layered conductivity nonuniformities

To obtain specific results from the general formulation described above, the following form of the model conductivity will be considered. For simplicity, the Hall parameter β will be taken as a constant, and $\sigma(y)$ is assumed to be of the form

$$\text{for } 0 \le y \le \delta, \qquad \sigma(y) = \sigma_w + (\sigma_o - \sigma_w)\frac{y}{\delta},$$

$$\text{for } \delta \le y \le h-\delta, \qquad \sigma(y) = \sigma_o, \tag{3-23}$$

$$\text{for } h-\delta \le y \le h, \qquad \sigma(y) = \sigma_w + (\sigma_o - \sigma_w)\frac{y}{h-\delta}.$$

This distribution represents layers of thickness δ of high or low conductivity over the electrodes and insulators. The conductivity in the the core of the gas is σ_o, and σ_w is the conductivity at the electrode-insulator wall. Such a distribution would be characteristic of heating or cooling near the electrode walls with δ representing a characteristic layer thickness. This distribution could also represent layers of frozen ionization over the electrodes and insulators, as suggested by Kerrebrock.[19,20]

The conductivity nonuniformity function G* has been calculated for this model distribution and is shown in Fig. 3-1 for values of δ/h and σ_w/σ_o. The non-dimensional transverse impedance $\overline{R}_T$ and Hall voltage $\overline{V}_H$ are shown in Figs. 3-2 through 3-5 for various values of σ_w/σ_o and β. In Fig. 3-2, the nondimensional impedance $\overline{R}_T$ is shown as a function of the Hall parameter β for various values of σ_w/σ_o. The nondimensional Hall voltage $\overline{V}_H$ is shown in Fig. 3-3 for these same cases. Also shown for reference is the value of $\overline{R}_T$ for continuous electrodes. It can be seen that the impedance is increased and the Hall voltage decreased as a result of the nonuniformities. This deterioration of performance becomes more pronounced for large Hall parameters. In Figs. 3-4 and 3-5 the effect of nonuniformities for a fixed value of Hall pa-

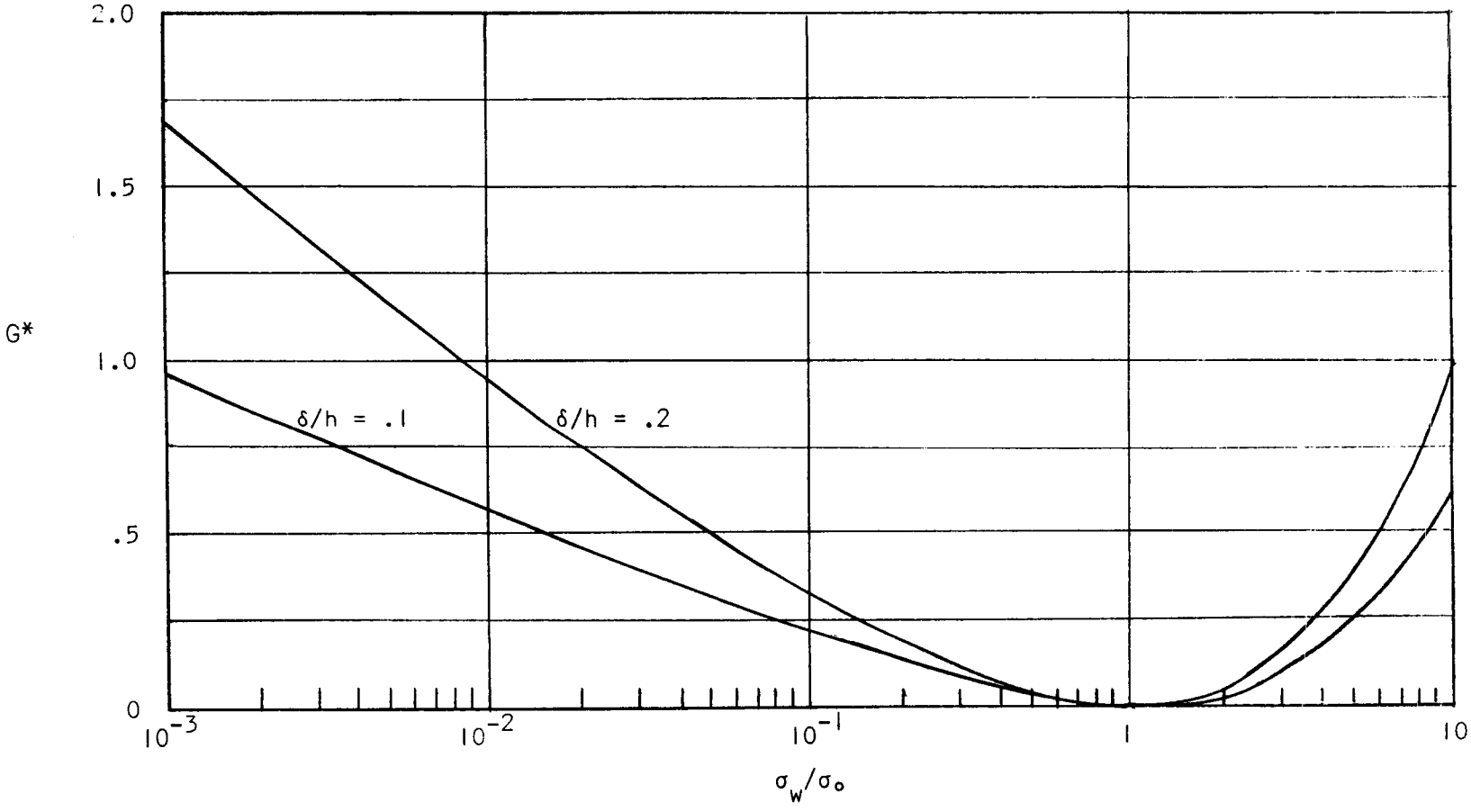

Fig. 3-1 Conductivity nonuniformity factor G* for the conductivity model given by Eq. (3-23)

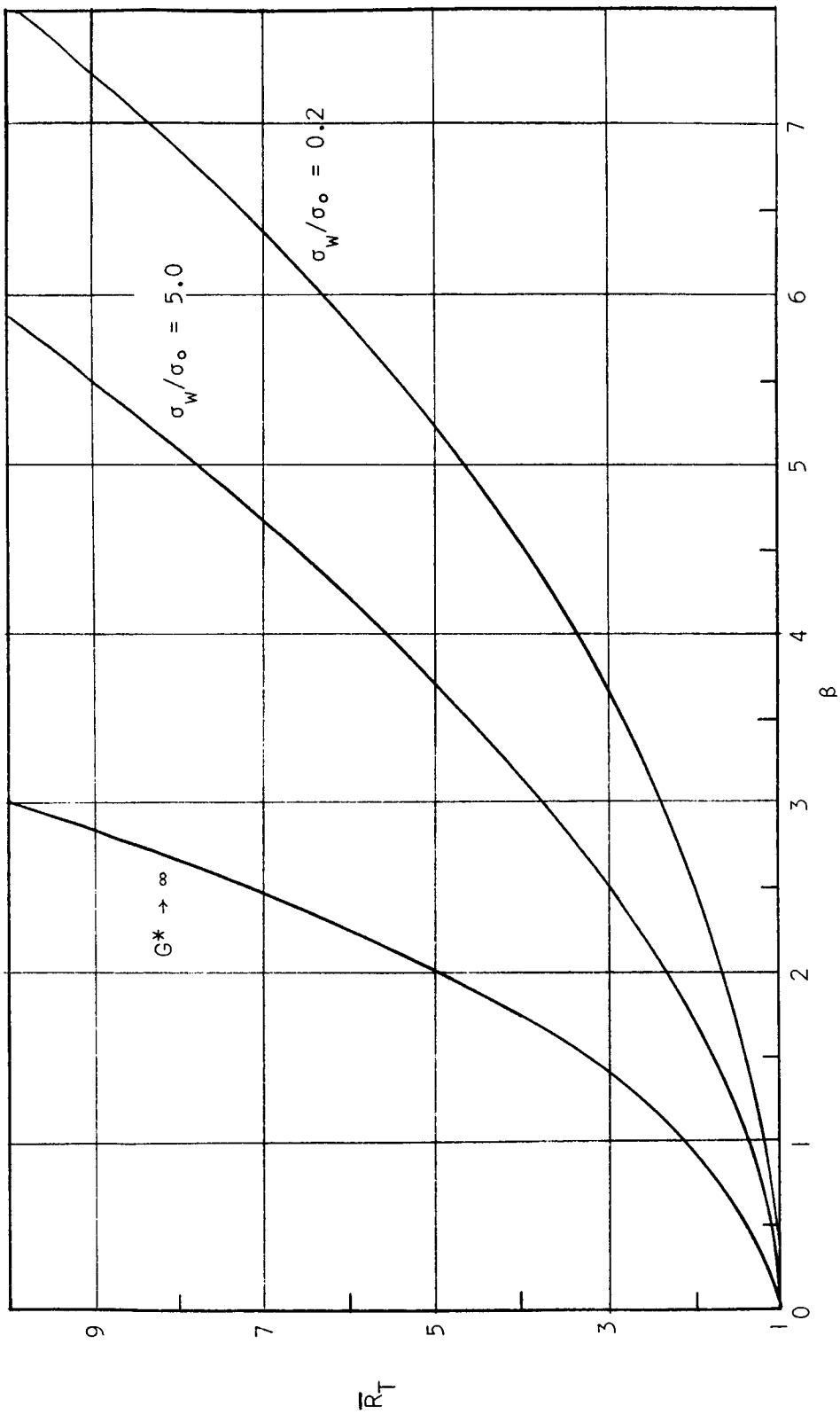

Fig. 3-2 Nondimensional transverse impedance $\bar{R}_T$ as a function of Hall parameter for infinitely fine segmented electrodes and several conductivity nonuniformities given by Eq. (3-23)

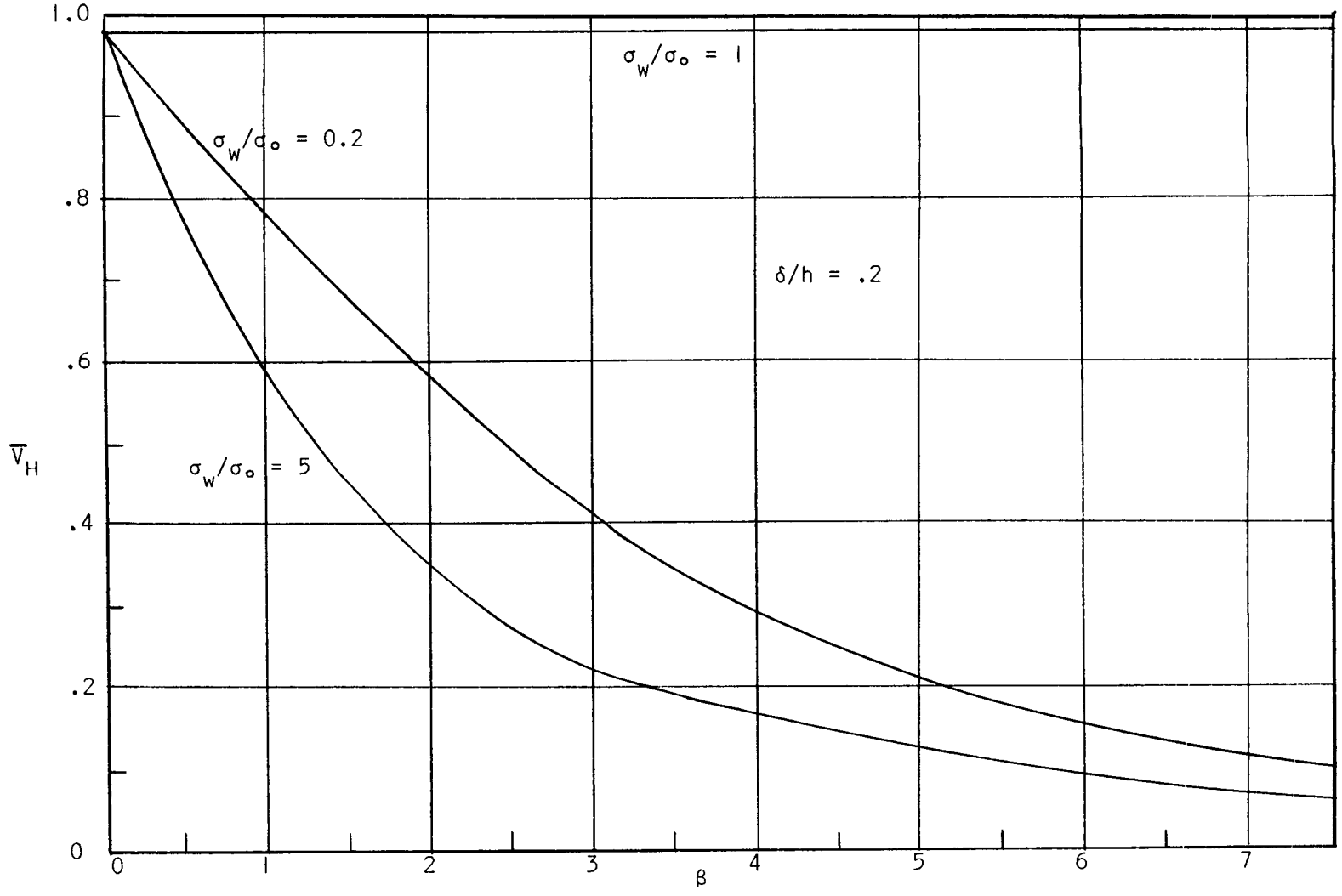

Fig. 3-3 Nondimensional Hall potential $\overline{V}_H$ as a function of Hall parameter for infinitely fine segmented electrodes and several conductivity nonuniformities given by Eq. (3-23)

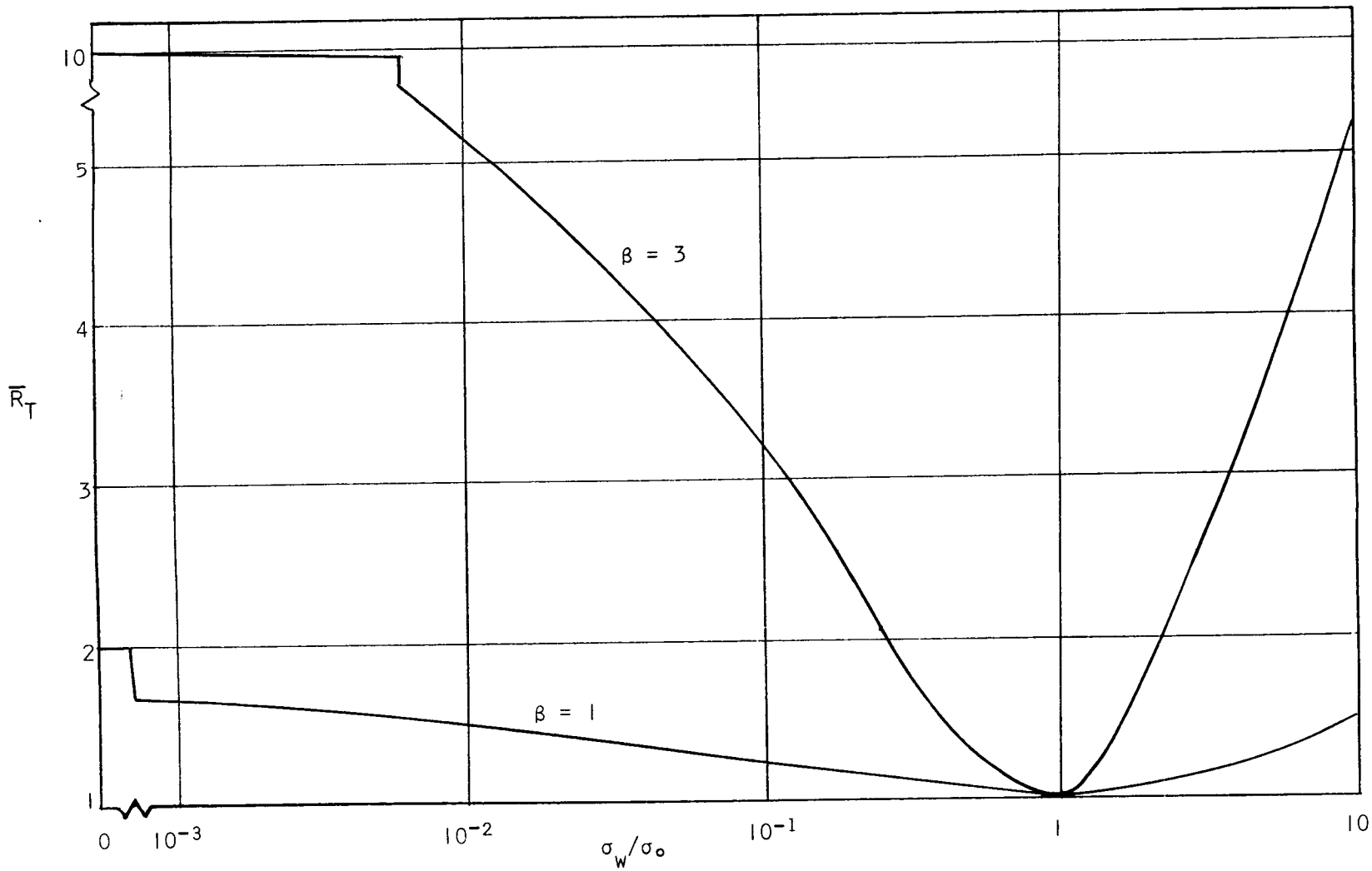

Fig. 3-4 Nondimensional transverse impedance $\overline{R}_T$ for infinitely fine segmented electrodes as a function of conductivity nonuniformity according to the model of Eq. (3-23). Note the asymptotic values of $\overline{R}_T \to 1 + \beta^2$ for strong conductivity nonuniformities.

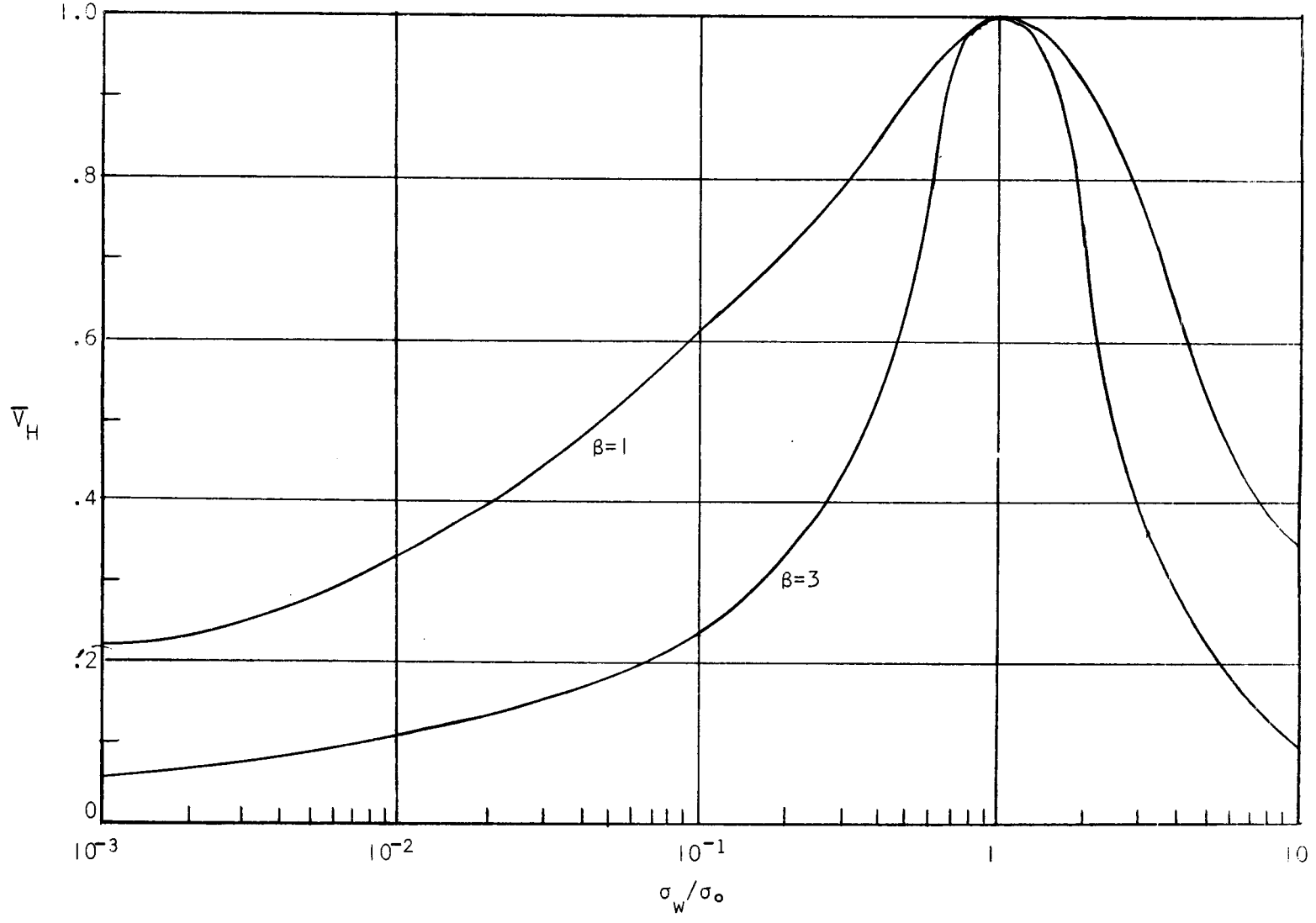

Fig. 3-5 Nondimensional Hall potential $\overline{V}_H$ for infinitely fine segmented electrodes as a function of conductivity nonuniformity according to the model of Eq.(3-23)

rameter is examined. As the nonuniformity is increased, the performance again exhibits deterioration. It should be noted that both high and low conductivity layers cause increased internal impedance, even though a high conductivity layer in the absence of Hall effects would lead to a decrease in internal impedance. This fact may be seen more clearly by examining R_{yy} normalized on $\frac{1}{\sigma_o}\left(\frac{h}{\ell}\right)$, the impedance of the gas if it were of uniform conductivity at the core value σ_o. This non-dimensional impedance is also shown in Fig. 3-4 and is always greater than unity.

It should also be noted that the performance degradation shown in Figs. 3-4 and 3-5 is more pronounced for high conductivity layers than for low conductivity layers.

3.2 Two-Dimensional Nonuniformities

3.2.1 The non-dimensional equations

In the absence of significant diffusion of charge due to electron pressure gradients and an electrical conductivity specified as a function of space within the channel, the governing equations for the potential Φ' and the flux function ψ were shown to be (section 2.1)

$$M_E(\Phi') = 0, \qquad M_J(\psi) = 0. \tag{3-24}$$

The operators M_E and M_J are defined in section 2.1 and contain the gradients of the given electrical conductivity distribution. The above equations may be non-dimensionalized as follows. Let V_o be a characteristic voltage and $I_o = \sigma_o V_o \ell/h$ a characteristic current per unit channel depth where σ_o is a characteristic conductivity. Let h, the channel height, be a characteristic length. A nondimensional potential

and flux function may be defined as

$$\bar{\Phi}' \equiv \frac{\Phi'}{V_o}, \qquad \bar{\psi} \equiv \frac{\psi}{I_o},$$

and nondimensional operators $\bar{M}_E$, $\bar{M}_J$ as

$$\bar{M}_E \equiv h^2 M_E, \qquad \bar{M}_J \equiv h^2 M_J. \tag{3-25}$$

The Eqs. (3-24) become

$$\bar{M}_E(\bar{\Phi}') = 0, \qquad \bar{M}_J(\bar{\psi}) = 0. \tag{3-26}$$

The boundary conditions discussed in section 2.4 become, in nondimensional form,

Periodicity:

$$\begin{aligned} \bar{\Phi}'(\bar{x}+\bar{\ell},\bar{y}) &= \bar{\Phi}'(\bar{x},\bar{y}) + \bar{V}_x', \\ \bar{\psi}(\bar{x}+\bar{\ell},\bar{y}) &= \bar{\psi}(\bar{x},\bar{y}) + \bar{I}_y, \end{aligned} \tag{3-27}$$

Conductor-insulator conditions in Field representation:

$$\begin{aligned} &\text{for } -\bar{a}/2 < \bar{x} < \bar{a}/2, \quad \bar{\Phi}'(\bar{x},0) = 0, \quad \bar{\Phi}'(\bar{x},1) = \bar{V}_y', \\ &\text{for } \bar{y} = 0,1 \text{ and either } -\bar{\ell}/2 < \bar{x} < -\bar{a}/2 \text{ or } \bar{a}/2 < \bar{x} < \bar{\ell}/2, \\ &\frac{\partial \bar{\Phi}'}{\partial \bar{y}} + \beta \frac{\partial \bar{\Phi}'}{\partial \bar{x}} = 0, \end{aligned} \tag{3-28}$$

Conductor-insulator conditions in current representation:

$$\text{for } -\bar{\ell}/2 < \bar{x} < -\bar{a}/2, \qquad \bar{\psi}(\bar{x},0) = 0, \quad \bar{\psi}(\bar{x},1) = -\bar{I}_x,$$

$$\text{for } \bar{a}/2 < \bar{x} < \bar{\ell}/2, \qquad \bar{\psi}(\bar{x},0) = \bar{I}_y, \quad \bar{\psi}(\bar{x},1) = \bar{I}_y - \bar{I}_x, \tag{3-29}$$

$$\text{for } y = 0,1 \text{ and } -a/2 < x < a/2, \qquad \frac{\partial\bar{\psi}}{\partial\bar{y}} - \beta\frac{\partial\bar{\psi}}{\partial\bar{x}} = 0 .$$

The nondimensional potential and total current are defined as

$$\bar{V}_x \equiv \frac{V_x}{V_o}, \qquad \bar{V}'_y \equiv \frac{V'_y}{V_o},$$

$$\bar{I}_x \equiv \frac{I_x}{I_o}, \qquad \bar{I}_y \equiv \frac{I_y}{I_o}.$$

The nondimensional lengths are

$$\bar{x} \equiv x/h, \quad \bar{y} \equiv y/h, \quad \bar{a} \equiv a/h, \quad \bar{\ell} \equiv \ell/h.$$

In the calculations which follow, the characteristic voltage V_o is selected as V'_y so that $\bar{V}'_y = 1$, $I_o = \sigma_o V'_y \ell/h$.

3.2.2 Layered conductivity nonuniformities

In the case of finitely segmented conductors, the solutions of the boundary value problem described by the foregoing equations with a model nonuniform conductivity were obtained numerically. (A discussion of the numerical procedures is given in Appendix A.) The effects of layered conductivity nonuniformities with finite electrode segments will now be described.

Consider a model distribution of σ according to Eq. (3-23) with a Hall parameter of unity. In such a situation property variations occur in the y direction and electrode-induced nonuniformities occur in the x direction. The current distribution for this case with a uniform conductivity is shown in Fig. 3-6 for reference. In Fig. 3-7, the current distribution for a low conductivity layer with $\delta/h = 0.2$, $\sigma_w/\sigma_o = 0.2$ is shown. It can be seen that the low conductivity layer tends to straighten the current in the core of the gas relative to the uniform conductivity case. This straightening effect results because the low conductivity gas near the insulators acts as a region of high electrical impedance in which the current tends not to flow. The current therefore tends to flow directly across the channel from electrode to electrode. In Fig. 3-8, the current distribution for a high conductivity layer with $\delta/h = 0.2$, $\sigma_w/\sigma_o = 5$ is shown. In this case, the high conductivity layer tends to short out the effect of the insulator since the high conductivity region over the insulators acts as a region of low impedance in which the current readily flows. The gas in the core is thus in the presence of an electrode wall which appears very much like a continuous electrode; thus the current in the core tends to flow at the Hall angle $\tan^{-1}(\beta)$. Near the electrode edge a large local axial component of current must exist to provide a path for the current attracted to the insulator region to flow into the electrode. It should also be noted that the dividing current streamline between electrode pairs has shifted from its position near the center of the insulator with a uniform conductivity towards the left hand lower electrode edge with a high conductivity layer.

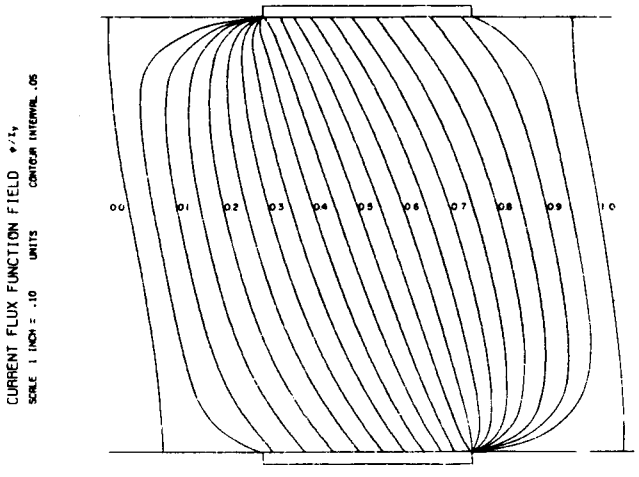

Fig. 3-6 Lines of constant current $\overline{\psi}$ for finitely segmented channel, $\ell/h = 1$, $a/\ell = .5$, $I_x = 0$, $\beta = 1$, uniform conductivity.

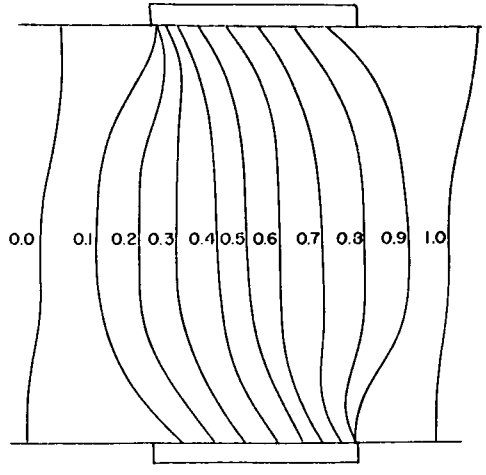

Fig. 3-7 Lines of constant current $\overline{\psi}$ for finitely segmented channel, $\ell/h = 1$, $a/\ell = .5$, $I_x = 0$, $\beta = 1$; low conductivity layer, $\sigma_w/\sigma_o = 0.2$, $\delta/h = 0.2$.

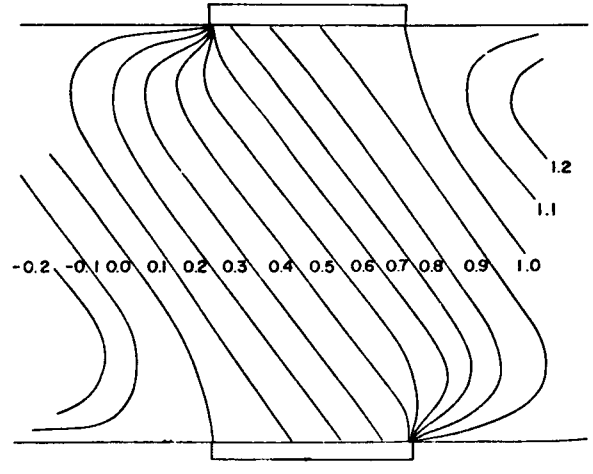

Fig. 3-8 Lines of constant current $\overline{\psi}$ for finitely segmented channel, $\ell/h = 1$, $a/\ell = .5$, $I_x = 0$, $\beta = 1$; high conductivity layer $\sigma_w/\sigma_o = 5$, $\delta/h = 0.2$.

In Fig. 3-9 the cumulative distribution of normal current over the electrode

$$I(x) = \int_{-\frac{a}{2}}^{x} J_y(\xi,0)d\xi = \psi(x,0) - \psi(-\tfrac{a}{2},0)$$

is shown for the foregoing cases. It can be seen that a layer of low conductivity gives rise to a more uniform distribution of current on the electrode, whereas a high conductivity layer introduces a greater nonuniformity in the current distribution relative to the uniform conductivity case.* These effects are explainable in terms of the large current which must enter the electrode at its edge when large currents are attracted to the region over the insulator.

In Figs. 3-10, 3-11, and 3-12 the potential distribution $\overline{\Phi}'(x,y)$ is shown for the same cases discussed above. In the case of a low conductivity layer, large potential drops occur over the electrodes, whereas in the case of the high conductivity layer, the principal potential drop occurs in the core except for the large drops near the electrode edges. Since the bulk of the current enters at the electrode edge, the bulk of the current flows through the large potential drop at the edge of the electrode which manifests an overall large internal impedance.

It may be observed that in both cases of high and low conductivity layers, the effect of the layers is to shield the current and potential distribution in the core from the finite segmentation effect. In both

*These results may be contrasted with the model employed by Kerrebrock[19,20] in which a uniform distribution of current is assumed to coexist on the electrode with a high conductivity layer.

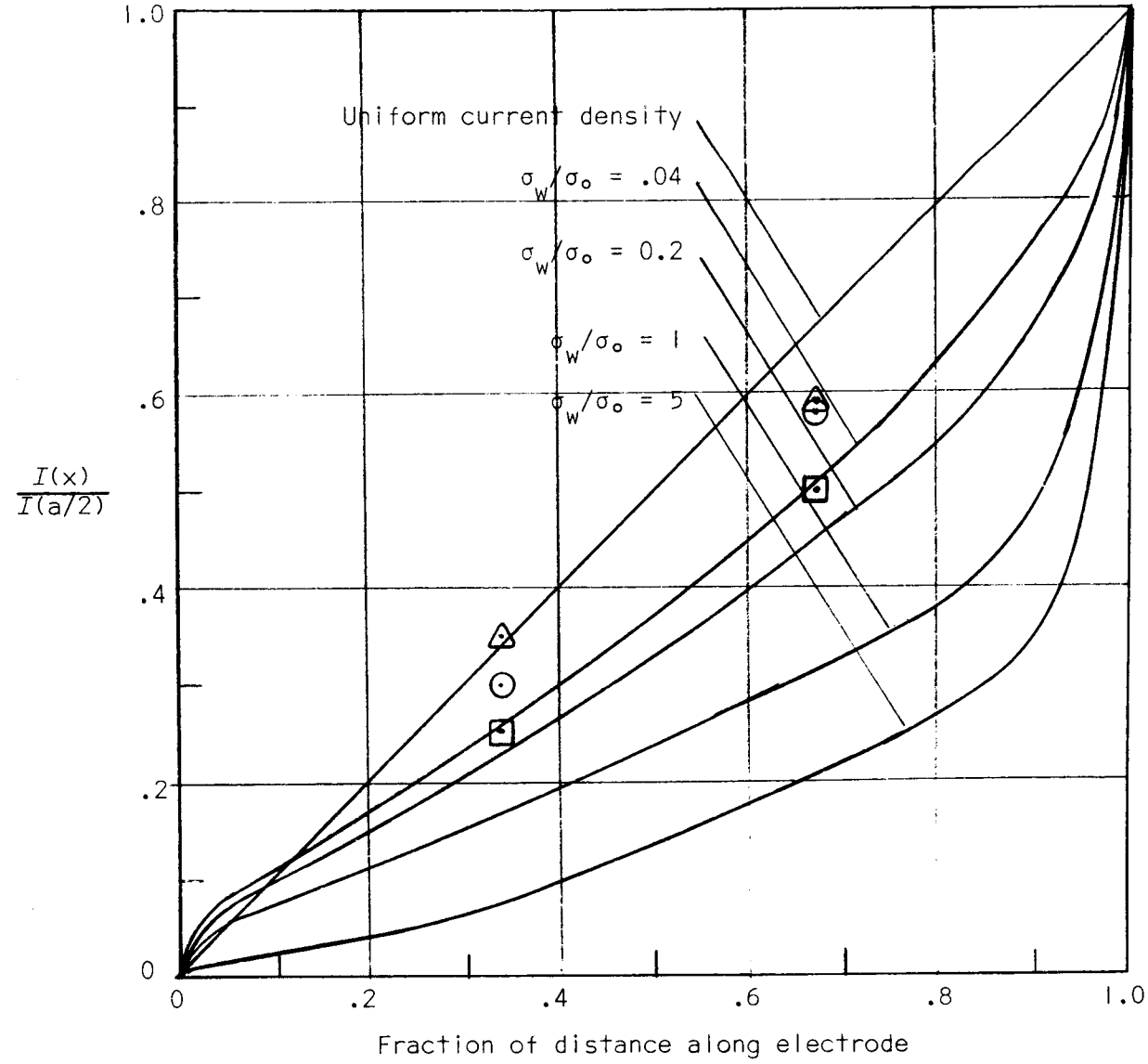

Fig. 3-9 Electrode current distribution for various degrees of conductivity nonuniformity for the cases in Figs. 3-6 through 3-8. Data points from Hoffman and Oates.[29]

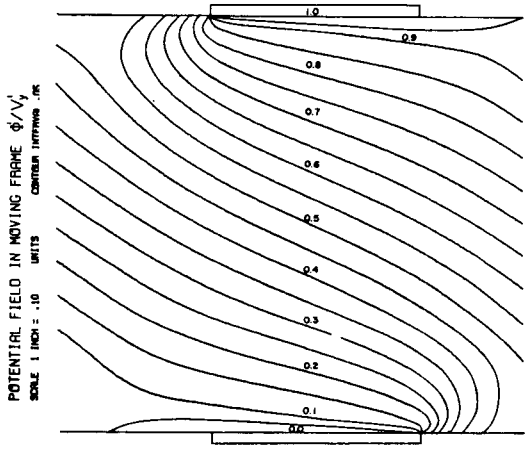

Fig. 3-10 Lines of constant potential $\overline{\Phi}'$ for finitely segmented channel, $\ell/h = 1$, $a/\ell = .5$, $I_x = 0$, $\beta = 1$; uniform conductivity.

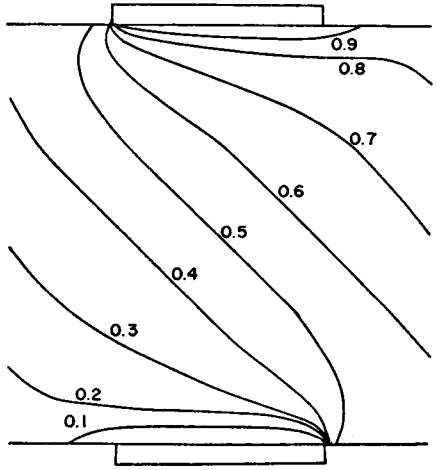

Fig. 3-11 Lines of constant potential $\overline{\Phi}'$ for finitely segmented channel, $\ell/h = 1$, $a/\ell = .5$, $I_x = 0$, $\beta = 1$; low conductivity layer, $\sigma_w/\sigma_o = 0.2$, $\delta/h = 0.2$.

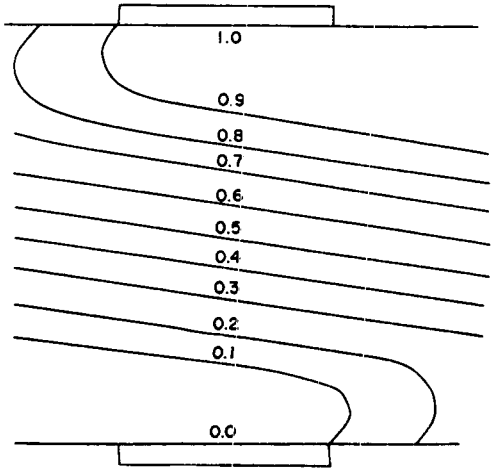

Fig. 3-12 Lines of constant potential $\overline{\Phi}'$ for finitely segmented channel, $\ell/h = 1$, $a/\ell = .5$, $I_x = 0$, $\beta = 1$; high conductivity layer, $\sigma_w/\sigma_o = 5$, $\delta/h = 0.2$.

cases, the current and potential distribution outside of the layers is remarkably uniform.

The distribution of the potential $\overline{\Phi}'$ on the insulator wall is shown in Fig. 3-13 for the cases discussed above.† It can be seen that although the low conductivity layer produces the greatest initial rise in potential, it then falls off below the uniform conductivity case. The high conductivity layer produces a consistently lower potential rise along the insulator relative to the uniform conductivity case.

The effect of high and low conductivity layers with large Hall paramaters has been examined. For reference purposes, the current distribution with uniform conductivity and $\beta = 3$ is shown in Fig. 3-14. The results which will now be discussed are for a uniform Hall parameter $\beta = 3$ and layered conductivity nonuniformities given by Eq. (3-23) with $\delta/h = 0.2$ and $\sigma_w/\sigma_o = 0.2$. The current distribution for low conductivity layers is shown in Fig. 3-15 and the detail region near the electrode is shown in Fig. 3-17. It is interesting to note that for this large value of β, the current in the layers flows at an angle near $\tan^{-1}(\beta)$, as was the case with uniform conductivity; however, in the core of the gas, the current is flowing at an angle considerably different than that with a uniform conductivity (Fig. 3-14). The core current for this high value of β tends to flow almost transverse to the channel walls, as contrasted to that for a uniform conductivity with $\beta = 3$.

The current distribution with a high conductivity layer with

†The relation of the potential $\overline{\Phi}'$ to the laboratory potential Φ is discussed in section 2.3.1.

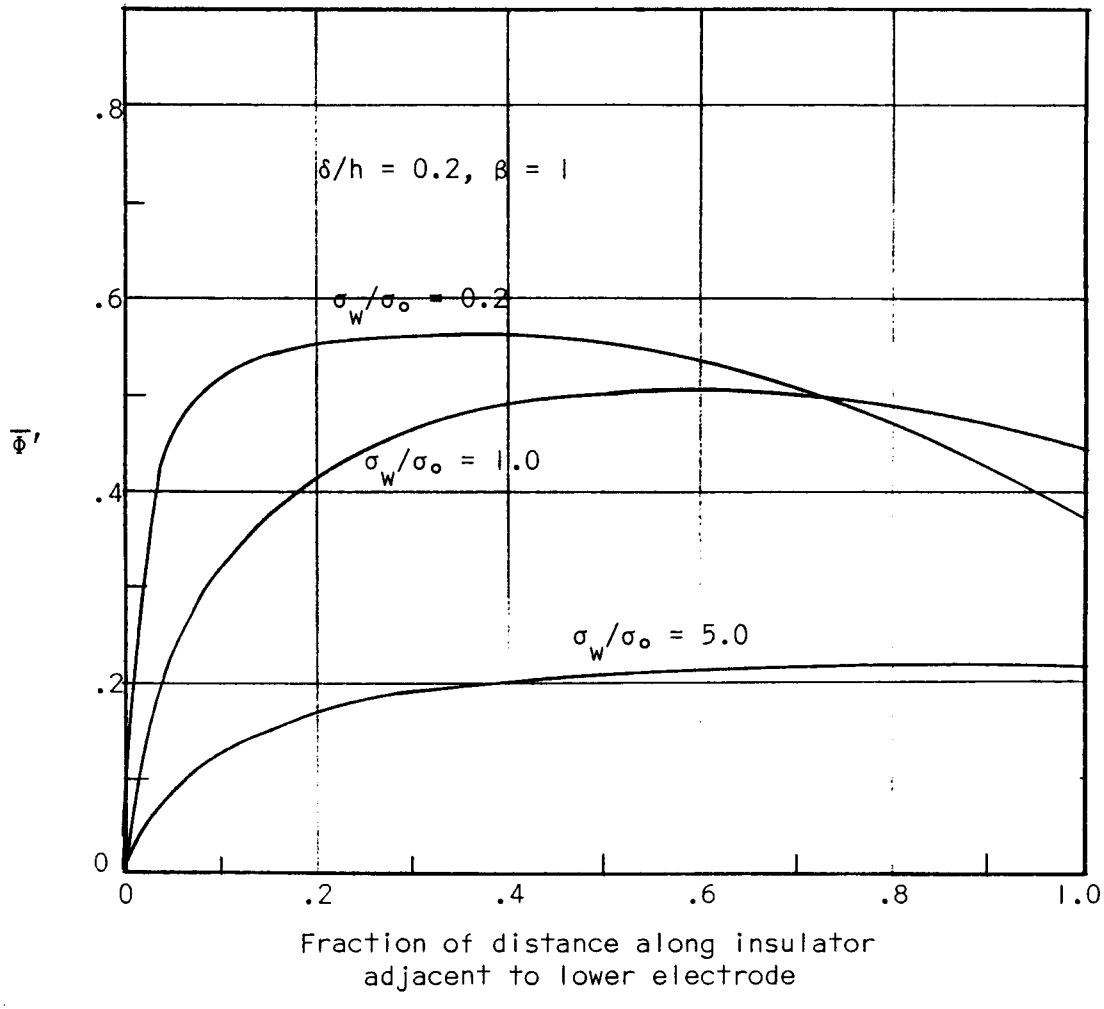

Fig. 3-13 Potential distribution $\bar{\Phi}'$ along insulator wall for various degrees of conductivity nonuniformity for the cases in Figs. 3-10 through 3-12

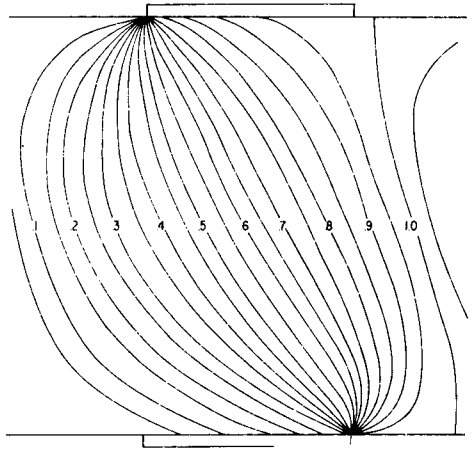

Fig. 3-14 Lines of constant current $\overline{\psi}$ for finitely segmented channel, $\ell/h = 1$, $a/\ell = .5$, $I_x = 0$, $\beta = 3$; uniform conductivity.

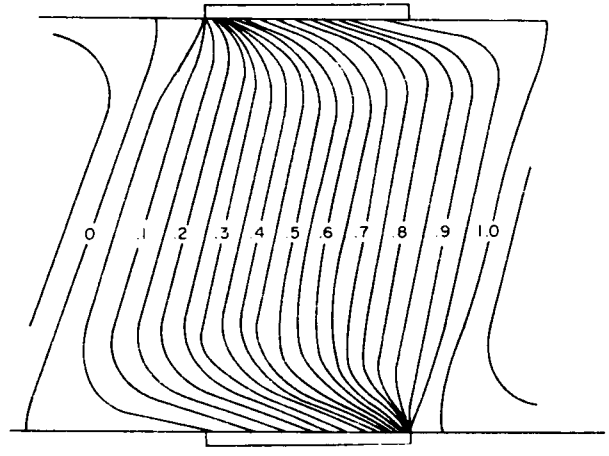

Fig. 3-15 Lines of constant current $\overline{\psi}$ for finitely segmented channel, $\ell/h = 1$, $a/\ell = .5$, $I_x = 0$, $\beta = 3$; low conductivity layer, $\sigma_w/\sigma_o = 0.2$, $\delta/h = 0.2$.

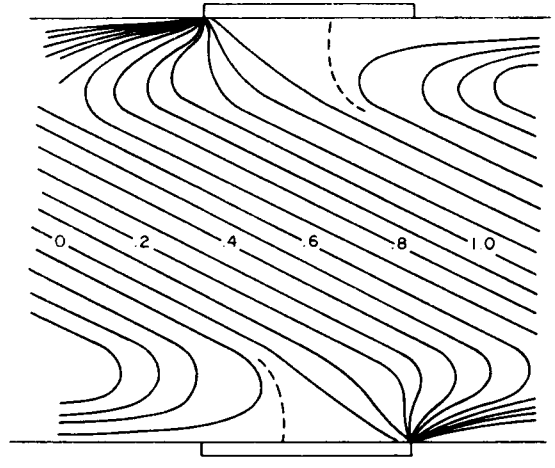

Fig. 3-16 Lines of constant current $\overline{\psi}$ for finitely segmented channel, $\ell/h = 1$, $a/\ell = .5$, $I_x = 0$, $\beta = 3$; high conductivity layer, $\sigma_w/\sigma_o = 5$, $\delta/h = 0.2$.

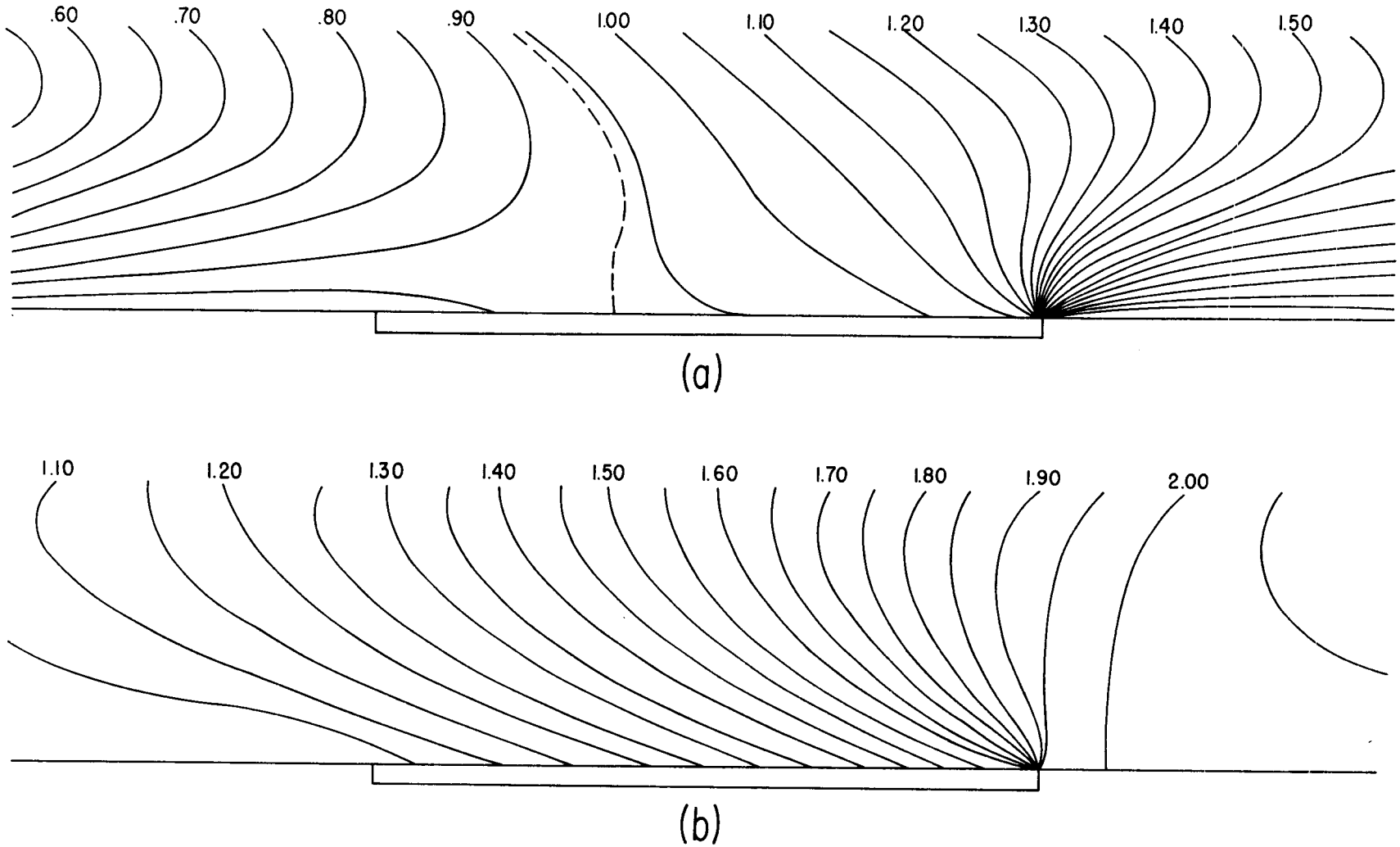

Fig. 3-17 Detail region of lines of constant current $\overline{\psi}$ near electrodes with low and high conductivity layers; $\ell/h = 1$, $a/\ell = .5$, $I_x = 0$, $\beta = 3$, $\delta/h = 0.2$; (a) high conductivity layer, $\sigma_w/\sigma_o = 5.0$, (b) low conductivity layer, $\sigma_w/\sigma_o = 0.2$.

σ_w/σ_o = 5 and a Hall parameter β = 3 is shown in Figs. 3-16 and 3-17. It can be seen that the trends established with a high conductivity layer and β = 1 persist. Note that the dividing current lines have moved onto the electrodes so that current is now entering the lower electrode at the downstream end and leaving the same electrode at the upstream end. This effect also occurs with uniform conductivity distributions with Hall parameters of the order β = 2 and values of the electrode to insulator length ratios a/ℓ near one as reported by Crown.[15]

The distribution of electrode current $I(x)$ for the layered model with β = 3 is shown in Fig. 3-18. In general, the trends established with β = 1 persist: low conductivity layers spread the current out over the electrode and high conductivity layers intensify the current at the electrode edges. The principal effect of the higher Hall parameter is to intensify the amount of current entering at the electrode edge. This more nonuniform distribution is then further made even more nonuniform by a high conductivity layer or more uniform by a low conductivity layer. With low conductivity layers, the tendency towards uniformity at high β is relatively less than that at lower β, as can be seen by comparing the high β results of Fig. 3-18 with the β = 1 results of Fig. 3-9. In the case of the high conductivity layer with a large Hall parameter, the current both eneters and leaves the electrode as shown by a decreasing $I(x)$ over the upstream edge of the electrode.

The potential distributions for the β = 3 cases discussed above are shown in Figs. 3-20 through 3-23 and the uniform conductivity distribution is shown in Fig. 3-19 for reference. Large potential drops

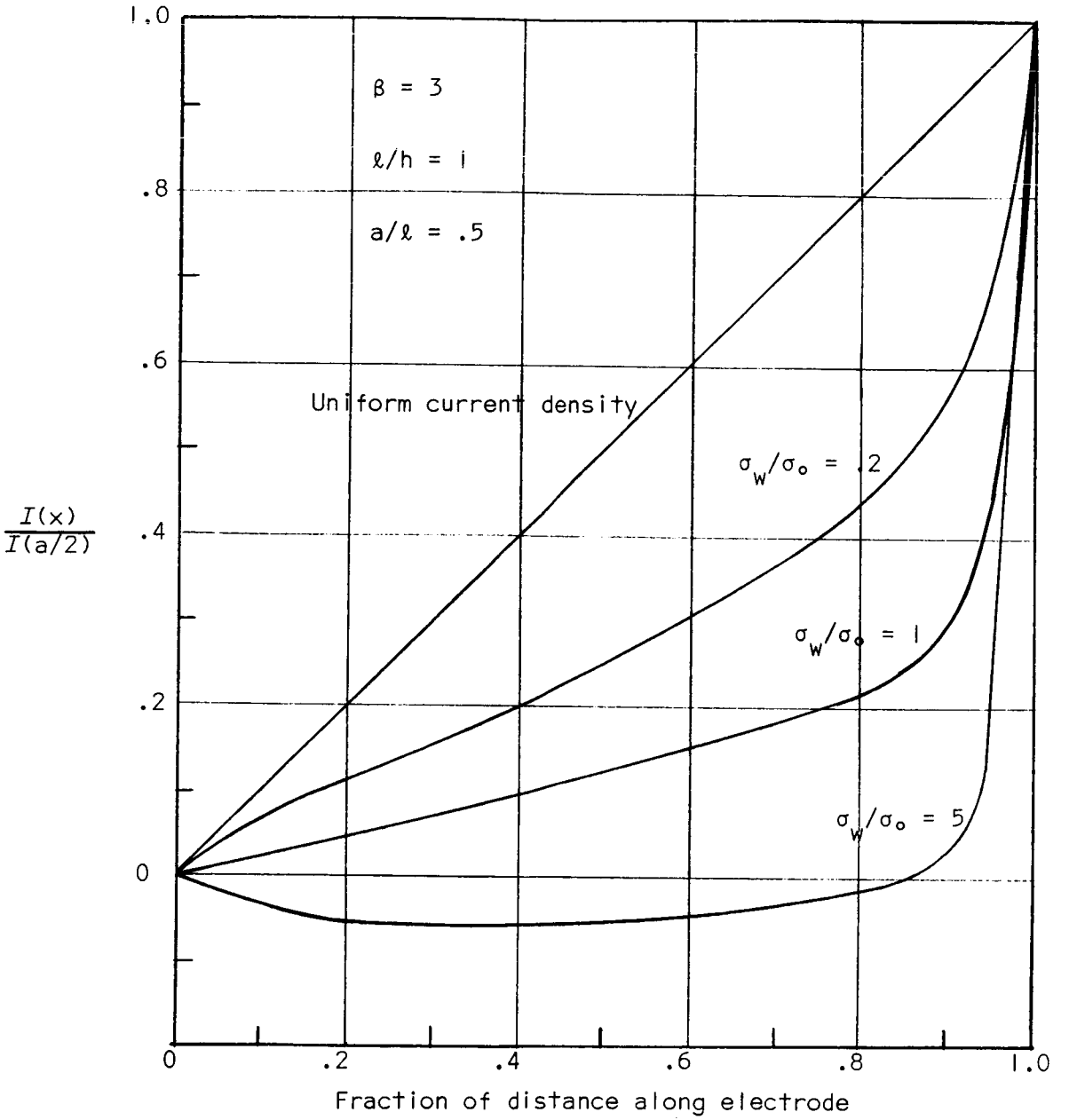

Fig. 3-18 Electrode current distribution for various degrees of nonuniformity for the cases in Figs. 3-14 through 3-16.

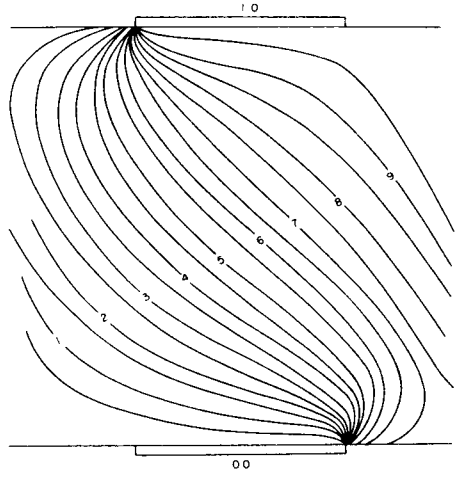

Fig. 3-19 Lines of constant potential $\overline{\Phi}'$ for finitely segmented channel, $\ell/h = 1$, $a/\ell = .5$, $I_x = 0$, $\beta = 3$; uniform conductivity.

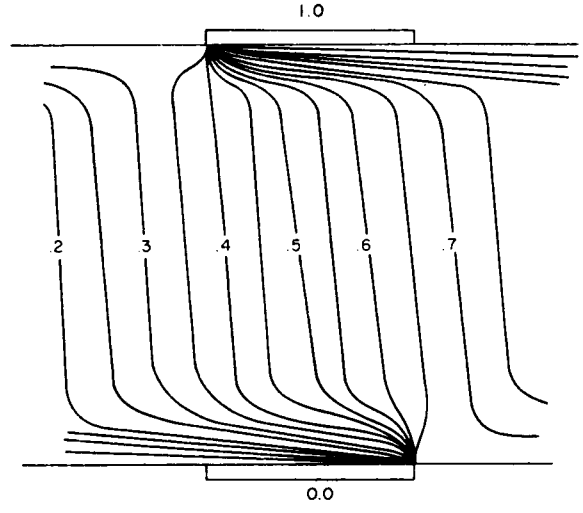

Fig. 3-20 Lines of constant potential $\overline{\Phi}'$ for finitely segmented channel, $\ell/h = 1$, $a/\ell = .5$, $I_x = 0$, $\beta = 3$; low conductivity layer, $\sigma_w/\sigma_o = 0.2$, $\delta/h = 0.2$.

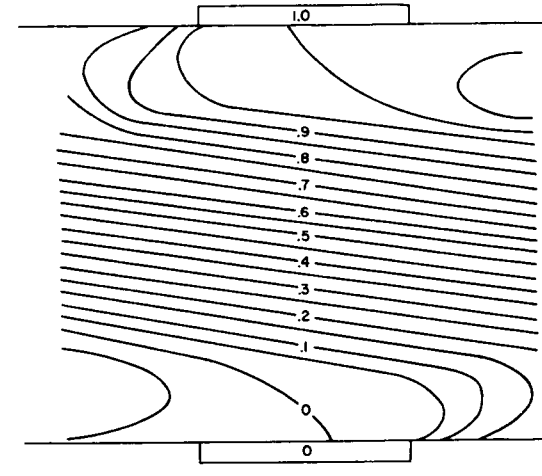

Fig. 3-21 Lines of constant potential $\overline{\Phi}'$ for finitely segmented channel, $\ell/h = 1$, $a/\ell = .5$, $I_x = 0$, $\beta = 3$; high conductivity layer, $\sigma_w/\sigma_o = 5$, $\delta/h = 0.2$.

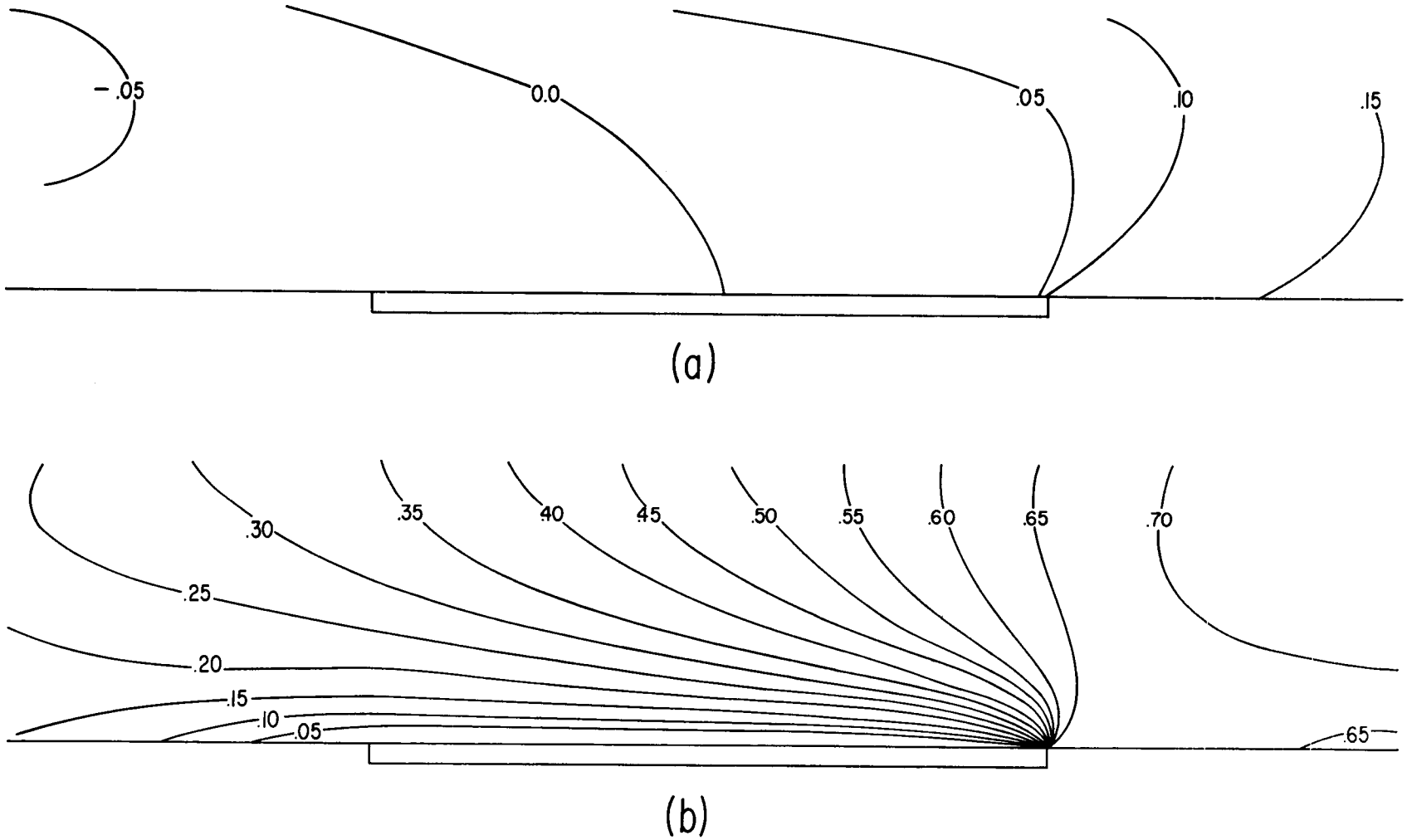

Fig. 3-22 Detail region of lines of constant potential $\overline{\Phi}'$ near electrodes with low and high conductivity layers; $\ell/h = 1$, $a/\ell = 0.5$, $I_x = 0$, $\beta = 3$, $\delta/h = 0.2$; (a) high conductivity layer, $\sigma_w/\sigma_o = 5.0$, (b) low conductivity layer, $\sigma_w/\sigma_o = 0.2$.

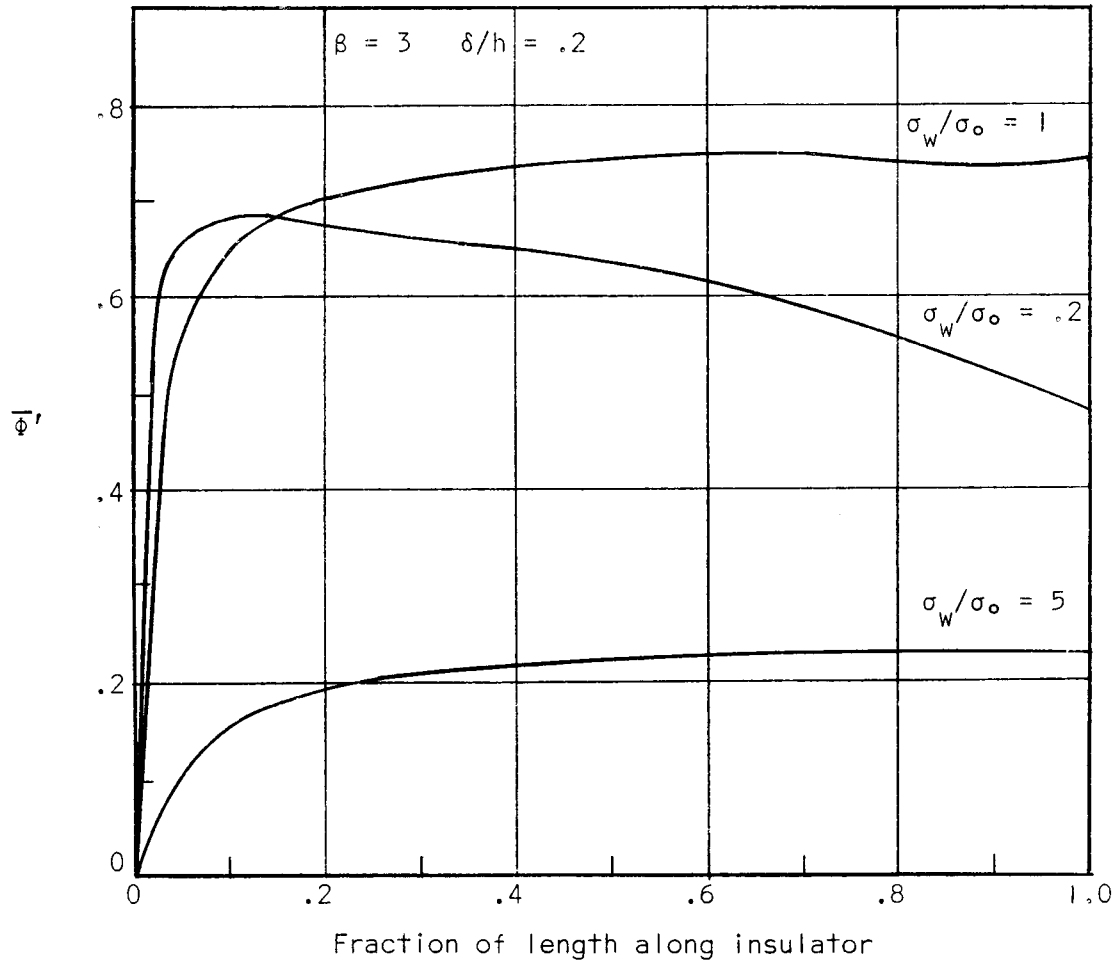

Fig. 3-23 Potential distribution $\overline{\Phi}'$ along insulator for various degrees of conductivity nonuniformity for the cases in Figs. 3-19 through 3-21

exist near the electrodes as would be expected for these low conductivity layers. With this larger value of the Hall parameter, the potential lines tend to approach a parallel distribution with respect to the current lines indicating that the current vector is tending to become normal to the electric field vector.

The distribution of potential along the insulator is shown in Fig. 3-23. The trends established for the potential distribution with $\beta = 1$ also persist with $\beta = 3$. Note that the maxima of the potential along the insulator shift towards the left edge of the lower electrode with low conductivity layers and towards the right edge with high conductivity layers. This result is due to the movement of the current dividing lines in those directions since the point of maximum potential on the insulator occurs at the "stagnation point" of the current dividing streamline.

All the foregoing layered model results with finite electrode segments lead to a nondimensional transverse impedance $\overline{R}_T$ and Hall voltage $\overline{V}_H$. The behavior of the impedance $\overline{R}_T$ for variable conductivity layers and a finite electrode segmentation $a/\ell = 0.5$, $\ell/h = 1$ as a function of β is shown in Fig. 3-24. Also shown for reference are the infinitely fine segmented and continuous electrode impedances. It can be seen that for large Hall parameters, the finite segmented impedance is bounded between the infinitely fine segmented impedance and the continuous electrode impedance. It should be noted that for low values of β, the continuous electrode impedance falls below the finite segmented impedance. This is because the need for segmentation to inhibit the Hall current

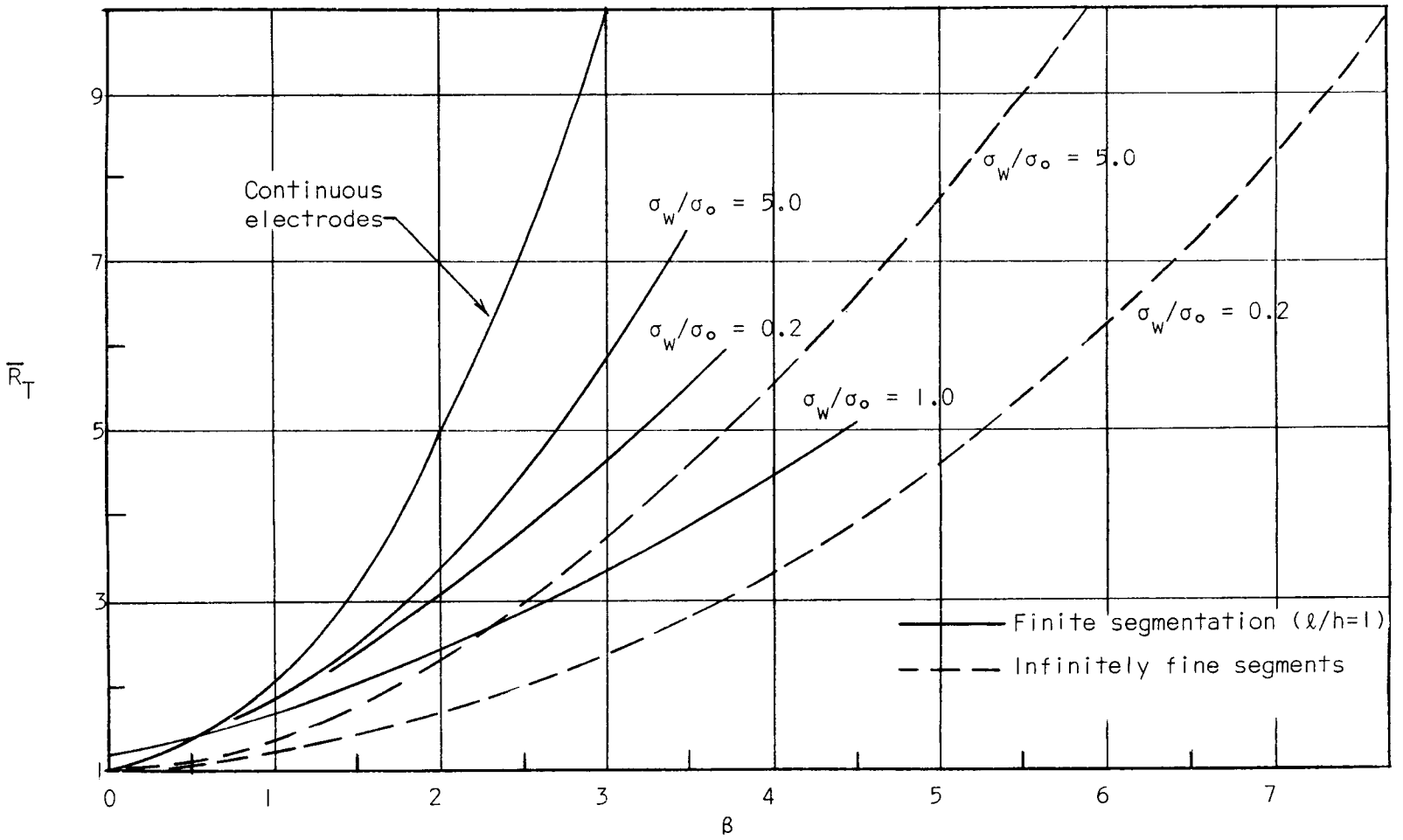

Fig. 3-24 Nondimensional transverse impedance $\overline{R}_T$ for finitely segmented electrodes with conductivity nonuniformity given by Eq. (3-23). Solid lines are finite segment results with $\ell/h = 1$, $a/\ell = .5$.

exist near the electrodes as would be expected for these low conductivity layers. With this larger value of the Hall parameter, the potential lines tend to approach a parallel distribution with respect to the current lines indicating that the current vector is tending to become normal to the electric field vector.

The distribution of potential along the insulator is shown in Fig. 3-23. The trends established for the potential distribution with $\beta = 1$ also persist with $\beta = 3$. Note that the maxima of the potential along the insulator shift towards the left edge of the lower electrode with low conductivity layers and towards the right edge with high conductivity layers. This result is due to the movement of the current dividing lines in those directions since the point of maximum potential on the insulator occurs at the "stagnation point" of the current dividing streamline.

All the foregoing layered model results with finite electrode segments lead to a nondimensional transverse impedance $\overline{R}_T$ and Hall voltage $\overline{V}_H$. The behavior of the impedance $\overline{R}_T$ for variable conductivity layers and a finite electrode segmentation $a/\ell = 0.5$, $\ell/h = 1$ as a function of β is shown in Fig. 3-24. Also shown for reference are the infinitely fine segmented and continuous electrode impedances. It can be seen that for large Hall parameters, the finite segmented impedance is bounded between the infinitely fine segmented impedance and the continuous electrode impedance. It should be noted that for low values of β, the continuous electrode impedance falls below the finite segmented impedance. This is because the need for segmentation to inhibit the Hall current

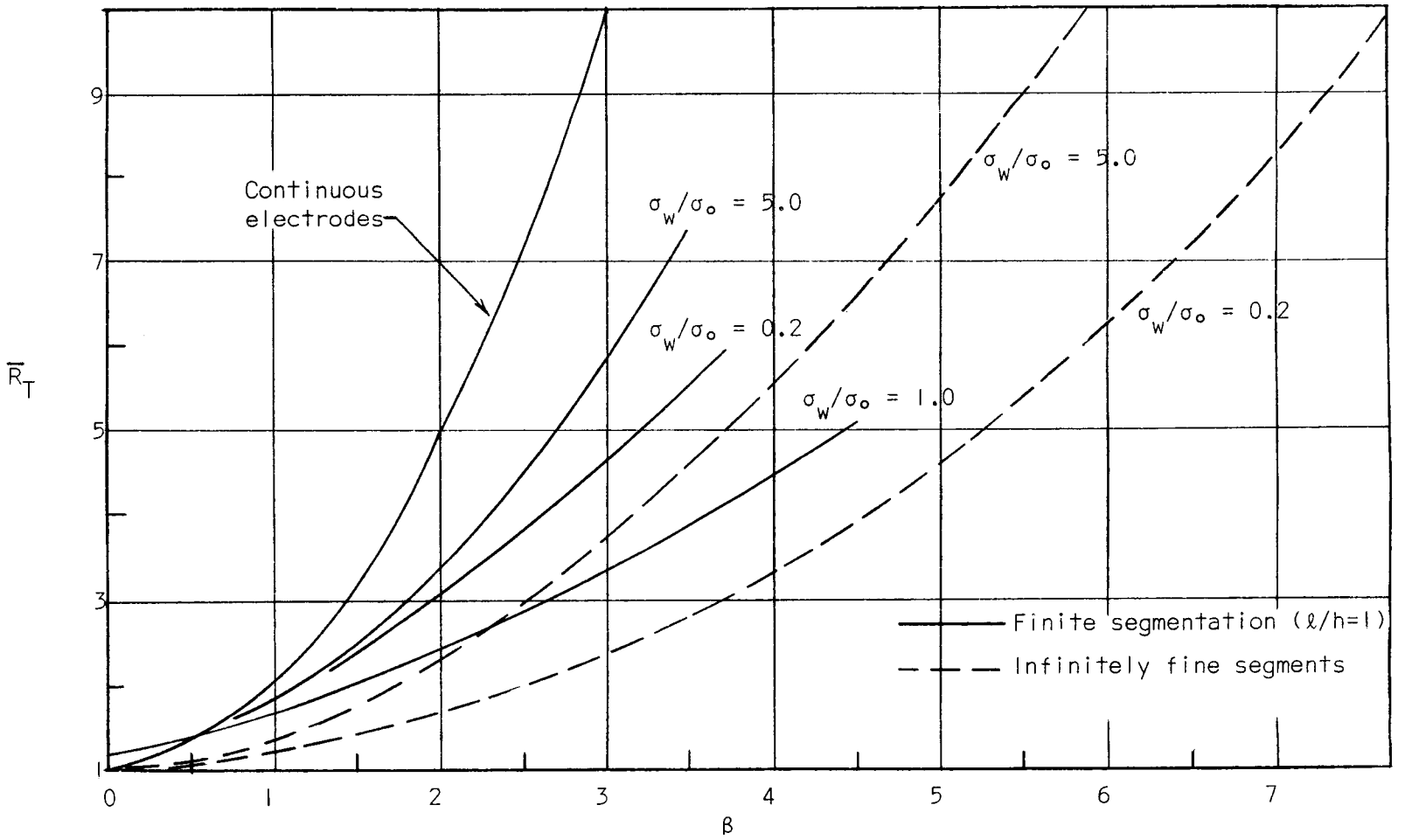

Fig. 3-24 Nondimensional transverse impedance $\bar{R}_T$ for finitely segmented electrodes with conductivity nonuniformity given by Eq. (3-23). Solid lines are finite segment results with $\ell/h = 1$, $a/\ell = .5$.

vanishes as β tends to zero. The finite coverage of the channel with finite segments at such low values of β then makes inefficient use of the full channel length and is thus detrimental to performance. In Fig. 3-25, the effect of variations in β on the nondimensional Hall voltage $\overline{V}_H$ is shown for various nonuniformities. The finite segmented Hall voltage can be seen to be depressed below the infinitely fine segmented value. In addition both finite and infinitely fine segmented performance is depressed by nonuniformities. This result emphasizes a general trend observed in all the calculations: geometrical nonuniformities (finite segmentation) and conductivity nonuniformities by themselves increase the internal impedance of the channel. Where both nonuniformity mechanisms occur simultaneously, they increase the impedance and depress the Hall voltage to a greater extent than could either nonuniformity mechanism by itself.

In Fig. 3-26 the variation of the transverse impedance $\overline{R}_T$ is shown as a function of the conductivity nonuniformity σ_w/σ_o for a fixed $\delta/h = 0.2$. It can be seen that the introduction of finite segments causes a greater increase in the internal impedance for small degress of nonuniformity than occurs at larger degrees of nonuniformity. This is because with strong nonuniformities, the effect of segmentation is virtually destroyed even if the segmentation is infinitely fine (cf. section 3.1.2). Thus, variations in segmentation with strong conductivity nonuniformities have little effect on performance. The nondimensional Hall voltage $\overline{V}_H$ is shown for these same cases in Fig. 3-27. It can be seen that the effect of finite segmentation is to reduce the Hall voltage below the ideal value for infinitely fine segmentation even with

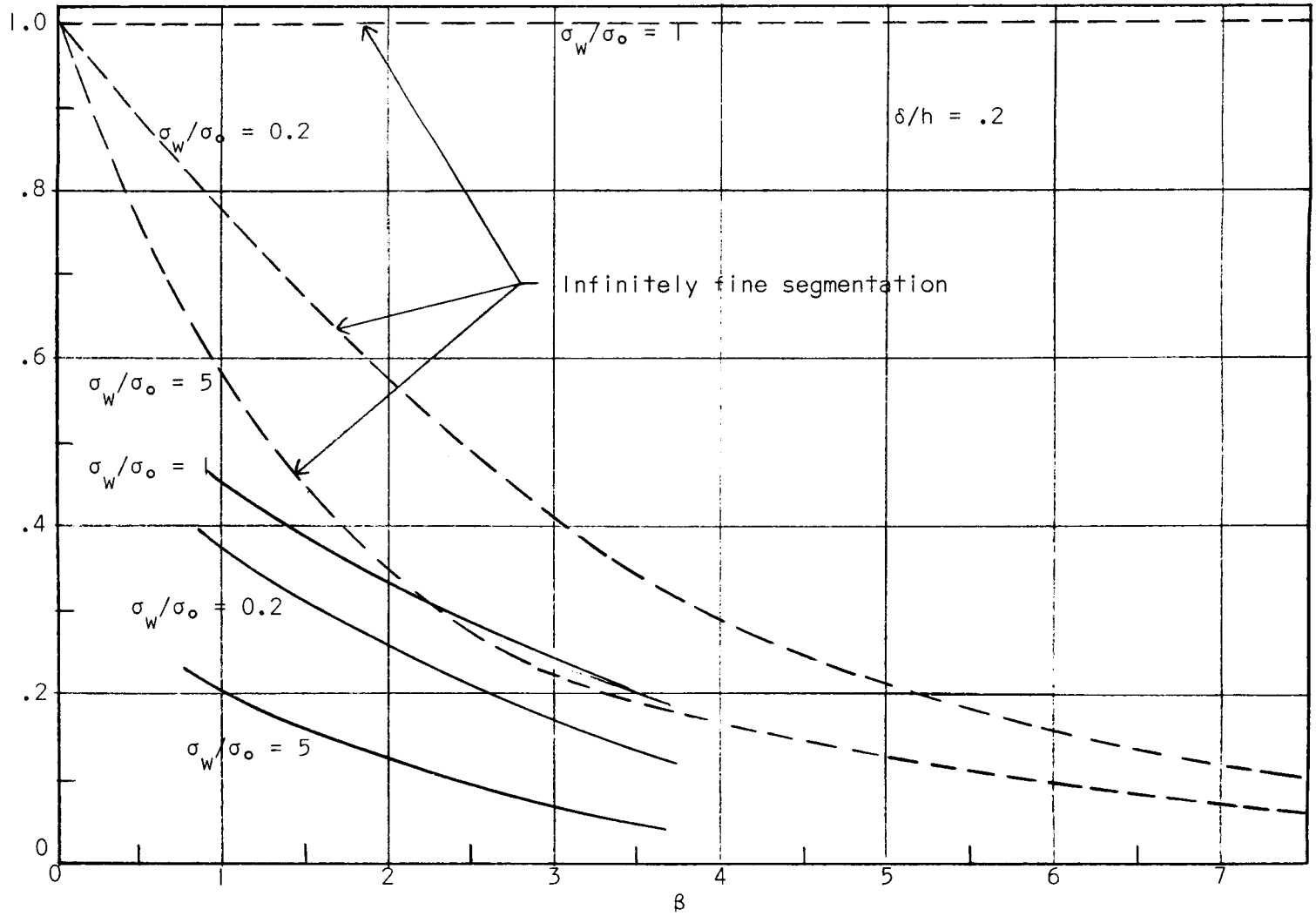

Fig. 3-25 Nondimensional Hall potential $\overline{V}_H$ for finitely segmented electrodes with conductivity nonuniformity given by Eq. (3-23). Solid lines are finite segment results with $\ell/h = 1$, $a/\ell = .5$.

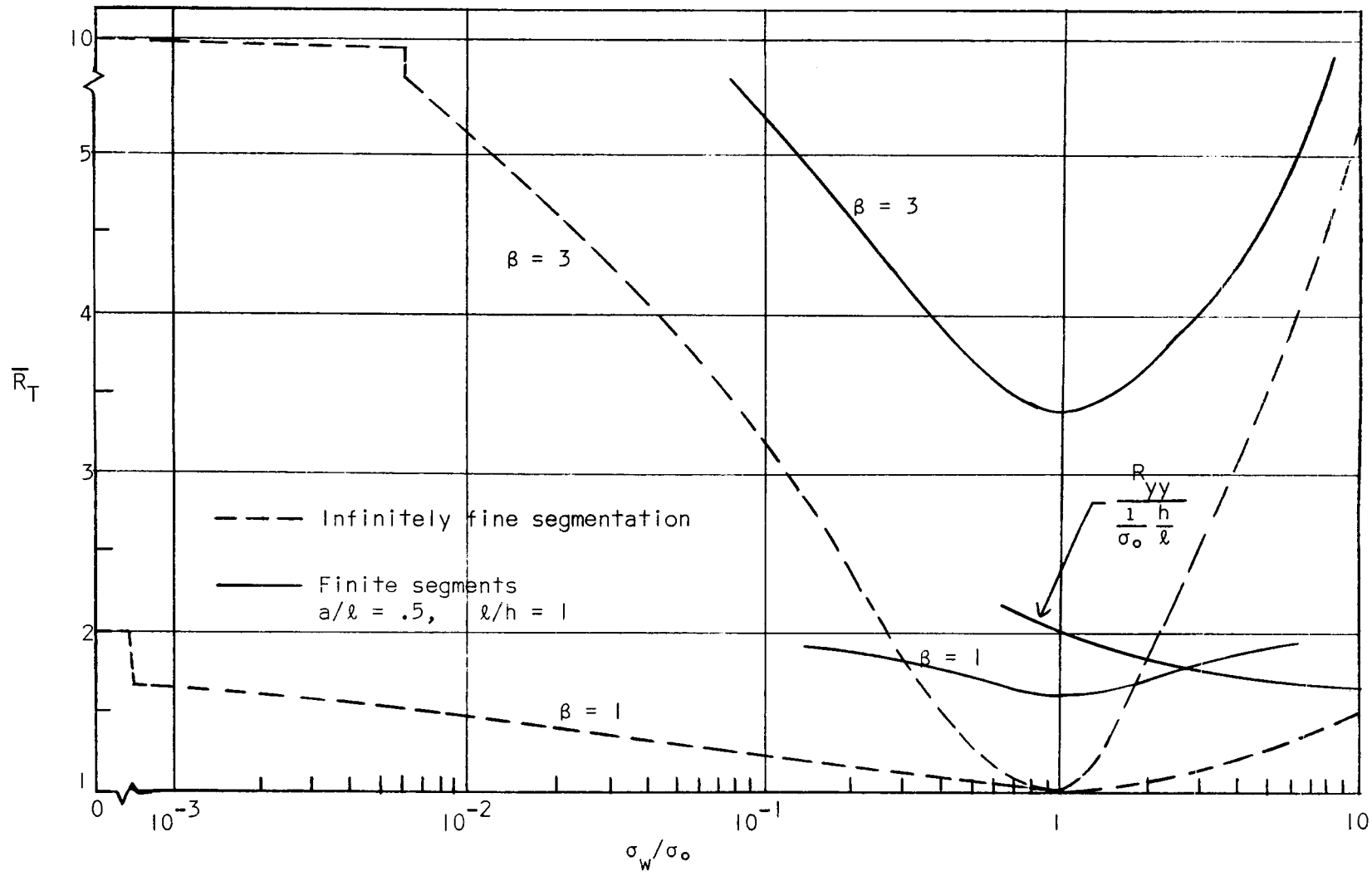

Fig. 3-26 Nondimensional transverse impedance $\overline{R}_T$ for finitely segmented electrode channel as a function of conductivity nonuniformity given by Eq. (3-23). Solid lines are finite segment results with ℓ/h = 1, a/ℓ = .5.

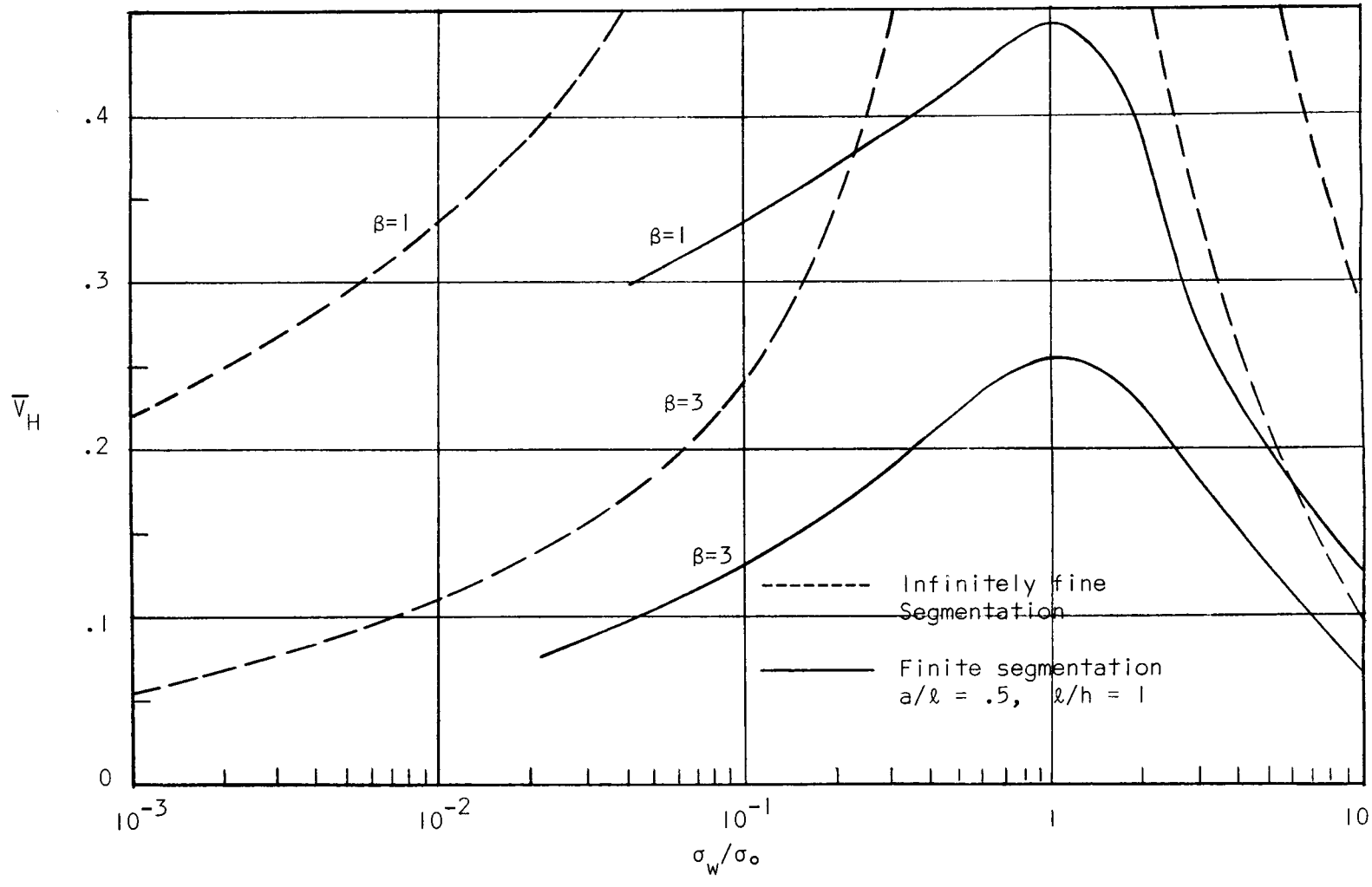

Fig. 3-27 Nondimensional Hall potential $\overline{V}_H$ for finitely segmented electrode channel as a function of conductivity nonuniformity given by Eq. (3-23). Solid lines are finite segment results with $\ell/h = 1$, $a/\ell = .5$.

uniform conductivity. The effect of nonuniformities with such finite segments is to further reduce the Hall voltage below the reduction due to finite segmentation alone.

3.2.3 Comparison with the measurements of Hoffman and Oates[29]

The electrode current distribution results shown in Fig. 3-9 for low conductivity layers with $\beta = 1$ may be compared with the measured distributions of Hoffman and Oates[29] which are also shown in Fig. 3-9. These investigators performed experiments on a finitely segmented channel with a potassium seeded argon flow. A center pair of electrodes in their channel was constructed with one of the electrodes divided into three parts but connected to a common bus. The current delivered to each part of the electrode could be measured so that the quantity $I(x)$ could be experimentally determined. The gas temperatures for the experiments were of the order of 1300° K and the cooled electrode walls were reported to range in temperature between 800° K and 1100° K. If the gas in the vicinity of the electrode wall was assumed to be at the reported electrode temperature and the electron concentration at the wall were assumed to be in equilibrium, a crude calculation which assumes a uniform mobility would yield $\sigma_w/\sigma_o \sim n_e^*(T_w)/n_e^*(T_o)$ where n_e^* is the equilibrium number density and T_w and T_o are the wall and core temperatures, respectively. For the reported values of T_w and T_o, the parameter σ_w/σ_o would be exceedingly small; however, it is not clear how closely the reported electrode temperature reflected the actual surface temperature of the electrodes. It may be qualitatively concluded, however, that the overall features of this experiment involved cooling near

the electrode walls which could be expected to give rise to a low conductivity layer over the electrodes.

The measured results shown in Fig. 3-9 indicate a considerably more uniform current distribution than that for a uniformly conducting gas. Although the finite emission and finite conduction characteristics of the electrode provide possible explanations for the more uniform current, the cool gas layer with a conductivity ratio of $\sigma_w/\sigma_o \lesssim .05$ also provides a plausible explanation of the experimental data. Conductivity nonuniformities may therefore play some role in the interpretation of current distribution measurements with Hall effects.

4. SOME THEORETICAL CONSIDERATIONS OF NONUNIFORM ELECTRICAL CONDUCTION WITH A NONEQUILIBRIUM CONDUCTIVITY

In this chapter consideration is given to the theoretical implications of the nonequilibrium conductivity model described in Section 2.3. The stability of uniform steady states according to this model is examined and the mathematical type of the steady state form of the equations is established.

4.1 Dynamic Instabilities in a Nonequipartition Magnetic Plasma

A study of certain aspects of the dynamic stability of a nonequipartition plasma in the presence of a magnetic field will now be undertaken. The motivation for this study is twofold. Firstly, steady state solutions of a nonuniform electrical conduction field with a nonequilibrium conductivity which are inherently unstable would not have steady state experimental counterparts of interest. Thus criteria which specify the stability of steady states governed by the nonequilibrium conductivity model of section 2.3 are required. Secondly, an important correspondence exists between the condition for stability of the nonsteady equations and the condition for uniform ellipticity of the steady equations. This correspondence will be discussed in section 4.3.

A general stability analysis of the conducting gas in a general nonuniform steady state would require inclusion of the full gas dynamic and electromagnetic equations. Such a treatment is beyond the scope of the present study. Instead, it will be assumed that the steady state

values of heavy species gas properties are little changed by the non-steady behavior of the electron number density and temperature and by the electric field and current.

A prerequisite to a systematic stability analysis is the solution of the steady state equations (2-7) through (2-10) subject to the boundary conditions discussed in chapter 2. Such solutions for finite sized electrodes, however, must be obtained numerically. It is therefore desirable to obtain information about the stability of a nonequipartition plasma in a magnetic field without solving the nonuniform steady state problem. This can be done to some degree by examining the stability of a steady state which is uniform in space. If such uniform steady states are found to be unstable, one would, in general, expect nonuniform steady states to be similarly unstable. The stability analysis presented here will therefore be restricted to uniform steady states.

Consideration is now directed to the region of the plasma where a uniform steady state exists. In this region a steady electric field $\vec{E}_o'$ is assumed to exist which produces a steady current $\vec{J}_o$ given by

$$\vec{J}_o = \overleftrightarrow{\sigma_o} \cdot \vec{E}_o'. \tag{4-1}$$

This current and field produce a local Joule heating which elevates the electron temperature to a value T_{e_o} according to Eqs. (2-30) and (2-31):

$$T_{e_o} = T + \gamma_{E_o}(\vec{E}_o')^2 = T + \gamma_{J_o}(\vec{J}_o)^2. \tag{4-2}$$

The electron number density which exists in this region is given by

$$n_{e_o} = n_e^*(T_{e_o}). \tag{4-3}$$

In the above, $\gamma_{E_o} \equiv \sigma_{\beta_o}/\theta_o n_{e_o}$, $\gamma_{J_o} \equiv 1/\sigma_o n_{e_o} \theta_o$, and a subscript "$_o$" indicates evaluation of the property in question at the state n_{e_o}, T_{e_o}.

The non-steady Eqs. (2-7), (2-8), (2-23), (2-24) are now expanded about the steady state described above as

$$\eta(x,y,t) = \eta_o + \eta'(x,y,t), \tag{4-4}$$

where η represents n_e, T_e, E_x' or E_y'. As implied by the expansion (4-4), the disturbances will be confined to the x,y plane. (The stability analysis may be carried out in either the field representation or the current representation; it is done here in the field representation.) The primed quantities may be viewed as small perturbations which are given to the steady state system. Since it is assumed that the heavy species properties of the gas are little influenced by the initial perturbations in the electron fluid properties, the state variables ρ, $\vec{u}$, T, ... maintain their steady state values as n_e, T_e, E_x', E_y' undergo perturbations about that steady state. The coefficients appearing in these equations which are functions of n_e, T_e, and $\vec{E}'$ are similarly expanded about the steady state; e.g., if η represents σ, σ_β, β, etc.,

$$\eta = \eta_o + \frac{\partial \eta}{\partial T_e} T_e' + \frac{\partial \eta}{\partial n_e} n_e'. \tag{4-5}$$

The stability analysis proceeds by substituting the forms (4-4) and (4-5) into the non-steady equations and neglecting terms involving prod-

ucts of the primed quantities. There results a linear system of equations in n_e', T_e', E_x'' , E_y'' .

The perturbation functions n_e', T_e', E_x'', E_y'' are assumed to possess Fourier decompositions for which typical components are

$$\eta' = \hat{\eta}\, e^{i(-\omega t + K_x x + K_y y)}, \tag{4-6}$$

where η again represents n_e, T_e, E_x', or E_y'. The Fourier amplitudes are denoted by "^". The frequency of the Fourier components is ω, and K_x, K_y are the components of the wave number $\vec{K}$. When the Fourier components (4-6) are substituted into the system of non-steady equations, there results a linear homogeneous algebraic system. The condition for non-trivial solutions leads to a dispersion relationship between ω and K_x, K_y. If the dispersion condition admits complex frequencies ω with positive imaginary parts for real $\vec{K}$, the perturbations grow in time and the equations are therefore said to be unstable.

Before proceeding with the substitution of the Fourier components, it is useful to nondimensionalize the non-steady equations which have been expanded in terms of the perturbation quantities n_e', T_e', E_x'', E_y'' . For this purpose, characteristic dimensional quantities are n_{e_o}, T_{e_o}, $E_o' = |\vec{E}_o'|$. A characteristic length is selected as $K^{-1} \equiv 1/\sqrt{K_x^2 + K_y^2}$ and a characteristic time as ω_r^{-1}, where ω_r is the real part of ω. Nondimensional quantities are then defined as

$$\bar{n}_e' \equiv n_e'/n_{e_o}, \qquad \bar{T}_e' \equiv T_e'/T_{e_o},$$

$$\bar{E}_x'' \equiv E_x''/E_o', \qquad \bar{E}_y'' \equiv E_y''/E_o',$$

$$\bar{x} \equiv xK, \qquad \bar{y} \equiv yK, \qquad \bar{t} \equiv t\omega_r,$$

$$\bar{K}_x \equiv K_x/K, \qquad \bar{K}_y \equiv K_y/K.$$

The non-steady equations in nondimensional form [Eqs. (2-7), (2-8), (2-30) and (2-31)] with $\vec{u}$ directed parallel to the x axis are then

Electron continuity:

$$\tau_i \left[\omega_r \frac{\partial}{\partial \bar{t}} + uK \frac{\partial}{\partial \bar{x}}\right] \bar{n}_e' - 2\left[\frac{\partial \bar{n}_e^*}{\partial \bar{T}_e} \bar{T}_e' - \bar{n}_e'\right] = 0, \qquad (4\text{-}7)$$

Electron energy:

$$\begin{aligned}
&\tau_e \left\{\left[\omega_r \frac{\partial}{\partial \bar{t}} + uK \frac{\partial}{\partial \bar{x}}\right]\left[\bar{\varepsilon}\, \bar{n}_e' + \bar{T}_e'\right] - (\ell_d K)\left[(\cos\delta + \right.\right. \\
&+ \beta_o \sin\delta) \frac{\partial \bar{n}_e'}{\partial \bar{x}} - (\sin\delta - \beta_o \cos\delta) \frac{\partial \bar{n}_e'}{\partial \bar{y}} + \\
&+ \frac{7}{2}(\cos\delta - \beta_o \sin\delta) \frac{\partial \bar{T}_e'}{\partial \bar{x}} + \frac{7}{2}(\beta_o \cos\delta + \\
&\left.\left. + \sin\delta) \frac{\partial \bar{T}_e'}{\partial \bar{y}}\right]\right\} - \omega_E \left[2(\cos\delta\, \bar{E}_x'' + \sin\delta\, \bar{E}_y'') + \right. \\
&\left. + \frac{\partial\, \ell n\, \gamma_{E_o}}{\partial \bar{n}_e} \bar{n}_e'\right] + \bar{T}_e' - (\ell q K)^2\, \bar{\nabla}^2\, \bar{T}_e',
\end{aligned} \qquad (4\text{-}8)$$

Current conservation:

$$\frac{\partial \bar{E}_x''}{\partial \bar{x}} + \frac{\partial \bar{E}_y''}{\partial \bar{y}} + (\ell_d K)\,\bar{\nabla}^2\,(\bar{n}_e' + \bar{T}_e') + \bar{F}_E(\bar{n}_e)\frac{\partial \bar{n}_e'}{\partial \bar{x}} + \bar{G}_E(\bar{n}_e)\frac{\partial \bar{n}_e'}{\partial \bar{y}} + \bar{F}_E(\bar{T}_e)\frac{\partial \bar{T}_e'}{\partial \bar{x}} + \bar{G}_E(\bar{T}_e)\frac{\partial \bar{T}_e'}{\partial \bar{y}} = 0, \tag{4-9}$$

Maxwell Faraday:

$$\frac{\partial \bar{E}_x''}{\partial \bar{y}} - \frac{\partial \bar{E}_y''}{\partial \bar{x}} = 0. \tag{4-10}$$

In the above equations,

$$\delta \equiv \tan^{-1}(E_y'/E_x'), \tag{4-11}$$

$$\tau_i \equiv 1/\alpha\, n_e^2, \tag{4-12}$$

$$\bar{\varepsilon} \equiv 1 + 2\varepsilon_i/3kT_e, \tag{4-13}$$

$$\omega_E \equiv (T_e/T-1)f_E, \tag{4-14}$$

$$\tau_e \equiv \frac{1}{\sum_j \frac{m_e}{m_j}\nu_{ej}}\, f_E, \tag{4-15}$$

$$\ell_d \equiv \frac{k(T_{e_o} - T)}{eE'}\, f_E \tag{4-16}$$

$$\ell_q^2 \equiv \frac{\lambda_e}{(1+\beta^2)\theta n_e} f_E, \tag{4-17}$$

where

$$f_E \equiv \frac{1}{1 - \gamma_E E'^2 \dfrac{\partial \ell n\, \gamma_E}{\partial T_e}}. \tag{4-18}$$

It is to be understood that the quantities defined in Eqs. (4-11) through (4-18) are to be evaluated at the steady state n_{e_o}, T_{e_o}, $\vec{E}_o'$ when used in Eqs. (4-7) through (4-9).

The nondimensional $\overline{F}_E$, $\overline{G}_E$ are obtained by nondimensionalizing F_E, G_E given by Eqs. (2-23) on E_o', n_{e_o}, and T_{e_o}. The operator $\overline{\nabla}^2$ represents the Laplacian nondimensionalized on h. It is to be noted that the time τ_e is proportional to the equipartition time between the electrons and the heavy species. Terms proportional to ℓ_d represent heat conduction and diffusion due to electron pressure gradients. Terms proportional to ℓ_q represent temperature gradient induced heat conduction in the electron fluid.

The Fourier components (4-6) may be substituted into Eqs. (4-7) through (4-10). In terms of the nondimensional frequency

$$\overline{\nu} \equiv -\overline{\omega} + \overline{K}_x \overline{x}$$

there results the following linear, homogeneous, algebraic system:

$$\begin{bmatrix} i\tau_i\omega_r\bar{\nu} + 2 & -2\dfrac{\partial \bar{n}_e^*}{\partial \bar{T}_e} & 0 & 0 \\ A & B & -2\omega_E \cos\delta & -2\omega_E \sin\delta \\ C & D & i\bar{K}_x & i\bar{K}_y \\ 0 & 0 & i\bar{K}_y & -i\bar{K}_x \end{bmatrix} \begin{Bmatrix} \hat{n}_e \\ \hat{T}_e \\ \hat{E}_x \\ \hat{E}_y \end{Bmatrix} = 0,$$

where

$$A = i\bar{\varepsilon}_o(\tau_e\omega_r\bar{\nu} - K\ell_d\Lambda_d^+) - \omega_E \frac{\partial\, \ell n\, \gamma_{E_o}}{\partial \bar{n}_e},$$

$$B = i(\tau_e\omega_r\bar{\nu} - \tfrac{7}{2}K\ell_d\Lambda_d^-) + (1 + \ell_q{}^2K^2),$$

$$C = -K\ell_d + i[\bar{F}_E(\bar{n}_e)\bar{K}_x + \bar{G}_E(\bar{n}_e)\bar{K}_y],$$

$$D = -K\ell_d + i[\bar{F}_E(\bar{T}_e)\bar{K}_x + \bar{G}_E(\bar{T}_e)\bar{K}_y],$$

and

$$\Lambda_d^+ \equiv \bar{K}_x(\cos\delta + \beta_o \sin\delta) + \bar{K}_y(-\beta_o\cos\delta + \sin\delta),$$

$$\Lambda_d^- \equiv \bar{K}_x(\cos\delta - \beta_o \sin\delta) + \bar{K}_y(\beta_o \cos\delta + \sin\delta).$$

The dispersion relationship follows by requiring that the determinant of the coefficient matrix vanish for nontrivial solutions. The result is the quadratic

$$a\bar{\nu}^2 + 2b\bar{\nu} + c = 0, \tag{4-19}$$

where

$$a = (\tau_i\omega_r)(\tau_e\omega_r), \tag{4-20}$$

$$b = -i\left[\frac{(\tau_i\omega_r)}{2}Q_{T_e} + (\tau_e\omega_r)\left(1 + \bar{\varepsilon}_o\frac{\partial\bar{n}_e^*}{\partial\bar{T}_e}\right)\right] - \frac{7}{4}K\ell_d\bar{\Lambda}_d, \tag{4-21}$$

$$c = -2Q + i(K\ell_d)\left[\frac{5}{2}\bar{\Lambda}_d + 2\frac{\partial\bar{n}_e^*}{\partial\bar{T}_e}\bar{\varepsilon}_o\Lambda_d^+ - 2\omega_E(\bar{K}_x\cos\delta + \bar{K}_y\sin\delta)\right]. \tag{4-22}$$

The functions Q_{T_e}, Q_{n_e} are quadratic forms in $\bar{K}_x$, $\bar{K}_y$:

$$Q_\eta = A_\eta\bar{K}_x^2 + 2B_\eta\bar{K}_x\bar{K}_y + C_\eta\bar{K}_y^2, \tag{4-23}$$

where η stands for either T_e or n_e. With the definition of a logarithmic derivative operator Δ_η,

$$\Delta_\eta(\ ) \equiv \eta_o\frac{\partial\ \ell n\ (\ )}{\partial\eta}, \tag{4-24}$$

the coefficients in Eqs. (4-23) are

$$\left.\begin{matrix}A_\eta\\C_\eta\end{matrix}\right\} = \theta_\eta + 2\omega_E\left[\Delta_\eta(\sigma_\beta)\left\{\begin{matrix}\cos^2\delta\\\sin^2\delta\end{matrix}\right\} \pm \beta_o[\Delta_\eta(\sigma_\beta) + \Delta_\eta(\beta)]\cos\delta\sin\delta\right], \tag{4-25}$$

$$B_\eta = 2\omega_E\{\Delta_\eta(\sigma_\beta)\cos\delta\sin\delta + \frac{\beta_o}{2}[\Delta_\eta(\sigma_\beta) + \Delta_\eta(\beta)]\ (\cos^2\delta - \sin^2\delta)\}$$

where

$$\theta_{T_e} \equiv 1 + \ell_q^2 K^2,$$
$$\theta_{n_e} \equiv -\omega_E \frac{\partial \ell n \gamma_{E_o}}{\partial \bar{n}_e}. \tag{4-26}$$

The quadratic form Q is defined as

$$Q \equiv Q_{T_e} + \left(\frac{\partial \bar{n}_e^*}{\partial \bar{T}_e}\right) Q_{n_e}.$$

The conditions for negligible heat conduction and diffusion are $(\ell_q K) << 1$ and $(\ell_d K) << 1$. In what follows, these effects will be neglected, and the effects of finite rates of ionization will be considered. (Some of the consequences of heat conduction and diffusion have been examined by Kerrebrock [22], while Dethlefson and Kerrebrock[31] consider the case of stability with Saha equilibrium.) For this case, Eqs. (4-20) through (4-22) reduce to

$$a = (\tau_i \omega_r)(\tau_e \omega_r), \tag{4-27}$$

$$b = -i\left[\frac{\tau_i \omega_r Q_{T_e}}{2} + \tau_e \omega_r \left(1 + \bar{\varepsilon}_o \frac{\partial \bar{n}_e^*}{\partial \bar{T}_e}\right)\right], \tag{4-28}$$

$$c = -2Q. \tag{4-29}$$

The solution for $\bar{\nu}$ is

$$\bar{\nu} = -i \frac{b_i \pm \sqrt{b_i^2 + ac}}{a},$$

where $b_i \equiv \mathrm{Im}(b)$. Since $\bar{\nu} = -\bar{\omega} + \bar{K}_x \bar{x}$ it follows that for $b_i^2 + ac > 0$,

$$\frac{\omega_i}{\omega_r} = \frac{b_i \pm \sqrt{b_i^2 + ac}}{a} . \tag{4-30}$$

Since it is true that a is always positive, it follows that for $c > 0$, there is always one root for which ω_i is positive; hence for stability ($\omega_i < 0$), it is required that $b_i < 0$ and $c < 0$. On the other hand, if $b_i^2 + ac < 0$, it follows that

$$\bar{\nu} = -i \frac{b_i \pm i \sqrt{|b_i^2 + ac|}}{a} ,$$

and

$$\frac{\omega_i}{\omega_r} = \frac{b_i}{a} . \tag{4-31}$$

The condition for stability is again $b_i < 0$. The stability conditions are thus, from Eqs. (4-28) and (4-29),

$$\frac{\tau_i \omega_r Q_{T_e}}{2} + \tau_e \omega_r \left(1 + \bar{\varepsilon}_o \frac{\partial \bar{n}_e^*}{\partial \bar{T}_e} \right) > 0, \tag{4-32}$$

$$Q > 0.$$

The quadratic form Q may be expressed as

$$Q = A\bar{K}_x^2 + 2B\bar{K}_x\bar{K}_y + C\bar{K}_y^2, \tag{4-33}$$

where

$$A = A_{T_e} + \frac{\partial \bar{n}_e^*}{\partial \bar{T}_e} A_{n_e}, \tag{4-34}$$

and similarly for B and C. The stability condition requires that the quadratic form Q be positive definite. It follows that this will be the case for all $\bar{K}_x$, $\bar{K}_y$ if

$$AC - B^2 > 0. \tag{4-35}$$

In terms of the operator

$$\Delta_*( ) \equiv \Delta_{T_e}( ) + \frac{\partial\, \ell n\, \bar{n}_e^*}{\partial \bar{T}_e} \Delta_{n_e}( ), \tag{4-36}$$

and the definition

$$\lambda_E \equiv \frac{2\omega_E}{\omega_E + f_E}, \tag{4-37}$$

the condition (4-35) may be written as

$$1 + \lambda_E \Delta_*(\sigma_\beta) - \left(\frac{\lambda_E \beta}{2}\right)^2 [\Delta_*(\sigma_\beta) + \Delta_*(\beta)]^2 > 0. \tag{4-38}$$

The above inequality may be rearranged to yield

$$\beta^2 < 4\frac{1 + \lambda_E\Delta_*(\sigma_\beta)}{\lambda_E{}^2[\Delta_*(\sigma_\beta) + \Delta_*(\beta)]^2} . \qquad (4\text{-}39)$$

When the mobility μ is uniform, $\Delta_*(\sigma_\beta) = \Delta_*(\sigma)$ and $\Delta_*(\beta) = 0$. The inequality (4-39) then becomes an explicit inequality for β. This condition contains the stability criterion of Dethlefson and Kerrebrock[31] as a special case. The instability which arises when the inequality (4-39) is violated has been termed an "electro-thermal" instability by Kerrebrock.[22]

As an illustration, assume that the mobility μ and energy exchange coefficient θ are weak functions of the electron temperature so that $\Delta_*(\beta) = 0$ and

$$\Delta_*(\sigma_\beta) = \frac{\partial\, \ell n\, \bar{n}_e{}^*}{\partial \bar{T}_e} . \qquad (4\text{-}40)$$

From the Saha equation (2-22) and the energy equation (4-2) it may readily be shown that for these assumptions $\lambda_E\Delta_*(\sigma_\beta)$ is always less than $\varepsilon_i/4kT_{e_o}$, where ε_i is the energy required to singly ionize an s species atom. The right hand side of the inequality (4-39) is a monotonically decreasing function of $\lambda_E\Delta_*(\sigma_\beta)$. Inserting the maximum $\lambda_E\Delta_*(\sigma_\beta) = \varepsilon_i/4kT_{e_o}$ into (4-39), the condition for stability becomes

$$\beta^2 < 4\,\frac{1 + \varepsilon_i/4kT_{e_o}}{(\varepsilon_i/4kT_{e_o})^2} . \qquad (4\text{-}41)$$

In the absence of a magnetic field, the inequality (4-41) is always

satisfied. In the absence of nonequipartition heating, $\lambda_E = 0$, and according to inequality (4-39) stability again prevails. Thus, with uniform mobility and energy exchange coefficient θ, instabilities may develop only with the simultaneous occurrence of the Hall effect and nonequipartition heating. If either of these effects is absent, the equations are stable. The inequality (4-41) places rather severe restrictions on β. For an alkali metal such as cesium or potassium at a gas temperature of 2000°K, $\varepsilon_i/4kT_{e_o} \sim 5$, and the inequality (4-41) therefore requires $\beta^2 < 24/25$.

From the solutions of (4-19) the growth rate of the disturbance is determined from

$$\frac{\omega_i}{\omega_r} = \frac{b_i \pm \sqrt{b_i^2 + ac}}{a}, \tag{4-42}$$

or

$$\omega_i = -\frac{(a_i\tau_i + a_e\tau_e)\left[1 \pm \sqrt{1 - \dfrac{2Q\tau_i\tau_e}{(a_i\tau_i + a_e\tau_e)^2}}\right]}{\tau_i\tau_e}, \tag{4-43}$$

where

$$a_i \equiv Q_{T_e}/2, \qquad a_e \equiv 1 + \bar{\varepsilon}_o \frac{\partial \bar{n}_e^*}{\partial \bar{T}_e}. \tag{4-44}$$

Near the equilibrium limit ($\tau_i \ll \tau_e$) the growth rate becomes

$$\omega_i \to -\frac{Q}{a_e\tau_e}$$

and the growth time $\tau = \omega_i^{-1}$ becomes

$$\tau \rightarrow -\left(\frac{a_e}{Q}\right)\tau_e \ . \tag{4-45}$$

The growth time is thus proportional to the effective energy transfer time τ_e. Near the frozen limit ($\tau_i >> \tau_e$)

$$\omega_i \rightarrow -\frac{Q}{a_i \tau_i} \ .$$

The growth time $\tau = \omega_i^{-1}$ in this limit is thus proportional to the ionization time τ_i:

$$\tau \rightarrow -\frac{a_i \tau_i}{Q} \ . \tag{4-46}$$

It can be seen that the controlling growth time is the longer of τ_i and τ_e and that the damping or growth of the disturbance is controlled by the sign of the quadratic form Q. (It should be noted that the coefficient a_e is always positive and that the coefficient a_i, which involves the quadratic form Q_{T_e} will generally be positive; indeed, if the mobility μ is assumed independent of electron temperature and if electron heat conduction effects are negligible, $Q_{T_e} = 1$.)

4.2 Static Instabilities in a Nonequipartition Plasma

It can be seen from Eq. (4-12) that the conductivity gradients tend to become infinite if

$$\gamma_E E'^2 \left(\frac{\partial \ell n\, \gamma_E}{\partial T_e}\right)_{\rho,T,\ldots,n_e} = 1. \qquad (4\text{-}47)$$

This condition is indicative of a phenomenon which Kerrebrock[1] has described as a "static instability". Physically, such an instability may appear when an increase in the temperature of the electrons causes the energy transfer to the heavy species in the gas to become less efficient. (This may occur for example if the average electron-heavy particle collision cross section decreases with an increase in the electron temperature. Thus, the electron temperature continues to rise as the collisional energy loss rate to the heavy species decreases.)

Since $E'^2\gamma_E = T_e - T$ is a positive quantity, the static instability may occur only if $(\partial\, \ell n\, \gamma_E/\partial T_e)_{\rho,T,\ldots,n_e}$ is positive. A sufficient condition for static stability of the conducting gas is then

$$(T_e - T)\left(\frac{\partial \ell n\, \gamma_E}{\partial T_e}\right)_{\rho,T,\ldots,n_e} < 1. \qquad (4\text{-}48)$$

As an illustration, assume that the momentum and energy transfer from the electron fluid are dominated by elastic collisions with a single heavy species which is denoted by a subscript ℓ. According to Eq. (2-33) the energy exchange coefficient is proportional to $\nu_{e\ell}$; thus $\gamma_E = \sigma_\beta/\theta n_e$ is proportional to $\nu_{e\ell}^{-2}$. To a good approximation, the collision frequency $\nu_{e\ell}$ may be expressed as $\nu_{e\ell} = n_e Q_{e\ell} \overline{C}_e$, where $\overline{C}_e$ is the electron mean thermal speed and $Q_{e\ell}$ is an average momentum transfer cross section. Since $\overline{C}_e$ is proportional to $T_e^{\frac{1}{2}}$, it can be seen that γ_E is proportional

to $Q_{e\ell}^{-2}T_e^{-1}$, and thus it follows that

$$\left(\frac{\partial\ \ell n\ \gamma_E}{\partial T_e}\right)_{\rho,T,\ldots,n_e} = -2\frac{\partial\ \ell n\ Q_{e\ell}}{\partial T_e} - \frac{1}{T_e}\ .$$

If the cross section increases with T_e for all T_e, the conducting gas is statically stable; on the other hand, if the cross section decreases with T_e, the gas is statically stable if

$$\left(-2T_e\frac{\partial\ \ell n\ Q_{e\ell}}{\partial T_e} - 2\right)T_e < \left(-2T_e\frac{\partial\ \ell n\ Q_{e\ell}}{\partial T_e} - 1\right)T.$$

In particular, if the heavy species considered is the ion fluid, where Q_{ei} is proportional to T_e^{-2}, the above condition becomes $T_e/T < 3/2$.

4.3 Type of the Steady Equations

An analysis of the type of the steady equations governing nonuniform conduction with a nonequilibrium conductivity is now presented. Such an analysis of type of the steady equations will bear upon the method of solution employed and the proper specification of boundary conditions.

The steady equations for the linear channel geometry described in chapter 2 are now considered. Attention is restricted to the case with negligible pressure gradient induced diffusion of charge and a velocity $\vec{u}$ directed parallel to the x axis.

To facilitate the examination of type, a matrix notation will be employed. Let the vector w_j have components (n_e, T_e, E_x', E_y'). Then

Eqs. (2-30), (2-31), (2-21), and (2-8) with the time derivative set equal to zero may be compactly written as

$$A_{ij} \frac{\partial w_j}{\partial x} + B_{ij} \frac{\partial w_j}{\partial y} + C_i = 0, \tag{4-49}$$

where a repeated subscript implies summation. The coefficient matrices A_{ij}, B_{ij} and the vector C_i in the field representation are

$$A_{ij} = \begin{pmatrix} u & 0 & 0 & 0 \\ (\frac{3}{2}kT_e + \varepsilon_i)u & \frac{3}{2}kn_e u & 0 & 0 \\ F_E(n_e) & F_E(T_e) & 1 & 0 \\ 0 & 0 & 0 & -1 \end{pmatrix}, \tag{4-50}$$

$$B_{ij} = \begin{pmatrix} 0 & 0 & 0 & 0 \\ 0 & 0 & 0 & 0 \\ G_E(n_e) & G_E(T_e) & 0 & 1 \\ 0 & 0 & 1 & 0 \end{pmatrix}, \tag{4-51}$$

$$C_i = \begin{pmatrix} \alpha n_e(n_e{}^{*2} - n_e{}^2) \\ \theta n_e(T_e - T) - \sigma_\beta (E')^2 \\ \Gamma_E \\ 0 \end{pmatrix}. \tag{4-52}$$

The type analysis of the system (4-49) proceeds (see, for example, Courant and Hilbert,[32] p. 176-177) by forming the matrix

$$A_{ij} - \lambda B_{ij} \tag{4-53}$$

and determining the characteristic directions λ from the condition

$$\mathrm{Det}(A_{ij} - \lambda B_{ij}) = 0. \tag{4-54}$$

If there are p distinct real values of λ which satisfy Eq. (4-54), where p is the number of components of w_j, the system is said to be *totally hyperbolic.* If there are p non-real values of λ which satisfy Eq. (4-54) the system is said to be *elliptic.* If the polynomial (4-54) for λ is of order less than p, the system is said to be *parabolic.* Using the forms for A_{ij}, B_{ij} given by Eqs. (4-50) and (4-51), the condition for λ is

$$u_o^2 \frac{3}{2} k n_{e_o} (1 + \lambda^2) = 0,$$

which is degenerate in λ. The system is therefore parabolic.

The case in which the convective term $u\partial n_e/\partial x$ is negligible in the energy equation is examined next. For this case, the energy equation may be written as

$$T_e = T + \gamma_E (E')^2. \tag{4-55}$$

Since the energy equation is now purely algebraic, the derivatives of T_e may be calculated in terms of the derivative of E'. Using Eq. (4-55) and observing that γ_E is a function of T_e, there results for the deriva-

tive of T_e (for $\xi = x$ or y)

$$\frac{\partial T_e}{\partial \xi} = \frac{2\gamma_E}{1 - \gamma_E (E')^2 \frac{\partial \ell n\, \gamma_E}{\partial T_e}} \left(E_x' \frac{\partial E_x'}{\partial \xi} + E_y' \frac{\partial E_y'}{\partial \xi} \right). \quad (4\text{-}56)$$

In the matrix formulation, w_j reduces to $w_j = (n_e, E_x', E_y')$ and the coefficients A_{ij}, B_{ij} become

$$A_{ij} = \begin{pmatrix} u & 0 & 0 \\ F_E(n_e) & 1 + \lambda_E \bar{F}_E(\bar{T}_e)\cos\delta & \lambda_E \bar{F}_E(\bar{T}_e)\sin\delta \\ 0 & 0 & -1 \end{pmatrix}, \quad (4\text{-}57)$$

$$B_{ij} = \begin{pmatrix} 0 & 0 & 0 \\ G_E(n_e) & \lambda_E \bar{G}_E(\bar{T}_e)\cos\delta & 1 + \lambda_E \bar{G}_E(\bar{T}_e)\sin\delta \\ 0 & 1 & 0 \end{pmatrix}, \quad (4\text{-}58)$$

$$C_i = \begin{pmatrix} \alpha n_e (n_e^{*2} - n_e^2) \\ \Gamma_E \\ 0 \end{pmatrix}. \quad (4\text{-}59)$$

In the above, δ and λ_E are defined in Eqs. (4-11) and (4-37). The condition (4-54) is now

$$a\lambda^2 + 2b\lambda + c = 0, \tag{4-60}$$

where

$$a = -[1 + \lambda_E \bar{G}_E(\bar{T}_e)\sin\delta],$$

$$b = \frac{1}{2}\lambda_E[\sin\delta\ \bar{F}_E(\bar{T}_e) + \cos\delta\ \bar{G}_E(\bar{T}_e)], \tag{4-61}$$

$$c = -[1 + \lambda_E \bar{F}_E(\bar{T}_e)\cos\delta].$$

This condition is degenerate in λ; hence, the system is again parabolic.

The case in which the convection effect in the electron continuity equation is negligible as well as the convection effect in the energy equation is now examined. The electron continuity equation reduces to the Saha equation (2-29) and thus

$$\frac{\partial n_e}{\partial \xi} = \frac{\partial n_e^*(T_e)}{\partial T_e}\frac{\partial T_e}{\partial \xi}. \tag{4-63}$$

The vector w_j is now $w_j = (E_x', E_y')$ and the coefficients are the same as those in the lower right hand corner of (4-57) and (4-58) with $\bar{F}_E$ and $\bar{G}_E$ replaced by $\bar{F}_E^*(\bar{T}_e)$, $\bar{G}_E^*(\bar{T}_e)$, where

$$\bar{F}_E^*(\bar{T}_e) = \bar{F}_E(\bar{T}_e) + \bar{F}_E(\bar{n}_e)\frac{\partial \bar{n}_e^*}{\partial \bar{T}_e}, \tag{4-64}$$

and similarly for $\bar{G}_E^*$. The characteristic directions λ for this system are determined by Eq. (4-60) where the a,b,c, are given by (4-61) with

$\overline{F}_E$, $\overline{G}_E$ replaced by $\overline{F}_E^*(\overline{T}_e)$, $\overline{G}_E^*(\overline{T}_e)$. The system is no longer degenerate in λ. The solutions for λ are real if

$$b^2 - ac > 0. \tag{4-65}$$

This condition is

$$b^2 - ac = -\{1 + \lambda_E \Delta_*(\sigma_\beta) - (\tfrac{1}{2}\lambda_E \beta)^2 [\Delta_*(\sigma_\beta) + \Delta_*(\beta)]\} > 0, \tag{4-66}$$

where the operator Δ_* is defined by Eq. (4-36).

In this case, in which the electrons are in ionization equilibrium at the local electron temperature, the Maxwell-Faraday, current conservation, and Ohm's Law equations may be compacted into a single second-order equation. This may be done in either the field or current representation by introducing the potential and flux functions Φ', ψ [Eqs. (2-5) and (2-6)]. The quasi-linear second-order operator L_E may be defined as

$$L_E \equiv A_E \frac{\partial^2}{\partial x^2} + 2B_E \frac{\partial^2}{\partial x \partial y} + C_E \frac{\partial^2}{\partial y^2} + D_E \frac{\partial}{\partial x} + E_E \frac{\partial}{\partial y}. \tag{4-67}$$

The system (4-49) may then be written as

$$L_E(\Phi') = 0, \tag{4-68}$$

where

$$\left.\begin{matrix} A_E \\ C_E \end{matrix}\right\} = 1 + \lambda_E \left[\Delta_*(\sigma_\beta) \left\{ \begin{matrix} \cos^2\delta \\ \sin^2\delta \end{matrix} \right\} \pm \beta [\Delta_*(\sigma_\beta) + \Delta_*(\beta)] \cos\delta \sin\delta \right], \tag{4-69}$$

and

$$B_E = \lambda_E\{\Delta_*(\sigma_\beta)\cos\delta\sin\delta + \frac{\beta}{2}[\Delta_*(\sigma_\beta) + \Delta_*(\beta)][\cos^2\delta - \sin^2\delta]\},$$

$$D_E = (q_E)_{n_e,T_e}, \tag{4-69}$$

$$E_E = (r_E)_{n_e,T_e}.$$

The same system may also be expressed in the current representation. The energy equation in the current representation is

$$T_e = T + \gamma_J J^2, \tag{4-70}$$

where $\gamma_J = 1/\sigma\theta n_e$. The counterpart of Eq. (4-56) in the current representation is

$$\frac{\partial T_e}{\partial \xi} = \frac{2\gamma_J}{1 - \gamma_J J^2 \dfrac{\partial\, \ell n\, \gamma_J}{\partial T_e}} \left(J_x \frac{\partial J_x}{\partial \xi} + J_y \frac{\partial J_y}{\partial \xi}\right). \tag{4-71}$$

A second-order quasi-linear operator L_J may be defined as

$$L_J \equiv A_J \frac{\partial^2}{\partial x^2} + 2B_J \frac{\partial^2}{\partial x \partial y} + C_J \frac{\partial^2}{\partial y^2} + D_J \frac{\partial}{\partial x} + E_J \frac{\partial}{\partial y}, \tag{4-72}$$

so that in the current representation, the system (4-49) for negligible heat conduction, convection, and pressure gradient induced diffusion becomes

$$L_J(\psi) = 0. \tag{4-73}$$

Following the same procedure used in developing Eqs. (4-69), there results

$$\left.\begin{matrix} A_J \\ C_J \end{matrix}\right\} = 1 - \frac{\lambda_J}{J^2}\left\{\Delta_*(\sigma)\left\{\begin{matrix} J_y^2 \\ J_x^2 \end{matrix}\right\} \mp \beta[\Delta_*(\sigma) - \Delta_*(\beta)]J_x J_y\right\},$$

$$B_J = \frac{\lambda_J}{J^2}\left\{\Delta_*(\sigma)J_x J_y - \frac{\beta}{2}[\Delta_*(\sigma) - \Delta_*(\beta)](J_x^2 - J_y^2)\right., \tag{4-74}$$

$$D_J = (q_J)_{n_e,T_e},$$

$$E_J = (r_J)_{n_e,T_e},$$

where

$$\lambda_J \equiv \frac{2\gamma_J J^2/T_e}{1 - \gamma_J J^2 \frac{\partial\, \ell n\, \gamma_J}{\partial T_e}}. \tag{4-75}$$

Equations (4-68) and (4-73) are second-order quasi-linear differential equations whose type depends on the positivity of negativity of the discriminant

$$D \equiv B^2 - AC, \tag{4-76}$$

where A,B,C are the coefficients in (4-67) or (4-72). When $D < 0$, these equations are elliptic, and when $D > 0$, the equations are hyperbolic. It is readily shown that in either representation $B^2 - AC = b^2 - ac$ consistent with the correspondence between a system of two first-order

equations and a single equation of second-order constructed from the first-order system.

The condition of uniform ellipticity is thus, from Eq. (4-76),

$$1 + \lambda_E \Delta_*(\sigma_\beta) - (\frac{1}{2} \lambda_E \beta)^2 [\Delta_*(\sigma_\beta) + \Delta_*(\beta)]^2 > 0, \qquad (4\text{-}77)$$

or

$$\beta^2 < 4 \frac{1 + \lambda_E \Delta_*(\sigma_\beta)}{\lambda_E^2 [\Delta_*(\sigma_\beta) + \Delta_*(\beta)]^2} . \qquad (4\text{-}78)$$

It is to be noted that in the absence of convection effects in the electron continuity and energy equations, the condition for uniform ellipticity presented above is precisely the same as that for the prevention of the electro-thermal wave instability discussed in section 4.1. It appears, therefore, that steady state solutions of the nonuniform conduction equations (4-68) or (4-73) when they are of hyperbolic type would be physically unstable.

In the event of uniform ellipticity, the boundary conditions are of the conventional Dirichlet or Neumann type discussed in Courant, Hilbert.[32] A discussion of the uniqueness of the solution with such boundary conditions is presented in appendix B.

5. NONUNIFORM CONDUCTION WITH A NONEQUILIBRIUM CONDUCTIVITY: IONIZATION EQUILIBRIUM

In this chapter detailed numerical solutions are obtained for the distributions of current, potential, electron number density, and electron temperature in a finitely segmented channel with nonequipartition electron heating. The electrons are assumed to be in Saha equilibrium at the local electron temperature. The internal impedance and Hall voltage for the Faraday mode of operation are compared with the results for infinitely fine segmented electrode channels.

5.1 Nondimensional Steady Equations

When electron pressure gradients are neglected ($\vec{E}_n << \vec{E}'$) and heat conduction and convection effects are neglected in the electron fluid, the governing equations for the potential Φ' and the flux function ψ were shown to be

$$L_E(\Phi') = 0, \qquad L_J(\psi) = 0. \tag{5-1}$$

The operators L_E, L_J are defined in Eqs. (4-67) and (4-72) and contain the electron temperature and number density. The electron energy equation in the field representation is

$$T_e = T + \gamma_E(\nabla\Phi')^2,$$

and in the current representation (5-2)

$$T_e = T + \gamma_J(\nabla\psi)^2.$$

The electron number density when Saha equilibrium prevails at the local electron temperature is given by

$$n_e = n_e^* = \left[(n_{s_o} - n_e)\, K(T_e)\right]^{\frac{1}{2}} \tag{5-3}$$

where n_{s_o} is the number density of ionizable seed atoms.

These equations and variables may be made nondimensional by introducing in addition to a characteristic voltage V_o and current I_o a characteristic temperature T_o and number density n_{e_o} where

$$n_{e_o} \equiv n_e^*(T_o).$$

If nondimensional variables and operators are defined as

$$\bar{\Phi}' \equiv \Phi'/V_o \qquad \bar{\psi} \equiv \psi/I_o$$

$$\bar{T} \equiv T/T_o \qquad \bar{T}_e \equiv T_e/T_o \qquad \bar{n}_e \equiv n_e/n_{e_o}$$

$$\bar{L}_E \equiv h^2 L_E \qquad \bar{L}_J \equiv h^2 L_J$$

$$\bar{x} \equiv x/h \qquad \bar{y} \equiv y/h$$

then the foregoing equations may be written as

$$\bar{L}_E(\bar{\Phi}') = 0, \qquad \bar{L}_J(\bar{\psi}) = 0, \tag{5-4}$$

$$\bar{T}_e = \bar{T} + \omega_E \left[\left(\frac{\partial \bar{\Phi}'}{\partial \bar{x}}\right)^2 + \left(\frac{\partial \bar{\Phi}'}{\partial \bar{y}}\right)^2\right], \tag{5-5}$$

$$\bar{T}_e = \bar{T} + \frac{\omega_J}{\bar{n}_e^{\,2}} \left[\left(\frac{\partial \bar{\psi}}{\partial \bar{x}}\right)^2 + \left(\frac{\partial \bar{\psi}}{\partial \bar{y}}\right)^2\right], \tag{5-6}$$

$$\bar{n}_e^{\,2} = f^{-1}(f^{-1} - \bar{n}_e) n_o \bar{T}_e^{\frac{3}{2}} \exp(-\bar{\varepsilon}_i/\bar{T}_e). \qquad (5\text{-}7)$$

In the above,

$$f \equiv n_{e_o}/n_{s_o}, \qquad \bar{\varepsilon}_i \equiv \varepsilon_i/kT_o,$$

$$n_o \equiv K(T_o)/n_{s_o}, \qquad \omega_E \equiv \frac{\sigma V_o^{\,2}}{\theta n_e T_o h^2},$$

$$\omega_J \equiv \frac{\sigma I_o^{\,2}}{\sigma_o^{\,2}\theta n_e T_o h^2}.$$

It is to be noted that if the electron mobility μ and the energy exchange coefficient θ are insensitive to the changing the electron temperature, then ω_E and ω_J may be assumed to be constants.

In the field representation it is appropriate to select $V_o = V_y'$, the actual induced voltage across the transverse electrodes which exists for a given gas velocity, magnetic field strength, and external load. The parameter ω_E then possesses a useful physical significance when the electron mobility and energy exchange coefficient may be assumed uniform. If the channel is infinitely finely segmented and $\bar{I}_x = 0$ (Faraday mode) and no nonuniformities exist, the solution of the first of Eqs. (5-4) is

$$\frac{\partial \bar{\Phi}'}{\partial \bar{x}} = -\beta, \qquad \frac{\partial \bar{\Phi}'}{\partial \bar{y}} = -1.$$

The energy equation in the field representation then becomes

$$\bar{T}_e - \bar{T} = \omega_E.$$

Since the gas temperature is uniform at T_o, it follows that $\bar{T} = 1$ and

$$\omega_E = \frac{T_e - T_o}{T_o} . \tag{5-8}$$

The parameter ω_E thus represents the electron temperature rise in an infinitely fine segmented electrode channel with constant voltage V_y' for the given physical parameters n_o, $\bar{\varepsilon}_i$, and f.

In the current representation the current I_o is selected as $I_o = I_y$, the actual current flowing across the transverse electrodes. If the channel is infinitely finely segmented and $\bar{I}_x = 0$ and no nonuniformities exist, the solution of the second of Eqs. 5-4 is

$$\frac{\partial \bar{\psi}}{\partial \bar{x}} = -h/\ell, \qquad \frac{\partial \bar{\psi}}{\partial \bar{y}} = 0.$$

The energy equation in the current representation is then

$$\bar{T}_e - \bar{T} = \frac{\omega_J}{\bar{n}_e^2} \left(\frac{h}{\ell}\right)^2 . \tag{5-9}$$

Since the gas temperature T is uniform at T_o, it follows that $\bar{T} = 1$ and

$$\omega_j = \left(\frac{\ell}{h}\right)^2 \left[\frac{T_e - T_o}{T_o}\right] \bar{n}_e^2 . \tag{5-10}$$

Thus, ω_j represents the product of the nondimensional temperature rise and the square of the nondimensional number density rise in an infinitely fine segmented MHD channel with a constant transverse current I_y. On comparing Eqs. (5-8) and (5-10) it can be seen that

$$\omega_J = \omega_E \bar{n}_e^2 \left(\frac{\ell}{h}\right)^2,$$

where V_o, which appears in ω_E and ω_J, is to be interpreted as the voltage which causes a current I_o to flow with conductivity σ_o: $V_o = I_o \frac{h}{\ell} \sigma_o^{-1}$.

In terms of the function $\zeta(\bar{T}_e)$, defined as

$$\zeta(\bar{T}_e) = n_o \bar{T}_e^{\frac{3}{2}} \exp\left(-\bar{\varepsilon}_i/\bar{T}_e\right), \tag{5-11}$$

the electron number density may be explicitly written as

$$\bar{n}_e = \frac{2f^{-1}}{1 + \sqrt{1 + 4/\zeta(\bar{T}_e)}}. \tag{5-12}$$

The logarithmic derivative of $\bar{n}_e$ which appears in the operators $\bar{L}_E$, $\bar{L}_J$ is

$$\frac{\partial\, \ell n(\bar{n}_e)}{\partial \bar{T}_e} = \frac{\frac{1}{\bar{T}_e}\left(\frac{3}{2} + \frac{\bar{\varepsilon}_i}{\bar{T}_e}\right)}{2 - \frac{\zeta(\bar{T}_e)}{2}\left(1 + \sqrt{1 + 4/\zeta(\bar{T}_e)}\right)}. \tag{5-13}$$

The boundary conditions in nondimensional form are identical to those given in Section 3.2.1.

5.2 Potential, Current, and Electron Temperature Distributions

In illustrating the effects of finite electrode segmentation with nonuniform Joulean heating and a nonequilibrium conductivity, the energy exchange coefficient θ, electron mobility μ, and gas state variables

$\rho, T, \ldots$ will be assumed to be uniform. The temperature T_o is selected as this uniform gas temperature so that $\overline{T} = 1$. As a typical case, these parameters are fixed at their values for equilibrium gas conditions typical of a slightly seeded cesium-argon mixture at one atmospheric pressure, $T_o = 2400°K$, mole seed fraction of 0.004, and an effective field $V_y'/h = 40$ volts/meter. For these values, $\omega_E \sim 0.5$. The geometrical parameters are selected as $\ell/h = 1$, $a/\ell = 0.5$. With the assumption of uniform mobility, the gas is always statically stable in the sense of inequality (4-49); however, the condition of uniform ellipticity (4-78) requires $\beta < 1.09$. The Hall parameter β will therefore be set equal to 1.0 for the purposes of studying only uniformly elliptic solutions of the steady equations. This choice of β allows a modest Hall effect without exceeding the criterion for uniform ellipticity.

The solutions of Eqs. (5-4) and (5-5) or (5-6) subject to the boundary conditions (2-36) and (2-37) or (2-38) are obtained numerically (c.f. appendix A). The current and potential fields for the above conditions are shown in Figs. 5-1 and 5-2 for the case $I_x = 0$. It can be seen that the effects of nonuniform Joulean heating have generally distorted the current distribution shown in Fig. 5-1. This current distribution may be compared with that when the conductivity is uniform shown in Fig. 3-6. It may be noted that with uniform conductivity the current flows at an angle very nearly equal to $\tan^{-1}(h/a)$ in the core of the gas; however, with nonuniform Joulean heating, the current flows very nearly at the Hall angle $\tan^{-1}(\beta)$. It may also be noted that the disturbance of the flow in the core by the finite segmentation penetrates more deeply into the core with a nonequilibrium conductivity than

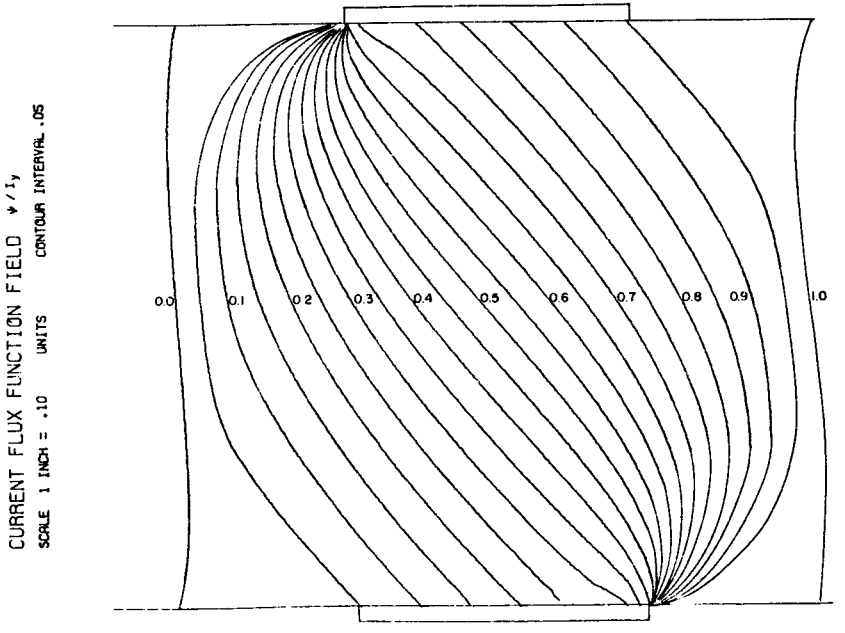

Fig. 5-1 Current distribution $\overline{\psi}$ with nonequilibrium conductivity; $\beta = 1$, $\ell/h = 1$, $a/\ell = .5$, $\overline{\varepsilon}_i = 20$, $\omega_E = .5$, $I_x = 0$.

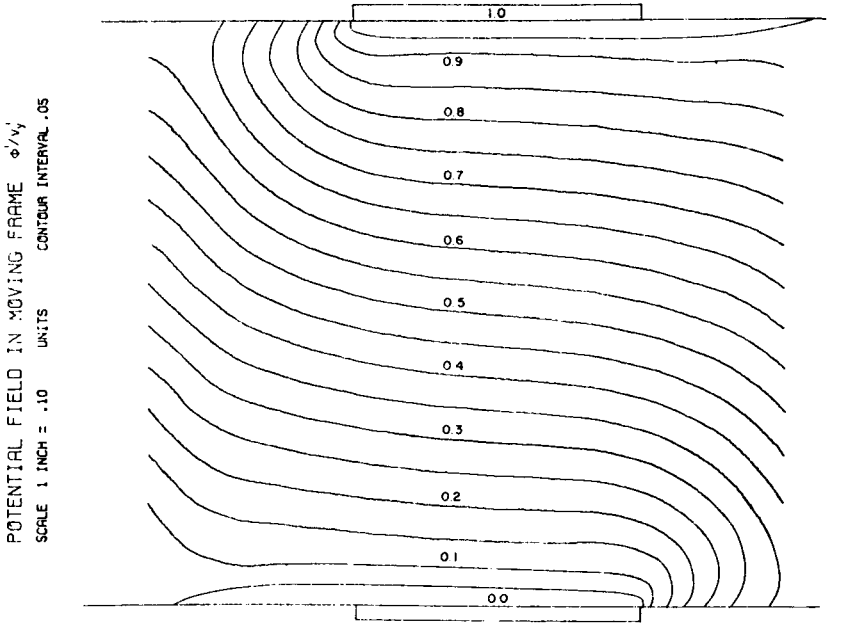

Fig. 5-2 Potential distribution $\overline{\Phi}'$ with nonequilibrium conductivity; $\beta = 1$, $\ell/h = 1$, $a/\ell = .5$, $\overline{\varepsilon}_i = 20$, $\omega_E = .5$, $I_x = 0$.

with a uniform conductivity.

The cumulative distribution of current on the electrode with non-equipartition heating is shown in Fig. 5-3. It can be seen that the current density is intensified at the right-hand singularity compared to the uniform conductivity case; indeed, this distribution is similar to the distribution with high conductivity layers (Fig. 3-8).

The potential $\overline{\Phi}'$ is shown for this case in Fig. 5-4 and may be compared with that shown in Fig. 3-10 for uniform conductivity. It may be noted that the parallel potential lines in the interelectrode region indicate that the Hall field E_x' has been effectively shorted out in this region by the nonuniform Joulean heating. This effect is consistent with the fact that the current in this region flows nearly at the Hall angle. The variation of the potential $\overline{\Phi}'$ along the insulator wall is shown in Fig. 5-4 where it is contrasted with the case for uniform conductivity. It can be seen that the total rise in potential along the insulator is below that for uniform conductivity. The rate of growth of the axial potential along the insulator is also less than that with a uniform conductivity.

The electron temperature distribution is shown in Fig. 5-5. It may be seen that high temperature zones occur over the singular points at the intersection of the electrodes and the insulators. It may be noted that a plateau of nearly uniform electron temperature $T_e/T = 1.40$ exists whose axis in the core lies approximately at the Hall angle. This electron temperature field may be contrasted with the Joule heating field J^2/σ for uniform conductivity shown in Fig. 5-6. It may again be observed that the disturbance created at the singular points at the

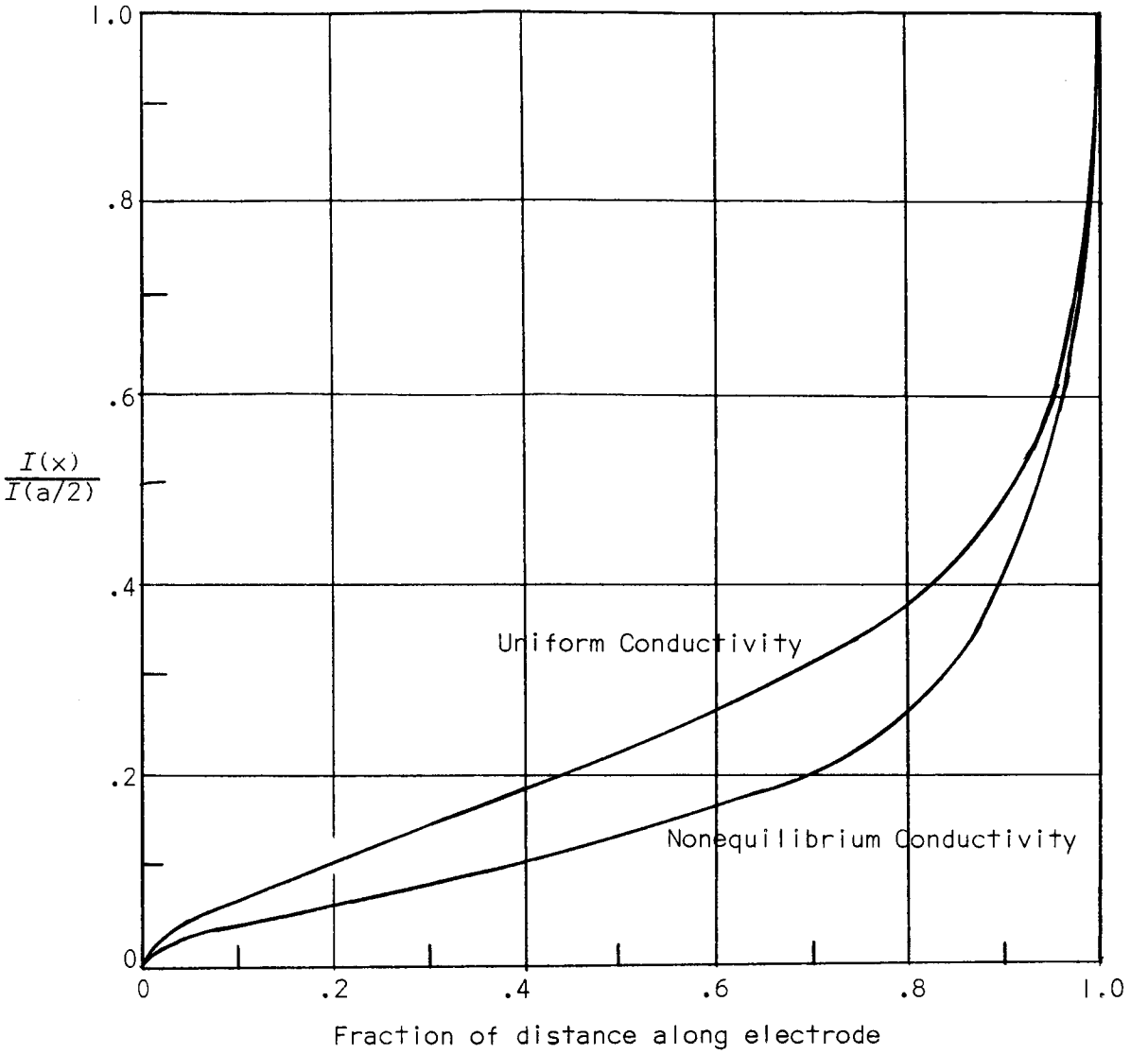

Fig. 5-3 Electrode current distribution with nonequilibrium conductivity; $\beta = 1$, $\ell/h = 1$, $a/\ell = .5$, $\bar{\varepsilon}_i = 20$, $\omega_E = .5$, $I_x = 0$

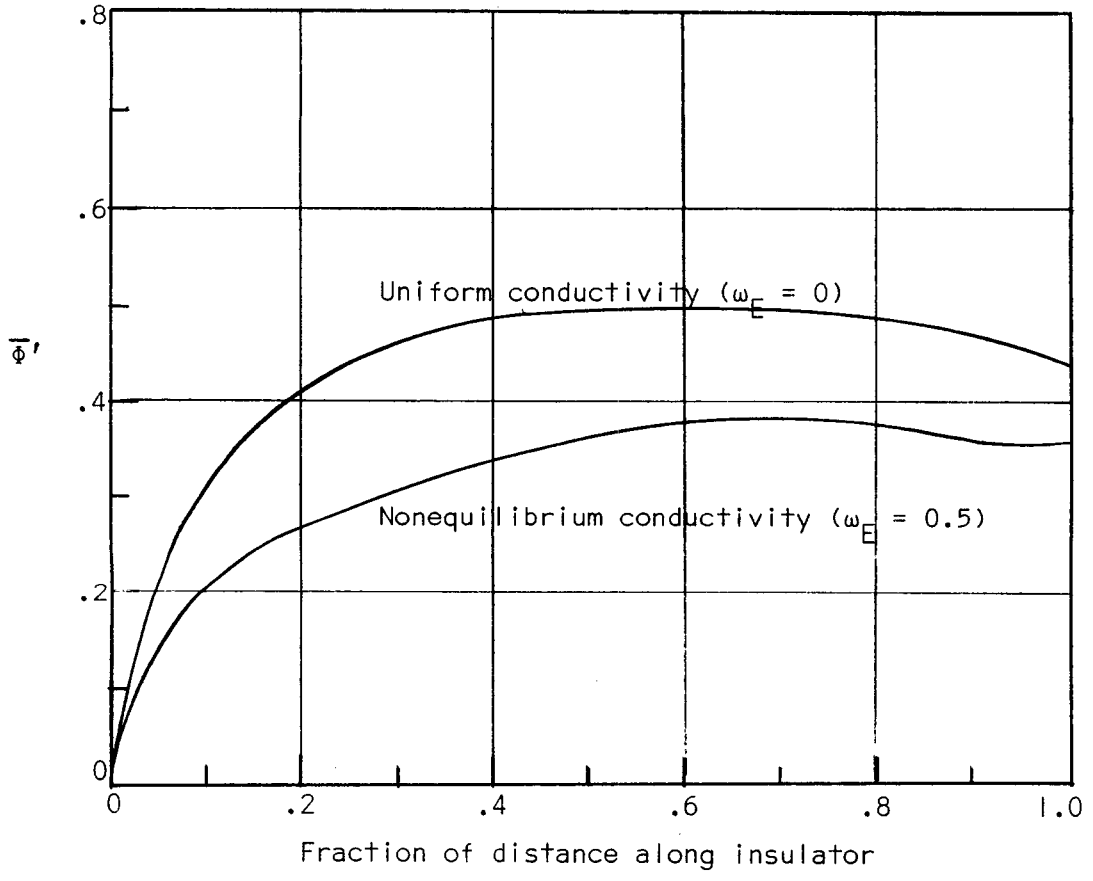

Fig. 5-4 Potential distribution $\overline{\Phi}'$ along insulator with nonequilibrium conductivity; $\beta = 1$, $\ell/h = 1$, $a/\ell = .5$, $\overline{\varepsilon}_i = 20$, $\omega_E = .5$, $I_x = 0$

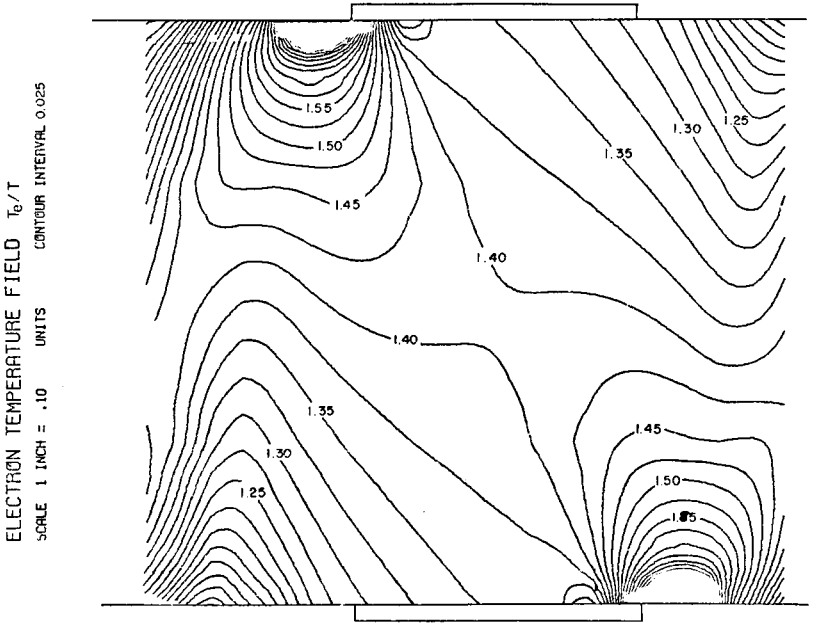

Fig. 5-5 Electron temperature field with nonequilibrium conductivity.

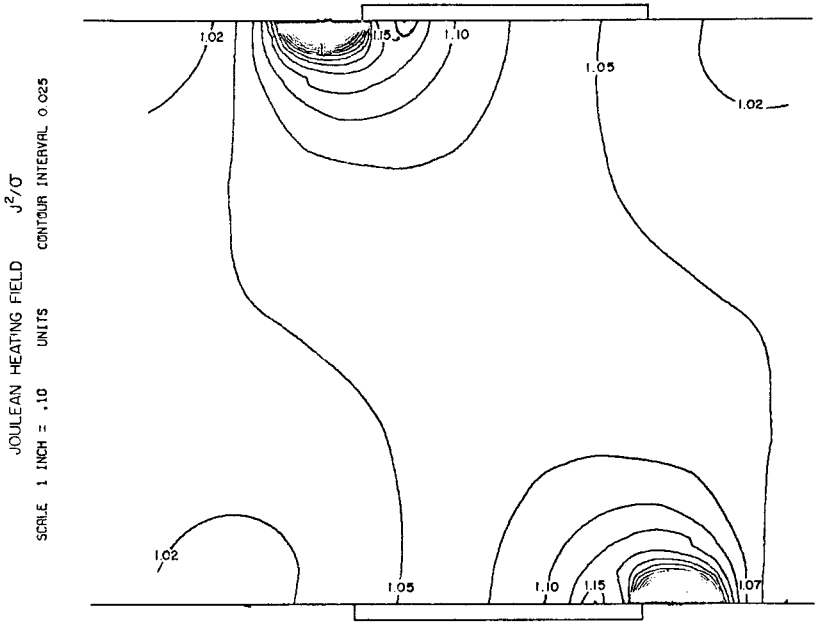

Fig. 5-6 Joulean heating field with uniform conductivity in arbitrary units.

electrode-insulator intersection penetrates more deeply into the core with nonuniform Joulean heating than with a uniform conductivity.

By virtue of the assumed Saha equilibrium at the local electron temperature, the electron number density is directly reflected in the electron temperature field. This temperature field possesses significant nonuniformities in the axial direction as well as in the transverse direction. Note in particular that there always exists a region in the axial direction where the electron heating vanishes (the current stagnation point on the insulator) and a region where the electron temperature in the absence of other dissipation effects is infinitely large (the singular points at the electrode-insulator intersections). Thus, for values of β of the order unity, there is no evidence of a highly conducting but axially uniform "shorting" layer over the insulators separating the electrodes. This result may be contrasted with the model treated by Kerrebrock[19,20] in which such a layer is postulated with a correspondingly large deterioration in channel performance. It should be pointed out, however, that such deterioration effects in the Kerrebrock model do not occur until Hall parameters considerably larger than one are reached. The conductivity model treated here, however, would be in the range in which the electro-thermal wave instability would be present for such large values of Hall parameter.

5.3 Internal Impedance and Hall Voltage

The combined effects of finite electrode size and the resulting nonuniform Joulean heating lead, as for other nonuniformities, to an increased transverse impedance and a depressed Hall voltage. For the

uniform conductivity case with finite electrodes ($\ell/h = 1$, $a/\ell = 0.5$, $\beta = 1$), $\overline{V}_H = 0.45$; but if nonuniform Joulean heating occurs with the electrons in Saha equilibrium at the nonuniform electron temperature, the Hall voltage for this example is reduced to $\overline{V}_H = 0.36$. The transverse impedance and Hall voltage with nonuniform Joulean heating are compared to those for continuous and infinitely fine segmented channels at the same gas conditions with the same effective field, $V'_y/h = 40$ volts/meter in Table 5-1.

TABLE 5-1

Electrode configuration and conductivity model	$\overline{R}_T = R_{yy}/R_{yy}(0)$	$\overline{V}_H = V'_x/(V'_x)_{ideal}$
Ideal continuous with nonequilibrium	0.30	0
Ideal segmented with nonequilibrium	0.05	1.0
Finite segmented with $\sigma=\sigma_o$	1.60	0.45
Finite segmented with nonequilibrium	0.12	0.36

It can be seen that the impedance is markedly higher than that for ideal segmented conductors but still somewhat below that for continuous electrodes with nonequipartition electron heating.

In Fig. 5-7 the effect of the departure of the electron temperature from the gas temperature for a fixed Hall parameter of unity is shown. It can be seen that the internal impedance relative to the internal im-

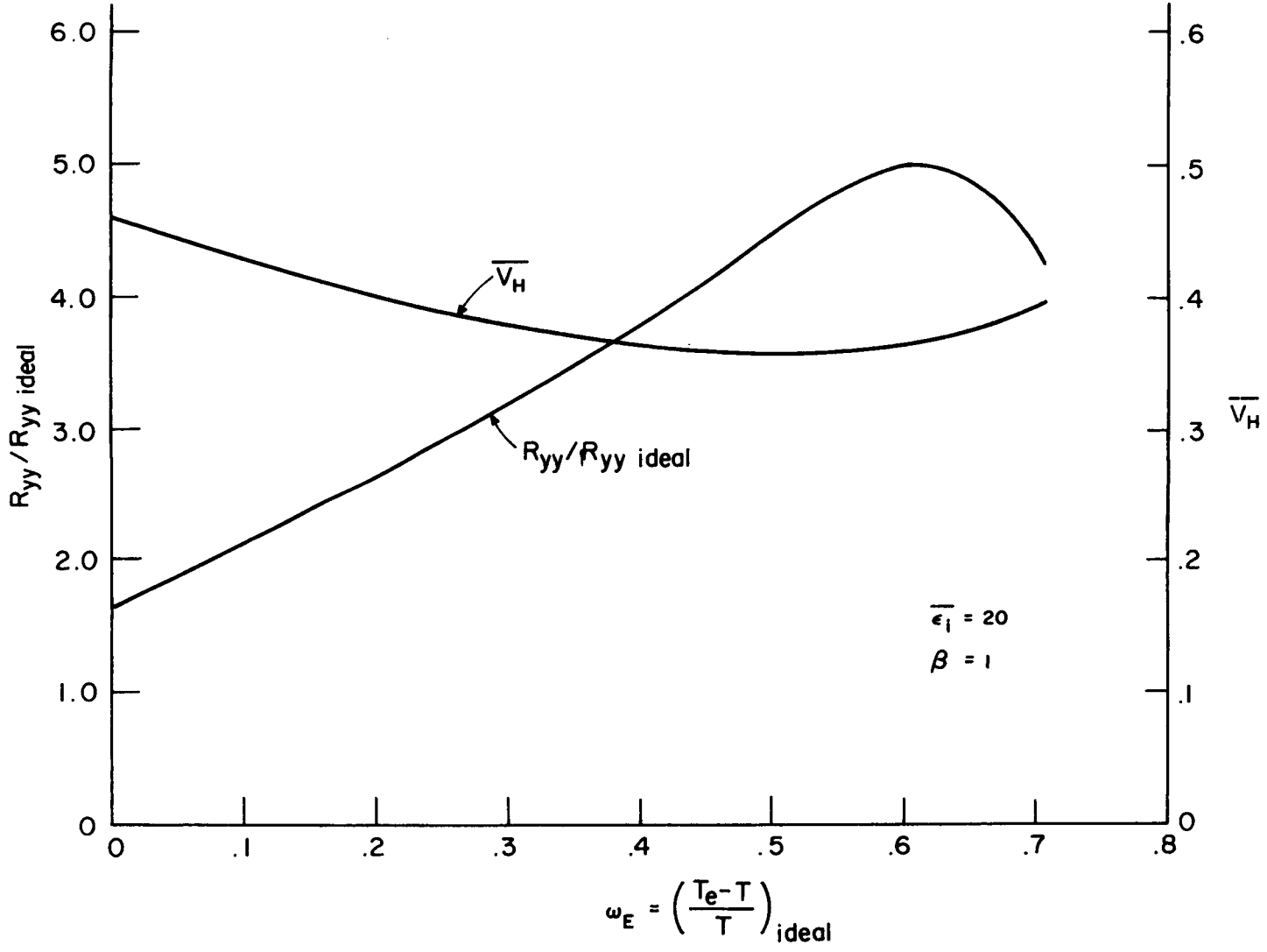

Fig. 5-7 Nondimensional internal impedance and Hall voltage with nonequilibrium conductivity; $\beta = 1$, $\ell/h = 1$, $a/\ell = .5$, $\overline{\epsilon}_i = 20$, $I_x = 0$. $R_{yy\ ideal}$ is the internal impedance of an infinitely fine segmented channel with uniform nonequilibrium heating at the same applied potential V_y'.

pedance of an infinitely fine segmented electrode generator increases as the electron temperature is allowed to respond to the Joulean heating and reaches a maximum near values of ω_E corresponding to maximum nonuniformity. As ω_E is increased further, the gas becomes more fully ionized and hence more uniform. The ratio of the actual impedance to the ideal segmented impedance begins to decrease back towards its value for uniform conductivity. The Hall voltage behaves in a corresponding fashion. As the departure of the electron temperature from the gas temperature increases, the higher conductivity near the edge of the electrodes and insulators decreases the Hall voltage. As further departures are allowed, the gas begins to reach full ionization of the seed and the Hall voltage begins to increase towards its uniform conductivity value.

6. FINITE RATE IONIZATION AND RECOMBINATION IN PERIODIC TEMPERATURE FIELDS

In this chapter the effects of finite rate ionization and recombination on the model discussed in chapter 5 are examined. The presence of such finite rate effects is shown to be suggested in the experimental results of Fischer.[28] *Qualitative observations about the manner in which finite rate effects would be manifested are presented. These observations are rendered more quantitative by a calculation of the number density response with finite rate effects to spatially periodic steady one-dimensional temperature disturbances. Such disturbances would be characteristic of the "hot spots" in segmented electrode channels due to current concentrations.*

6.1 Electron Number Density Antisymmetry with Hall Effect and Finite Rate Ionization

In chapter 5 it was shown that for the orientation of the magnetic field shown in Fig. 2-1 regions of very high electron temperature corresponding to large concentrations of current develop assymetrically at the leading edge of the upper electrode and at the downstream edge of the lower electrode. When the electrons are allowed to achieve Saha equilibrium at the local electron temperature, these regions of high electron temperature directly reflect regions of high electron number density.

The equilibrium electron number density distribution may be disturbed by gas dynamic convection if the recombination frequency is not

large. Under such circumstances it may be concluded that the electron number density which would tend to develop at the "hot spots" under equilibrium conditions will tend to be distributed preferentially in the downstream direction when convective nonequilibrium effects are present. Thus, near the electrodes, it would be expected that the electron number density at the upper electrode would be higher than the electron number density at the lower electrode. This is because the electrons generated at the lower "hot spot" are immediately convected over the adjacent insulator segment whereas the electrons generated at the upper "hot spot" are immediately convected over the upper electrode. Such an effect in a linear MHD channel has been observed by Fischer.[28] In Fig. 6-1, Fischer's measurements of the radiation intensity distribution between an electrode pair along a line intersecting the midpoints of the insulators is shown. The plasma for this case was generated in a 135 m/sec, 2100°K potassium-seeded argon flow. This radiation intensity is proportional to the population of an excited potassium state; however, because of the convective nonequilibrium, it is not clear that this state is in equilibrium with either the electron temperature or the electron number density. The radiation is probably an index of both temperature and number density effects. It can be seen that the intensity is higher along the insulator wall which is immediately downstream of the "hot spot" than along the upper insulator wall which is immediately upstream of the "hot spot". A reversal of the current (and hence the cathode and anode) has little effect on this distribution; thus, electrode sheath effects do not appear to be dominant.

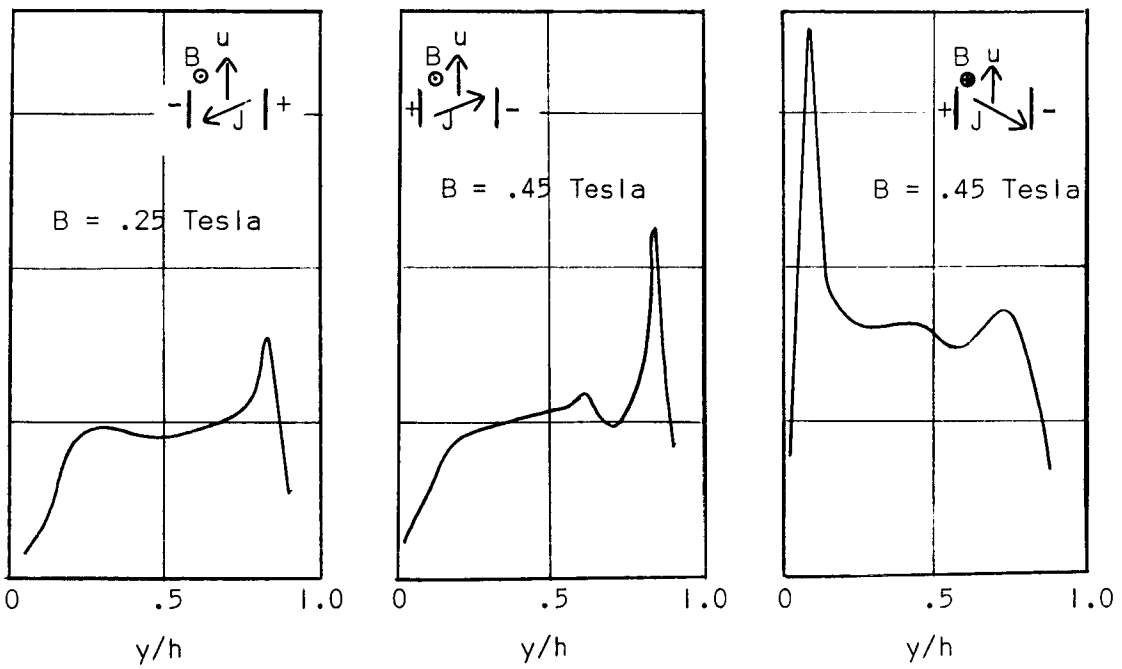

Fig. 6-1 Radiation intensity measurements of Fischer along a traverse across the channel intersecting the midpoints of opposed insulator segments

6.2 Recombination Times and Residence Times in Flowing Noble-Gas, Alkali-Metal Plasmas

The foregoing observations may be rendered somewhat more precise by calculation of the magnitude of convective nonequilibrium effects expected in a segmented electrode MHD channel. In the range of operating temperature anticipated for alkali metal seeded noble gas MHD generators (approximately 2000°K) the recombination is principally of the three-body type. A theory for three-body recombination has been given by Hinnov and Hirschberg.[24] If the net rate of production of electrons is denoted $\dot{n}_e$, then

$$\dot{n}_e = \alpha n_e (n_e^{*2} - n_e^2), \tag{6-1}$$

where α is the recombination coefficient and n_e^* is the equilibrium number density at temperature T_e; the recombination frequency is

$$\nu_r = \alpha n_e^2. \tag{6-2}$$

In appendix C values of ν_r for various values of T_e and n_e are calculated according to the theory for $\alpha(T_e)$ of Hinnov and Hirschberg. In particular, it is shown that the recombination frequency in a 2000°K plasma seeded with a few tenths of a percent of alkali metal vapor is of the order of 10^3 sec^{-1}. For a plasma flow of approximately 100 m/sec (which would represent a lower limit of velocity for MHD generators) and an electrode of 1 cm in length, the plasma residence time over the electrode is of the order of 10^{-4} sec. Since the corresponding time for ionization or recombination is only 10^{-3} sec, it can be seen that convective non-

equilibrium is easily achieved in such low electron number density plasmas.

6.3 Electron Continuity Equation with Ionization and Recombination

A study of one-dimensional nonuniformities in electron temperature and number density will now be made with the aim of obtaining a more precise evaluation of the decay and response of the electron number density to periodic temperature hot spots. The steady-state electron continuity equation from section 2.3 for a velocity $\vec{u}$ parallel to the x axis and independent of x with negligible ion current is

$$u \frac{\partial n_e}{\partial x} = \alpha n_e (n_e^{*2} - n_e^2). \tag{6-3}$$

From the work of Hinnov and Hirschberg,[24]

$$\alpha(T_e) = 5.6 \times 10^{-27} (kT_e)^{-\frac{9}{2}}, \tag{6-4}$$

where kT_e is expressed in electron volts. The electron continuity equation may be nondimensionalized on characteristic values n_{e_o}, T_o, and period length ℓ to become

$$\bar{u} \frac{\partial \bar{n}_e}{\partial \bar{x}} = \bar{\alpha}\, \bar{n}_e (\bar{n}_e^{*2} - \bar{n}_e^2), \tag{6-5}$$

where

$$\bar{n}_e = n_e / n_{e_o}, \qquad \bar{n}_e^* = n_e^*(T_e)/n_{e_o},$$

$$\bar{u} = u/\ell\nu_r, \qquad \bar{\alpha} = \alpha(T_e)/\alpha(T_o) = (T_e/T_o)^{-\frac{9}{2}},$$

$$\bar{x} = x/\ell.$$

The recombination frequency at the reference temperature is $\nu_r = \alpha(T_o)n_e^{*2}(T_o)$. The periodic boundary condition for Eq. (6-5) is

$$\bar{n}_e(\bar{x} + 1) = \bar{n}_e(\bar{x}). \tag{6-6}$$

Since ℓ/u represents the average residence time of the plasma in the period of length ℓ, and $1/\nu_r$ represents the average time between recombination events, it can be seen that the parameter $\bar{u}$ represents the ratio of the recombination time to the plasma residence time. Thus, when $\bar{u} \to 0$, the electron number density is in equilibrium in the section of length ℓ, and when $\bar{u} \to \infty$, the electron number density is frozen in the section of length ℓ.

6.4 Spatially Periodic Solutions of the Electron Continuity Equation

In appendix D it is shown that the nonlinear rate equation (6-5) may be transformed into a linear equation, and that the solution of Eq. (6-5) subject to the boundary condition (6-6) is

$$\bar{n}_e = \frac{1}{\bar{u}}\left[F(\bar{x}) + \frac{e^{-\lambda(\bar{x})/\bar{u}}}{1 - e^{-\lambda(1)/\bar{u}}}F(1)\right]^{-\frac{1}{2}}, \tag{6-7}$$

where

$$\lambda(\bar{x}) \equiv 2\int_0^{\bar{x}} \bar{\alpha}\,[\bar{T}_e(\eta)]\bar{n}_e^{*2}[\bar{T}_e(\eta)]d\eta, \tag{6-8}$$

$$F(\bar{x}) \equiv 2\int_0^{\bar{x}} \bar{\alpha}\,[\bar{T}_e(\eta)]e^{-[\lambda(\bar{x}) - \lambda(\eta)]}d\eta. \qquad (6\text{-}9)$$

It is shown (appendix D) that in the frozen limit where $\bar{u} \to \infty$, the solution (6-7) becomes

$$\bar{n}_e = \left(\frac{\int_0^1 \bar{\alpha}\,\bar{n}_e{}^{*2}d\eta}{\int_0^1 \bar{\alpha}\,d\eta} \right)^{\frac{1}{2}}. \qquad (6\text{-}10)$$

Thus in the frozen limit, the number density becomes uniform in the axial direction x and is equal to a root mean square average of the Saha number density weighted against the recombination coefficient.

6.5 Number Density Response to Spatially Periodic Temperature Pulses

As an application of the foregoing results, consider a model of the high temperature zones which occur periodically at the intersection of the insulators and electrodes of a segmented magnetohydrodynamic channel. A simple model of such an effect is an electron temperature pulse of the form shown in Fig. 6-2:

$$T_e(x) = \begin{cases} T_{e_o}, & 0 \le x \le \frac{a-\delta}{2} \\ T_{e_{max}}, & \frac{a-\delta}{2} \le x \le \frac{a+\delta}{2} \\ T_{e_o}, & \frac{a+\delta}{2} \le x \le \ell \end{cases} \qquad (6\text{-}11)$$

where δ represents the spatial extent in the axial direction over which the pulse extends and $T_{e_{max}}$ represents the temperature within the pulse.

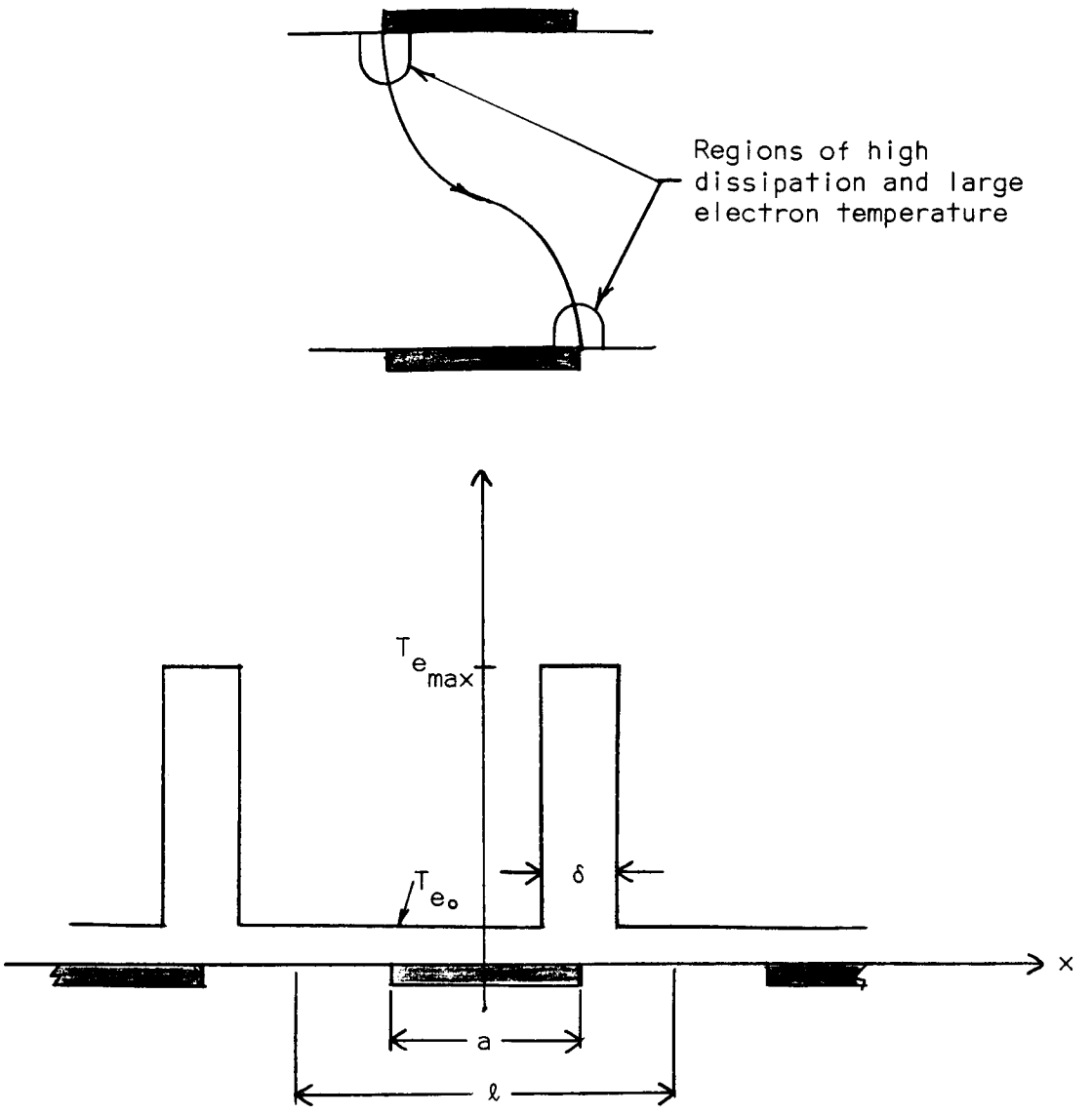

Fig. 6-2 Periodic temperature pulses in a finitely segmented MHD channel

The temperature over the remainder of the insulator and electrode is selected at the reference temperature and is denoted T_{e_o}.

The electron number density response to such a temperature distribution is shown in Fig. 6-3 for various values of the parameter $\bar{u}$, for $\delta/\ell = 0.2$, $T_{e_{max}}/T_{e_o} = 1.5$, $\varepsilon_i/kT_{e_o} = 20$. The equilibrium limit ($\bar{u} = 0$) and the frozen limit ($\bar{u} \to \infty$) are to be noted. It can be seen that as $\bar{u}$ is increased, the electron number density responds less sharply to the temperature pulse and also decays less sharply. This effect tends to spread the region of high electron number density over the insulator region on the downstream side of the temperature "hot spot".

It should be noted that with values of $\bar{u}$ as high as 10 or 20 (representing the ratio of ionization time to residence time), the electrons are still a large degree away from their frozen value; indeed, it appears that values of $\bar{u} \geq 200$ are required before the fluctuation in electron number density is less than 10% over the period.

In Fig. 6-4, the average value of the electron number density denoted $\langle \bar{n}_e \rangle$ in the range $0 \leq \bar{x} \leq 1$ is shown as a function of $\bar{u}$. The frozen limit value $\bar{n}_{e_{frozen}}$ and the average equilibrium value $\langle \bar{n}_e^* \rangle$ are also shown. It may be observed that the maximum value of $\langle \bar{n}_e \rangle$ occurs for $\bar{u} \sim 1$.

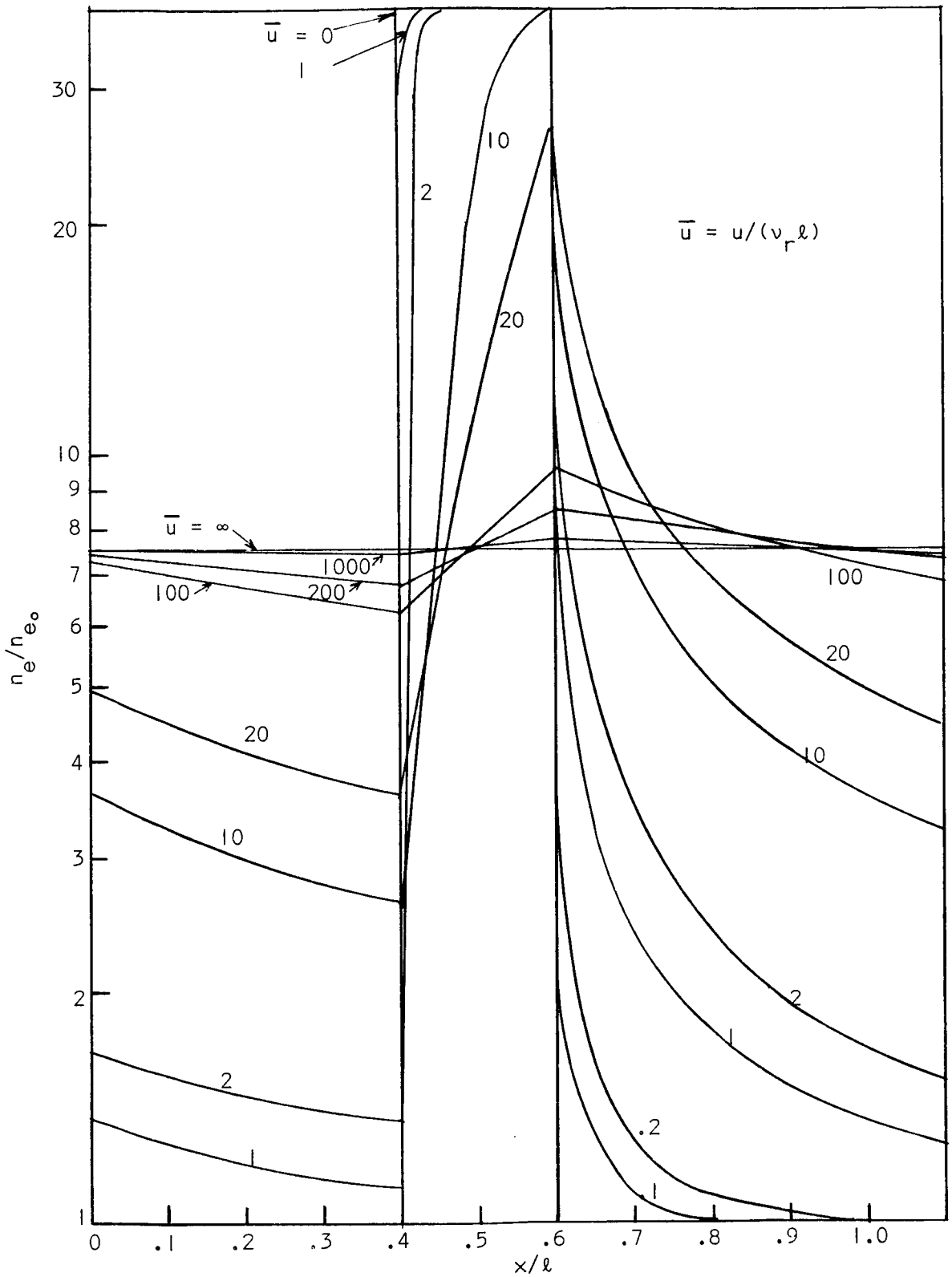

Fig. 6-3 Electron number density response to periodic temperature pulses

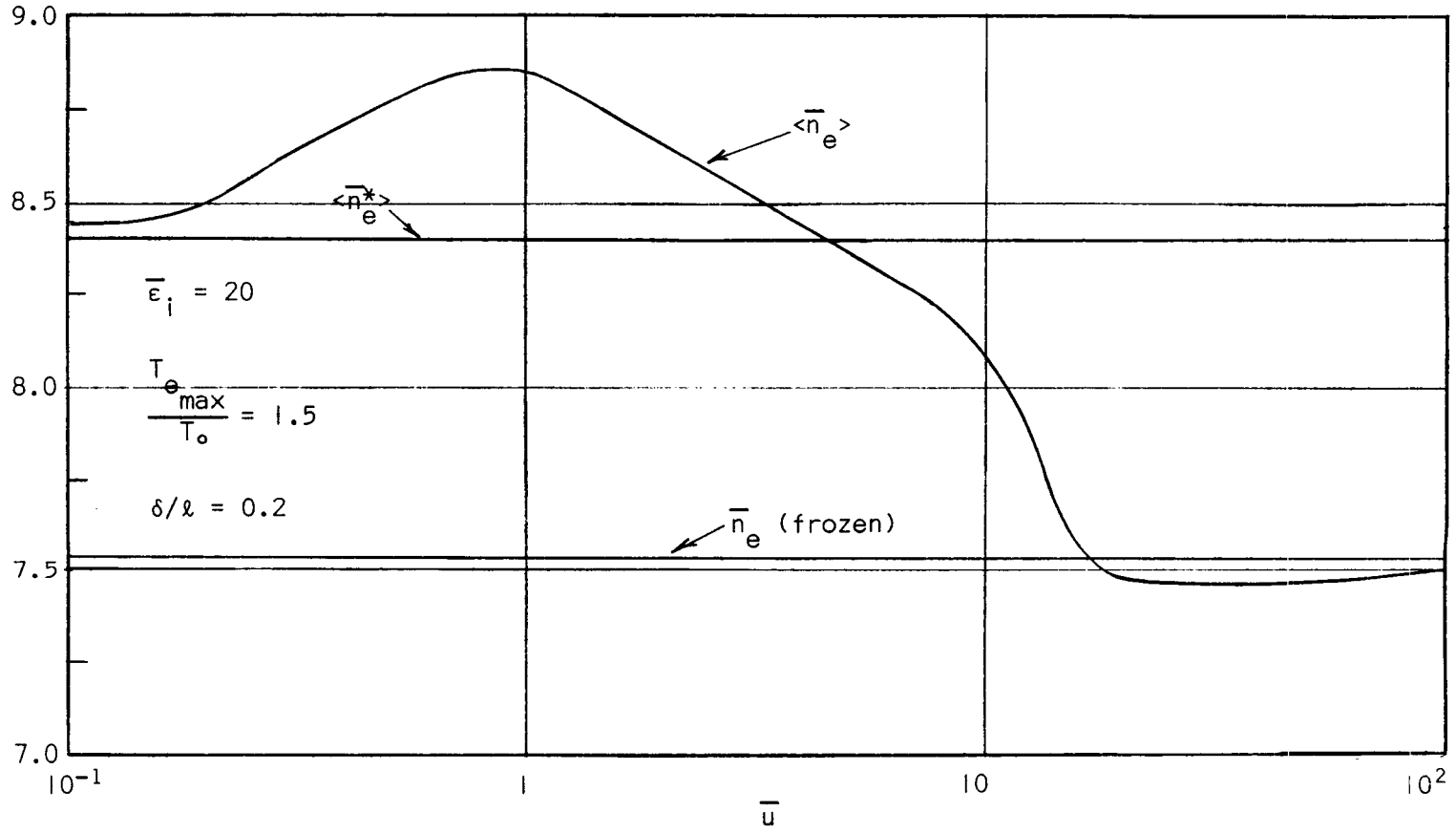

Fig. 6-4 Average electron number density over one period with periodic temperature disturbances for various degrees of convective nonequilibrium

7. NONUNIFORM ELECTRICAL CONDUCTION WITH A NONEQUILIBRIUM CONDUCTIVITY: FINITE RATE EFFECTS

In this chapter, consideration is given to the effects of finite rates of ionization and recombination due to convective nonequilibrium on electrical conduction in a finitely segmented magnetohydrodynamic channel with nonequilibrium conductivity. The electron temperature is assumed to be determined by a simple balance between Joulean heating and collisional energy loss to the heavy species in the gas as discussed in chapters 2 and 5. The electron number density, however, is governed by the more complete electron continuity equation discussed in chapter 6. Detailed numerical solutions are obtained for the distribution of potential, current, electron temperature, and electron number density. The results of this model are contrasted with those obtained for the model discussed in chapter 5, in which the electrons were assumed to be in ionization equilibrium at the local electron temperature. A specific calculation is made for the approximate conditions and geometry of the experiment of Fischer.[28] *It is shown that certain of Fischer's measurements are explainable in terms of a convective nonequilibrium effect.*

7.1 Nondimensional Steady Equations

The nondimensional steady equations governing the potential $\bar{\Phi}'$ or flux function $\bar{\psi}$, electron temperature $\bar{T}_e$, and number density $\bar{n}_e$ from sections 3.2, 5.1, and 6.3 are

Current Conservation and Maxwell-Faraday:

$$\overline{M}_E(\overline{\Phi}') = 0, \qquad \overline{M}_J(\overline{\psi}) = 0, \tag{7-1}$$

Electron Energy:

$$\overline{T}_e = \overline{T} + \omega_E \left[\left(\frac{\partial\overline{\Phi}'}{\partial\overline{x}}\right)^2 + \left(\frac{\partial\overline{\Phi}'}{\partial\overline{y}}\right)^2\right],$$

$$\overline{T}_e = \overline{T} + \frac{\omega_J}{\overline{n}_\epsilon^2}\left[\left(\frac{\partial\overline{\psi}}{\partial\overline{x}}\right)^2 + \left(\frac{\partial\overline{\psi}}{\partial\overline{y}}\right)^2\right], \tag{7-2}$$

Electron Continuity:

$$\overline{u}\,\frac{\partial\overline{n}_e}{\partial\overline{x}} = \overline{\alpha}\,\overline{n}_e(\overline{n}_e{}^{*2} - \overline{n}_e{}^2). \tag{7-3}$$

The operators $\overline{M}_E$, $\overline{M}_J$ are defined as

$$\overline{M}_{E,J} \quad \frac{\partial^2}{\partial\overline{x}^2} + \frac{\partial^2}{\partial\overline{y}^2} + \overline{q}_{E,J}\,\frac{\partial}{\partial\overline{x}} + \overline{r}_{E,J}\,\frac{\partial}{\partial\overline{y}}\,. \tag{7-4}$$

For uniform electron mobility μ, the coefficients $\overline{q}_{E,J}$, $\overline{r}_{E,J}$ from Eqs. (2-11) and (2-12) are

$$\overline{q}_E = \frac{\partial\,\ell n\,\overline{n}_e}{\partial\overline{x}} + \beta\,\frac{\partial\,\ell n\,\overline{n}_e}{\partial\overline{y}},$$

$$\overline{r}_E = \frac{\partial\,\ell n\,\overline{n}_e}{\partial\overline{x}} - \beta\,\frac{\partial\,\ell n\,\overline{n}_e}{\partial\overline{y}}, \tag{7-5}$$

$$\bar{q}_J = -\frac{\partial\, \ell n\, \bar{n}_e}{\partial \bar{x}} + \beta \frac{\partial\, \ell n\, \bar{n}_e}{\partial \bar{y}}\,,$$

$$\bar{r}_J = -\frac{\partial\, \ell n\, \bar{n}_e}{\partial \bar{x}} - \beta \frac{\partial\, \ell n\, \bar{n}_e}{\partial \bar{y}}\,. \qquad (7\text{-}6)$$

Equations (7-1), (7-2), and (7-3) are three equations governing $\bar{\Phi}'$ or $\bar{\psi}$, $\bar{T}_e$ and $\bar{n}_e$. From section 4.3, this system of steady state equations is parabolic, provided $\bar{u} \neq 0$. From section 4.1, it was shown that the electro-thermal wave instability may still occur even with finite rates of ionization. The condition for the prevention of this instability will be discussed in the example below.

7.2 Potential, Current, Electron Temperature, and Electron Number Density Distributions

In illustrating the effects of finite rates of recombination in a finitely segmented electrode channel, the energy exchange coefficient θ, electron mobility μ, and gas state variables $\rho, T, \ldots$ will be assumed uniform; the coefficient ω_E is then constant. As a typical case, let $\omega_E = 0.5$ which corresponds to a slightly seeded cesium argon mixture at one atmosphere pressure, $T = 2400°K$, mole seed fraction of 0.004, and an effective field of $V_y'/h \sim 40$ volts/meter. Geometrical parameters are selected as $\ell/h = 1$, $a/\ell = 0.5$. Uniform mobility precludes static instabilities of the form discussed in section 4.2. By selecting the Hall parameter at $\beta = 1$ for these conditions, the electro-thermal wave instability is prevented according to inequality (4-41). The extent of the effect of finite rates of recombination is contained in the nondimen-

sional parameter $\bar{u}$ which represents the ratio of ionization time to residence time of an electron over the period length ℓ. As a typical value illustrating finite rate effects, let $\bar{u} = 10$.

The solution of Eqs. (7-1) through (7-3) subject to the boundary conditions (2-35), (2-36), and (2-37) or (2-38) are obtained numerically. The potential, current, electron temperature, and electron number density fields are shown in Figs. 7-1 through 7-4 for $\bar{I}_x = 0$. Attention should be directed to the four singular points, one of which occurs at each electrode edge as shown in Fig. 2-1. For the orientation of magnetic field shown in Fig. 2-1, the Hall effect causes an intensification at the singular points at the downstream edge of the lower electrode and the upstream edge of the upper electrode. In what follows, these intensified singularities (or concentrations of current) are referred to as the "strong" singularities.

The most significant aspect of the current distribution shown in Fig. 7-1 is the loss of symmetry between the upper electrode-insulator wall and the lower wall as a result of the finite rate effects. It may be noted that the strong singularity at the downstream edge of the lower electrode is now stronger than that on the upstream edge of the upper electrode. This fact may be verified by counting the number of current lines entering the singular point in both cases. This distribution may be contrasted with that shown in Fig. 5-1 for Saha equilibrium in which the strong singularities on the upper and lower wall are equal.

The potential distribution shown in Fig. 7-2 reflects behavior that may be interpreted in terms of the current distribution discussed above. Lack of symmetry between upper and lower electrodes is manifest, the

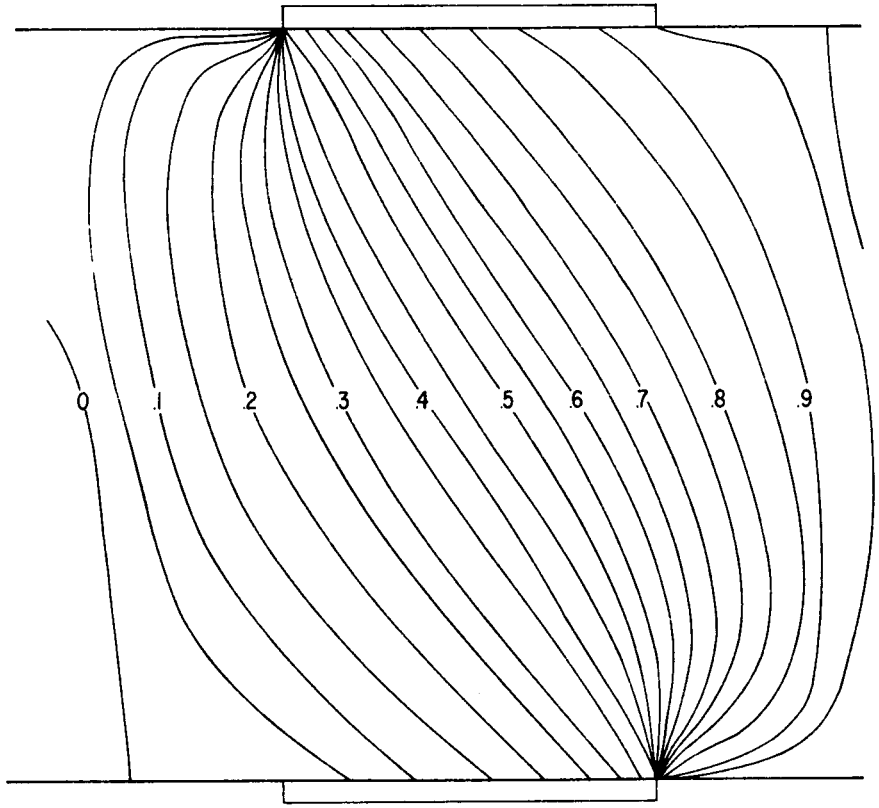

Fig. 7-1 Current distribution $\overline{\psi}$ with finite rates of ionization. $\omega_E = 0.5$, $\overline{u} = 10$, $\beta = 1$, $\overline{\varepsilon}_i = 20$.

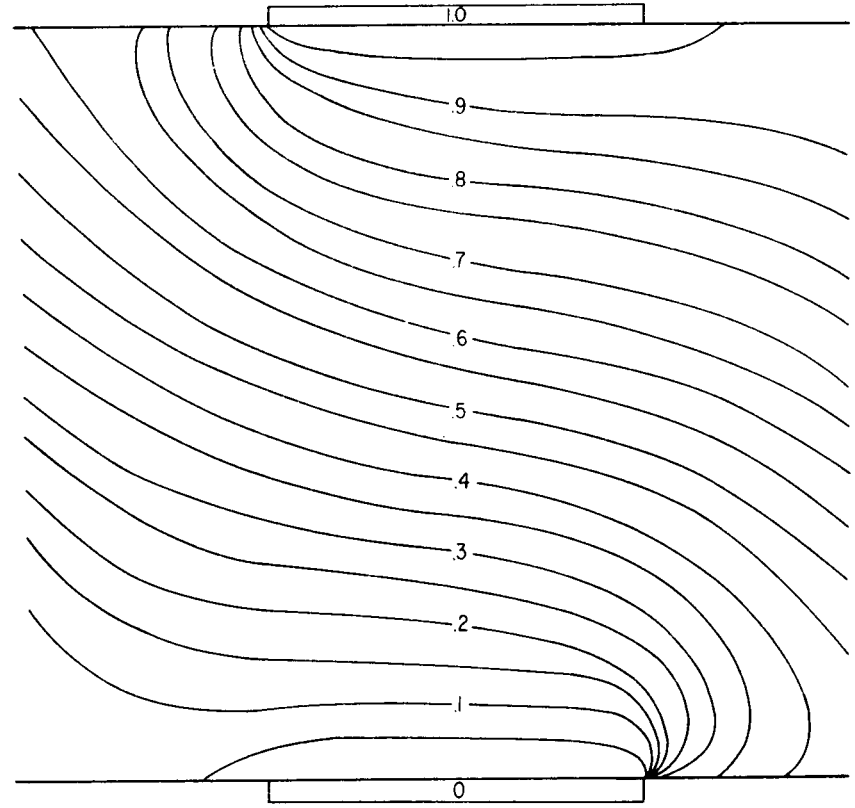

Fig. 7-2 Potential distribution $\overline{\Phi}'$ with finite rates of ionization. $\omega_E = 0.5$, $\overline{u} = 10$, $\beta = 1$, $\overline{\varepsilon}_i = 20$.

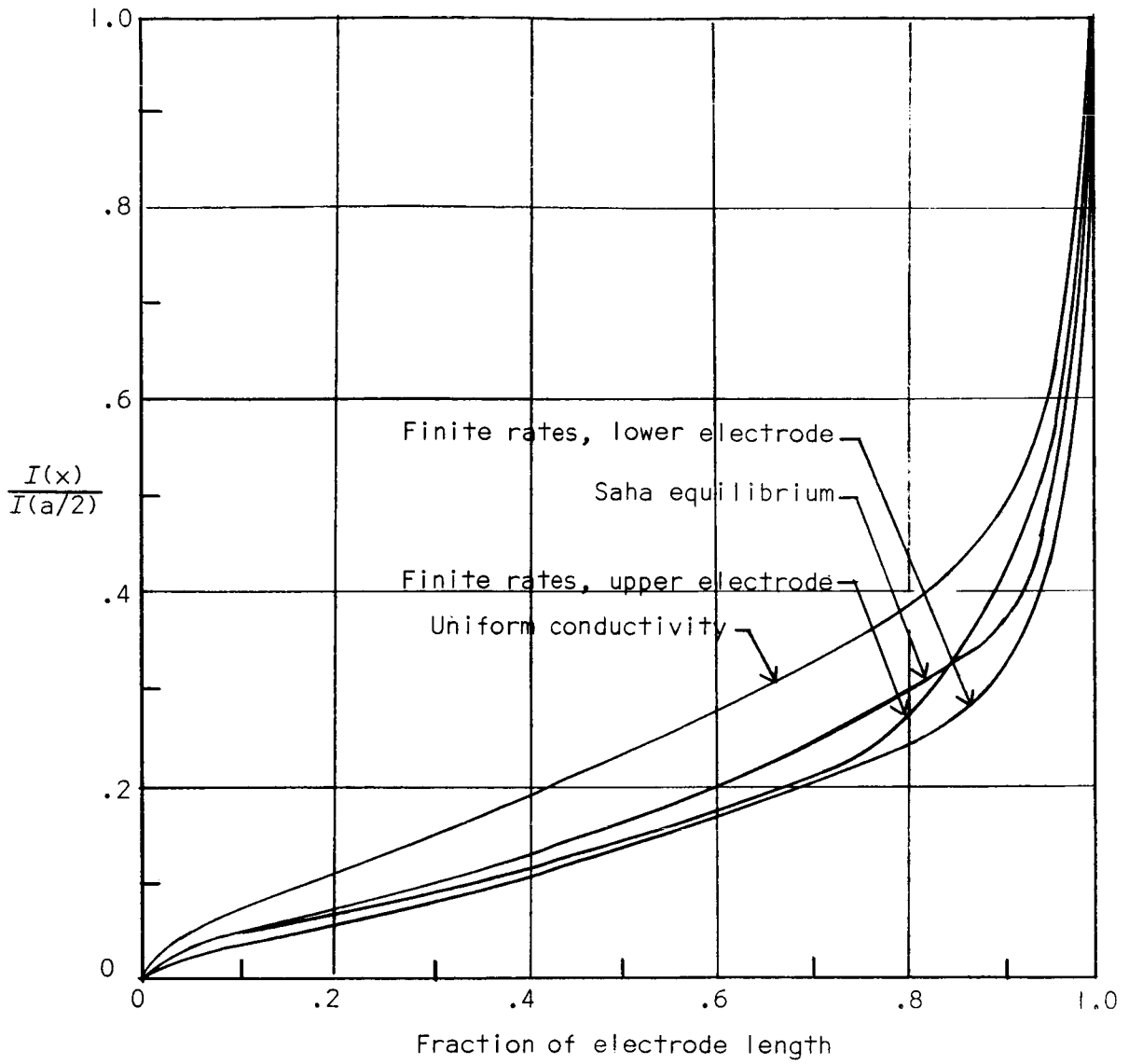

Fig. 7-3 Current distribution along electrode for the case shown in Fig. 7-1

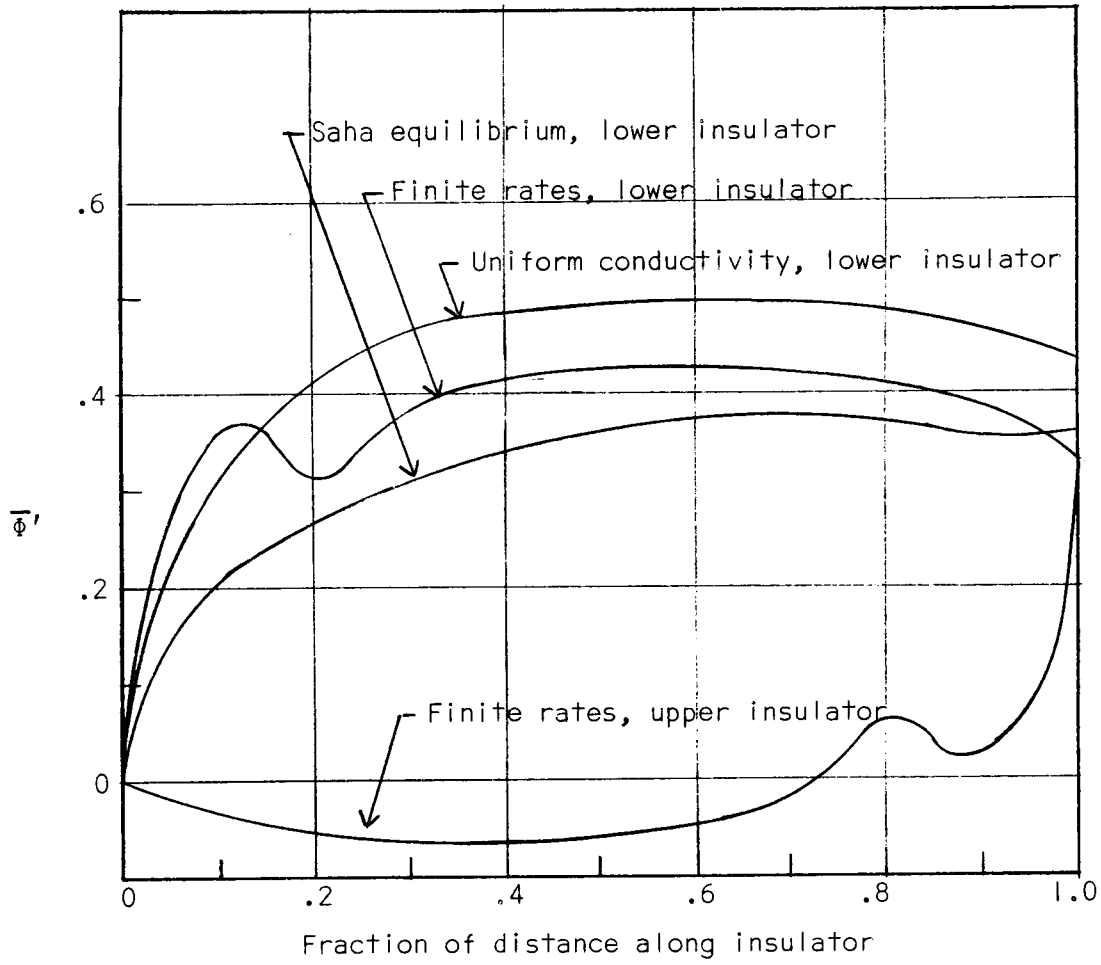

Fig. 7-4 Potential distribution along insulator for the case shown in Fig. 7-2

potential drop at the lower electrode edge being greater than that at the upper electrode edge.

The electron number density distribution shown in Fig. 7-6 evidences definite finite-rate effects. The electrons created near the "hot spots" at the electrode-insulator intersections are convected downstream as seen in the shift of the constant-number-density contours. It can be seen that this shift in the electron number density does not produce a corresponding strong shift in the electron temperature field (Fig. 7-5). Such a shift might be expected if the higher conductivity region attracts a larger current to the downstream regions which in turn produces greater Joulean heating in those regions, thereby producing higher electron temperatures. The electron temperature contours, however, are not as strongly displaced as the electron number density contours. This electron temperature field with finite rate effects may be contrasted with the equilibrium temperature field shown in Fig. 5-5.

The effect of finite rates on the electrode current distribution is shown in Fig. 7-3. It can be seen that the lower electrode which is immediately upstream of the strong singularity has a more nonuniform current distribution than it possessed in the Saha equilibrium case of chapter 5. This effect results because, on the lower electrode, the electrons are convected downstream of the singularity directly onto the insulator, thereby attracting more current to the edge of the electrode. The upper electrode on the other hand possesses a current distribution (except near the strong upstream singularity) which is more uniform than the Saha equilibrium case. This is so because, on the upper electrode, the electrons generated at the strong upstream singularity are immediately

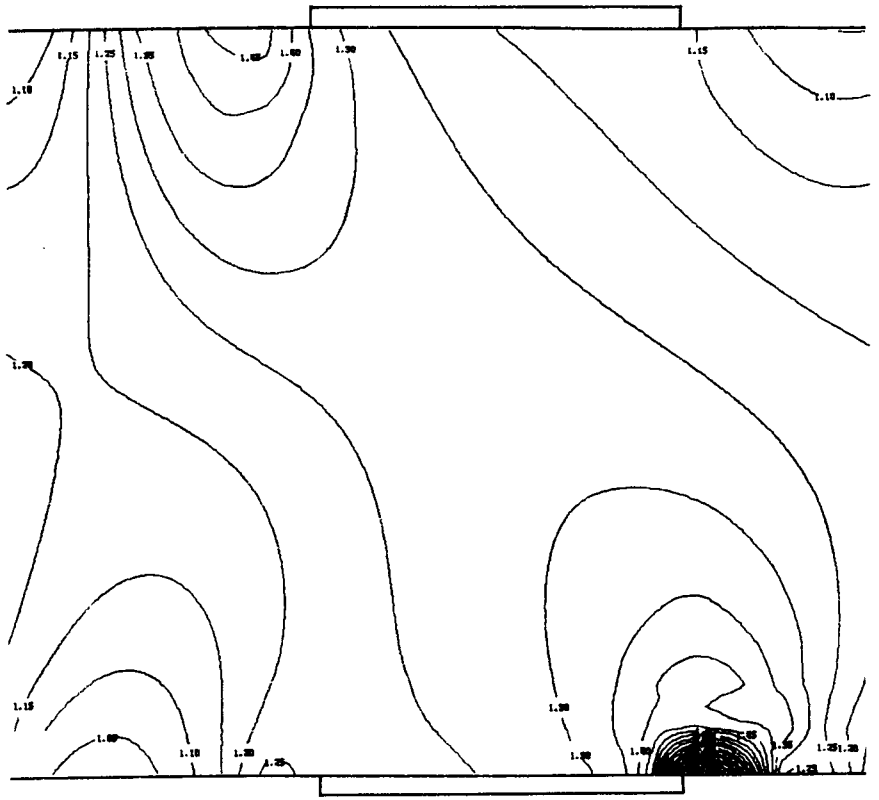

Fig. 7-5 Electron temperature distribution $\overline{T}_e$ for the case shown in Figs. 7-1 and 7-2.

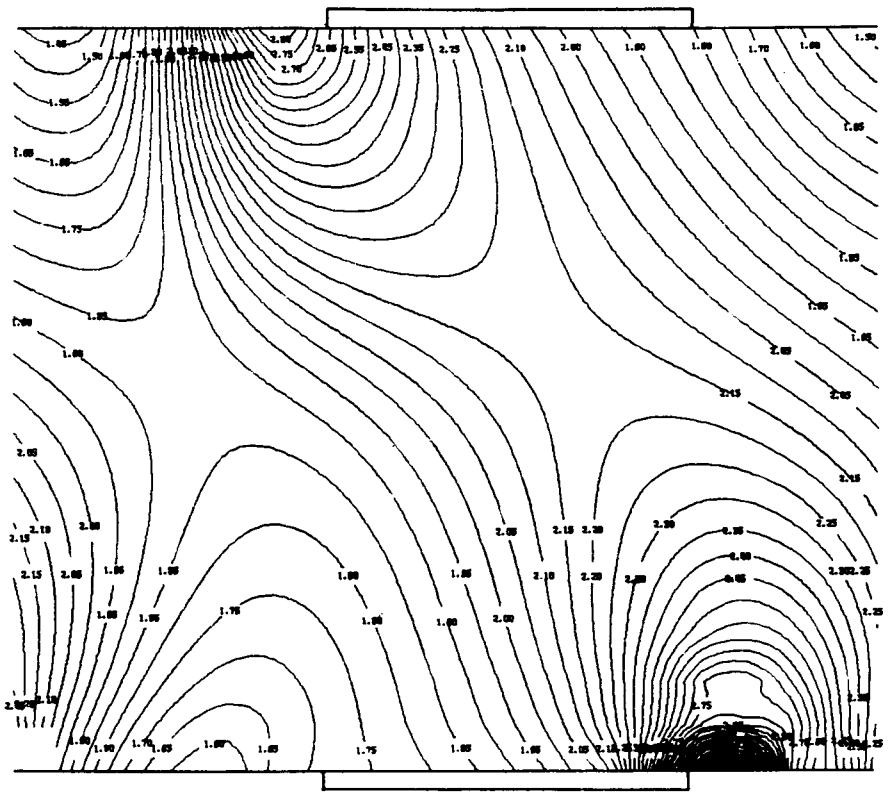

Fig. 7-6 Electron number density distribution $\ell n(\overline{n}_e)$ for the case shown in Figs. 7-1 and 7-2.

convected onto the electrode. These electrons then generate a higher conductivity over the electrode portion adjacent to the strong singularity. This effect then tends to spread the current out in the regions adjacent to the strong singularity. Since the overall effect of finite rates is to generate a layer of high conductivity over the electrodes and insulators, the region of the electrode near the strong singularity still manifests strong current nonuniformity relative to the case with Saha equilibrium. This follows from the results of chapter 3, where it was shown that a high conductivity layer over the insulators and electrodes produces a more nonuniform distribution of current on the electrode. This convective effect therefore explains the shift in the relative strength of the singularities of the upper and lower electrode walls discussed above.

The distribution of potential $\overline{\Phi}'$ on the insulator is shown in Fig. 7-4. Although the potential rises more rapidly than for the Saha equilibrium case, the overall rise along the insulator is less than that for Saha equilibrium.

7.3 Internal Impedance and Hall Voltage

The internal impedance and Hall voltage for this case are shown in Table 7.1, where the results for the Saha equilibrium calculation are also shown for comparison. It can be seen that the finite rate effect produces a conducting layer over the insulator which does tend to reduce the Hall voltage relative to the Saha equilibrium case for this value of $\overline{u} = 10$. The internal impedance has also been increased relative to the Saha equilibrium case as a result of the Hall shorting effect

TABLE 7.1

CONDUCTIVITY MODEL	$\bar{R}_T \equiv R_{yy}/R_{yy}(0)$	$\bar{V}_H \equiv V_x'/V_{x_{ideal}}'$
Uniform Conductivity at σ_o	1.60	0.45
Nonequilibrium Conductivity with Saha Equilibrium	0.15	0.36
Nonequilibrium Conductivity with Finite Rates	0.22	0.32

$\bar{\varepsilon}_i = 20, \quad \beta = 1, \quad \omega_E = 0.5, \quad \ell/h = 1, \quad a/\ell = 0.5$

7.4 Comparison with the Measurements of Fischer

It was pointed out in chapter 6 that the distribution of radiation intensity measured by Fischer[28] could be explained as a convective non-equilibrium effect. A calculation using conditions similar to those of Fischer's experiment is now described. The conditions of the potassium seeded argon flow for which a comparison will be attempted are

$$T = 2100°K$$

$$u = 135 \text{ m/sec}$$

$$\ell = 1.2 \text{ cm}$$

$$n_{s_o} \sim 2\times10^{16}\text{cm}^{-3}$$

$$h = 2.0 \text{ cm}$$

$$a/\ell = 0.5$$

From appendix C, the reference recombination frequency ν_r corresponding to this condition is about 10^3 sec^{-1}. The nondimensional parameter $\bar{u} \equiv u/\ell\nu_r$ is therefore approximately 10. The applied magnetic field for this case was 0.25 Tesla. Based on the gas composition data available, the Hall parameter β was approximately 3. For these low degrees of ionization and the cross section behavior of potassium and argon, static instabilities discussed in section 4.3 will not arise. From section 4.1 it was shown that even with finite rate effects, the electro-thermal wave instability may still occur and that the onset of this instability is still governed by the inequality (4-39). If a uniform mobility is assumed, the condition (4-39) for the prevention of the electro-thermal wave instability is $\beta \gtrsim 0.8$ ($\bar{\varepsilon}_i = 23$ for the above data). Because of the assumption of uniform mobility, this condition is probably overly conservative; nevertheless, it appears that the conditions of Fischer's experiment corresponded closely to those for the onset of the electro-thermal wave instability.

For the comparison with the above experiment, the nondimensional gas properties were set at $\bar{\varepsilon}_i = 20$, $\omega_E = 0.5$. The geometrical parameters were set at $\ell/h = 0.6$, $a/\ell = 0.5$. The convective nonequilibrium parameter $\bar{u}$ was set at 10.0. The current, potential, electron number density and electron temperature distributions for this calculation are shown in Figs. 7-7 through 7-10 and possess the same general trends as those discussed previously. It should be noted that the lack of symmetry between the upper and lower electrode walls discussed previously is clearly evident in the electron temperature and number density distributions. The intense singularity occurs on the lower wall, and a

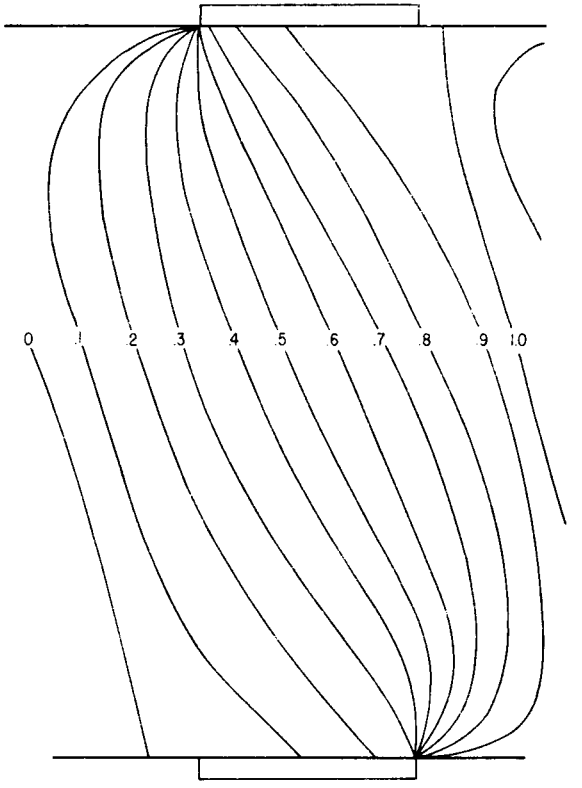

Fig. 7-7 Current distribution $\overline{\Psi}$ with finite rates of ionization and the geometry of Fischer's experiment. $\ell/h = 0.6$, $\omega_{\Gamma} = 0.5$, $\overline{u} = 10$, $\beta = 1$, $\overline{\varepsilon}_i = 20$.

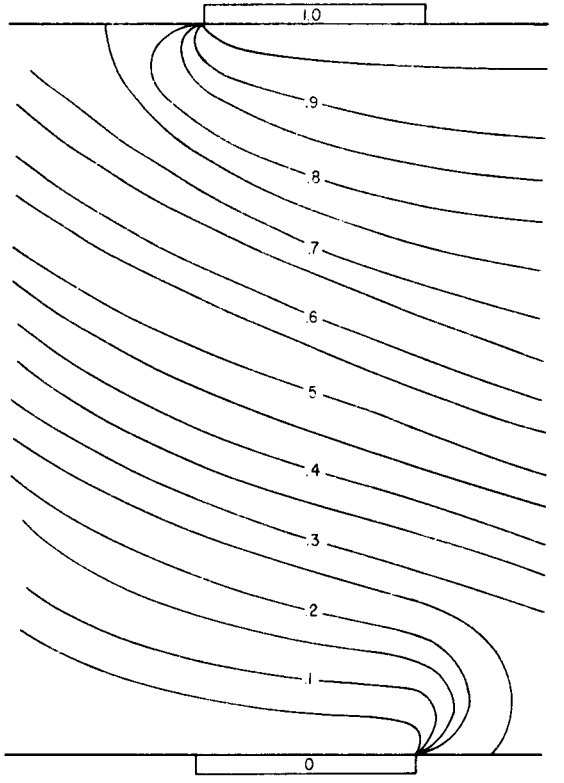

Fig. 7-8 Potential distribution $\overline{\Phi}'$ with finite rates of ionization for the case shown in Fig. 7-7.

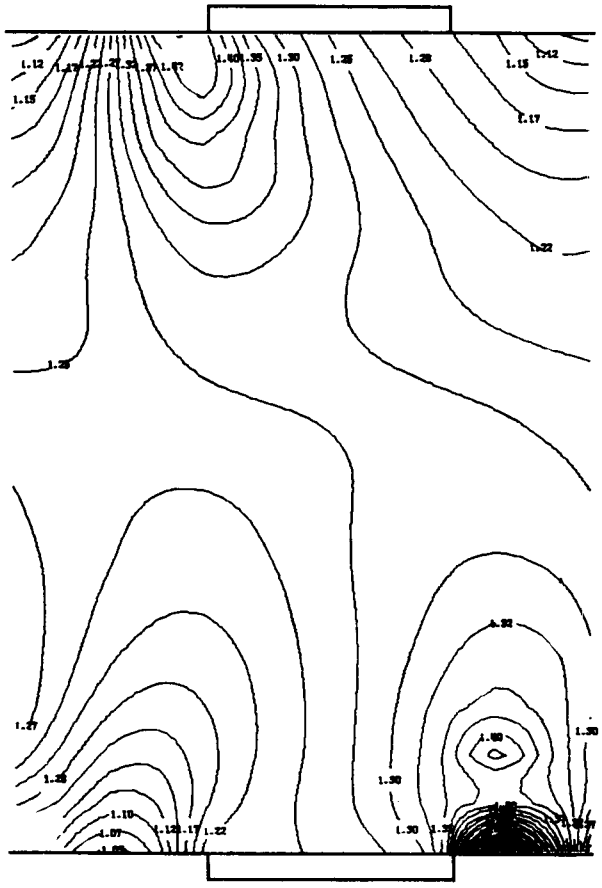

Fig. 7-9 Electron temperature distribution $\bar{T}_e$ for the case shown in Fig. 7-7.

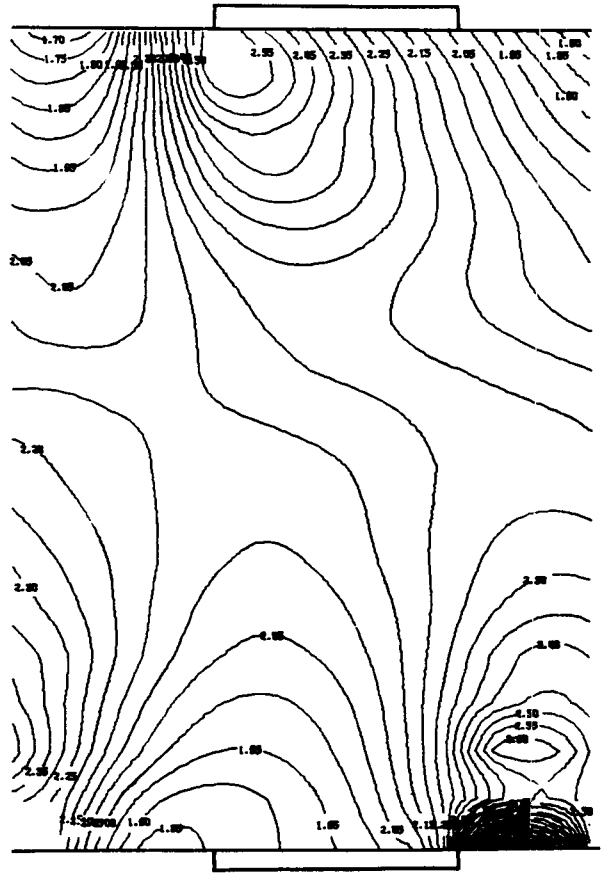

Fig. 7-10 Electron number density distribution $\ell n(\bar{n}_e)$ for the case shown in Fig. 7-7.

considerably weaker singularity occurs on the upper wall. Further insight into this convective nonequilibrium effect may be obtained with reference to Fig. 7-11. In the absence of significant convection effects, the "hot spots" generated at opposite electrode edges as a result of the Hall effect would be expected to develop regions of high temperature and electron number density which extend equally in both the upstream and downstream directions. A traverse along the dashed line shown in Fig. 7-11 would then reveal a symmetric variation in either temperature or number density across the channel. On the other hand, in the presence of gas dynamic convection, the distributions in number density and temperature tend to become distorted in the downstream direction and the traverse along the dashed line no longer reveals a symmetric distribution. The results of the calculation in terms of number density and temperature along the dashed line shown in Fig. 7-11 are shown in Fig. 7-12. These results are compared with Fischer's measurements (in terms of the photomultiplier tube signal of the radiation intensity). It may be noted that a reversal of the magnetic field reverses the direction of the anti-symmetry. It can be seen that, although the distortion of the intensity is much sharper for Fischer's measurements, the trends in number density and temperature in the calculation are similar. Note that the number density shows a sharper variation than does the electron temperature.

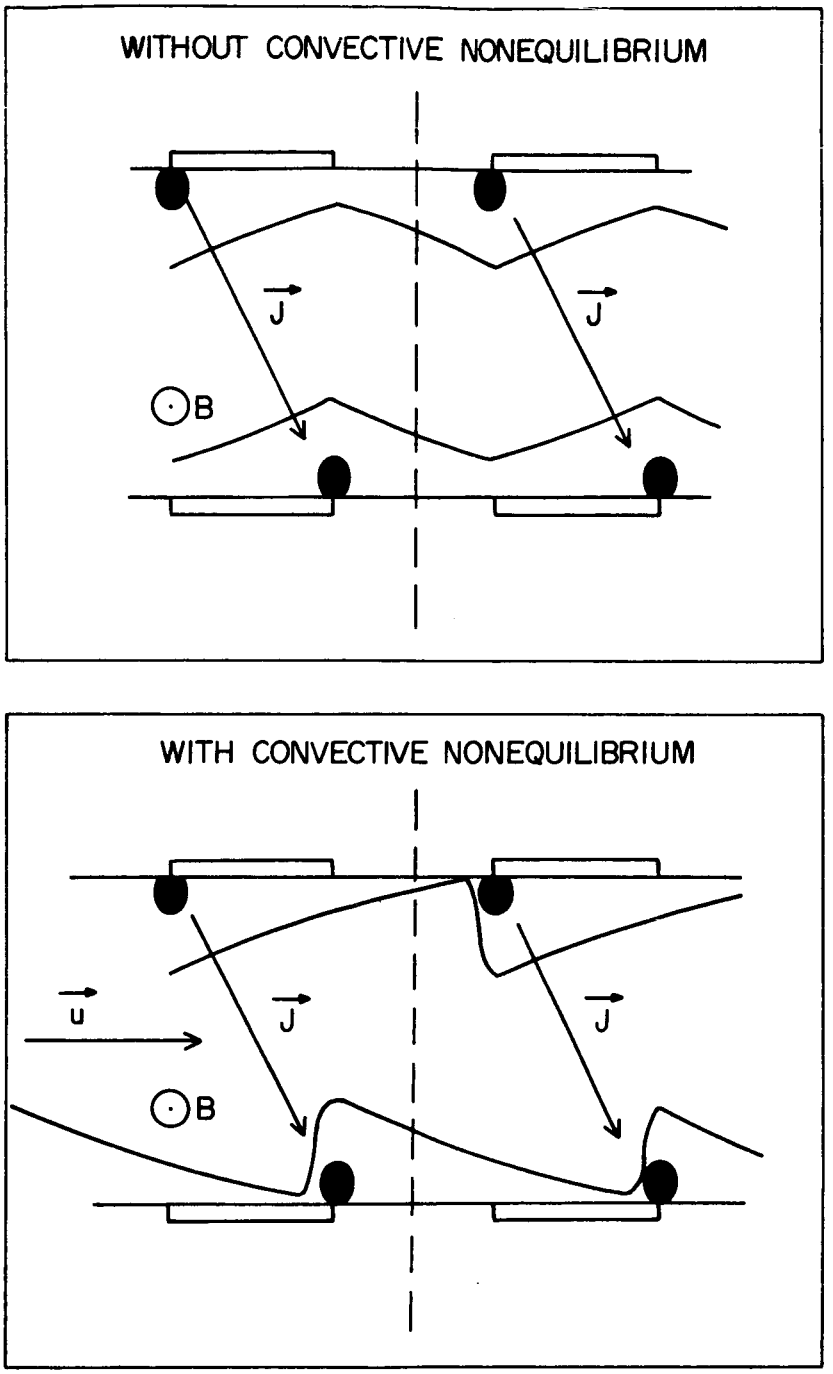

Fig. 7-11 Convective nonequilibrium effects in a finitely segmented MHD channel.

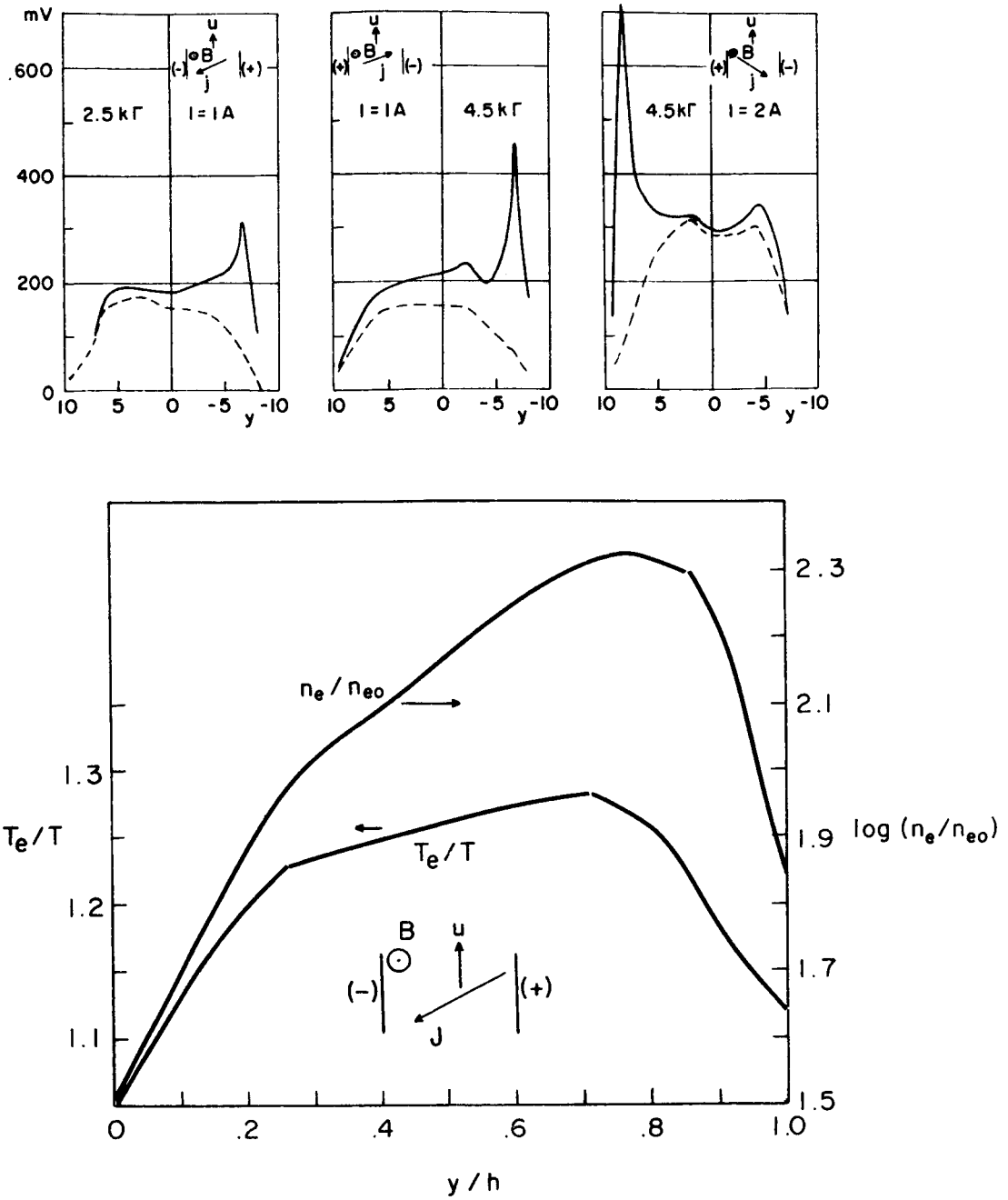

Fig. 7-12 Comparison of calculated electron temperature and number density profiles with the radiation intensity measurements of Fischer.[28] From reference 28, the photomultiplier tube signal in mv is approximately proportional to the electron temperature over this range .

8. SUMMARY AND CONCLUSIONS

A basic theoretical study has been made of some of the effects of nonuniform conductivity on electrical conduction in magnetohydrodynamic channels. Two basic models have been proposed which exhibit such effects. The first model requires as input information the spatial distribution of conductivity throughout the channel. The second model incorporates the effects of electron fluid heating and electron ionization and recombination on the conductivity distribution in a self-consistent calculation.

Studies made with the first model have shown that low conductivity layers over the electrodes and insulators in the presence of a strong magnetic field have two important effects on the current distribution relative to the uniform conductivity case. The first effect is a straightening of the current lines in the core of the channel such that the current tends to flow vertically across the channel from electrode to electrode. The second effect is a more uniform distribution of current on the electrode relative to the uniform conductivity case. This uniformity effect was shown to be consistent with the experimental measurements of Hoffman and Oates.[29] When layers of high conductivity over the electrodes and insulators were examined with the same model, it was shown that the current in the core tends to flow at the Hall angle. For large Hall parameters, the current flows nearly parallel to the channel axis in the core. In addition, the current distribution on the electrode becomes increasingly more nonuniform relative to the case with uniform conductivity.

Studies made with the second model described above revealed the existence of an ionization instability. This instability had previously been predicted by Kerrebrock.[22] A detailed examination of the effects of finite rates of ionization on this instability revealed that the condition for the onset of the instability is unchanged from that with infinitely fast ionization. It was also shown that in the absence of pressure gradient induced diffusion of charge and electronic heat conduction, the growth rate of the instability was proportional to the longer of either the effective ionization time of electrons or the effective collisional energy transfer time from the electron fluid. This model under steady state conditions was also shown to be described by a system of equations of mixed type if the ionization was in equilibrium at the local electron temperature. It was shown that if the Hall parameter is small enough, the equations of this model will always be uniformly elliptic. Further, in the absence of pressure gradient induced diffusion and heat conduction, it was shown that the condition for uniform ellipticity of these steady equations is identical to the condition for the prevention of the ionization instability described previously.

Numerical studies made with the steady state form of the second model were carried out for Hall parameters such that the equations were uniformly elliptic. When the ionization was in equilibrium at the local electron temperature, it was shown that the more intense electron heating at the electrode edges tends to reduce the Hall potential. This effect occurs because of an enhanced conductivity which occurs in this region of high electron temperature. When the electrons were allowed to be driven out of ionization equilibrium by gas dynamic convection and finite rates, it was shown that the current concentrations on one of the

electrode walls became less intense while on the opposite electrode wall the current concentrations became more intense. These effects were also shown to be consistent with the experimental measurements of Fischer.[28]

In general it was shown that all types of conductivity nonuniformities considered led to a degradation of performance of MHD generator channels as reflected in increased internal impedance of the conducting gas and depressed Hall voltage. Although several important effects of the nonuniform conductivity have been exhibited and contrasted with the limited experimental data available, it is clear that much more remains to be understood. Perhaps the foremost among these is the ionization instability in a strong magnetic field. As was pointed out in chapter 4, MHD devices which are expected to operate with large Hall parameters and a nonequilibrium conductivity will most likely be subject to such instabilities. The steady state theory of chapters 5 and 7 is not applicable in such cases (being restricted to $\beta \lesssim 1$), and a proper formulation of a quasi-steady theory of such effects does not now exist. Experimental data on such instabilities is also quite limited. Rigorous design procedures for the performance of nonequilibrium MHD devices cannot be established until further progress is made in these areas.

APPENDIX A

NUMERICAL SOLUTION OF THE EQUATIONS GOVERNING ELECTRICAL CONDUCTION IN NONUNIFORM MEDIA

A.1 Differential Equations and Boundary Conditions

It was shown in chapters 2 and 4 that the potential Φ' and flux function ψ in a medium characterized by either a model conductivity nonuniformity or by a nonequilibrium conductivity were governed by the differential equation

$$L(\phi) = 0, \tag{A-1}$$

where

$$L \equiv A\frac{\partial^2}{\partial x^2} + 2B\frac{\partial^2}{\partial x \partial y} + C\frac{\partial^2}{\partial y^2} + D\frac{\partial}{\partial x} + E\frac{\partial}{\partial y}. \tag{A-2}$$

In the above, ϕ represents either the potential Φ' or the flux function ψ, and the A, B, C, D, E are general coefficients which are functions of x, y, $\partial\phi/\partial x$, and $\partial\phi/\partial y$. As described in chapters 2 and 4, these coefficients are different for Φ' and ψ. In what follows, however, both cases will be treated by considering the general operator L. In addition, it will be assumed that all variables have been nondimensionalized as discussed in chapters 3, 5, and 7. In what follows, this nondimensionalization will not be explicitly denoted by the bar notation. The boundary conditions appropriate to the differential equation (A-1) were shown to be of the form

$$\phi = \text{constant on insulating (conducting) surfaces}$$

$$\frac{\partial \phi}{\partial y} + \eta \frac{\partial \phi}{\partial x} = 0 \text{ on conducting (insulating) surfaces parallel to the x axis} \qquad \text{(A-3)}$$

where $\eta = \pm\beta$.

A.2 Formulation of Difference Equations

The development of difference equations for the differential equations (A-1) and (A-3) will now be described. For this purpose, let a square lattice of mesh width $\delta > 0$ be defined for the coordinate system shown in Fig. 2-1 by the nodes $x = m\delta$, $y = n\delta$, where $m = 0, \pm 1, \pm 2, \ldots$; $n = 0, 1, 2, \ldots$. The notation $\phi(m,n)$ will be used to indicate the function ϕ at the point x,y whose discrete coordinates are m,n. The derivatives appearing in the operator (A-2) may be calculated from the expansion of $\phi(x,y)$ about the point x,y whose discrete coordinates are m,n. This procedure yields the following expressions for $\partial^2\phi/\partial x^2$, $\partial^2\phi/\partial y^2$, $\partial^2\phi/\partial x \partial y$, $\partial\phi/\partial x$, $\partial\phi/\partial y$:[34,36]

$$\frac{\partial^2 \phi}{\partial x^2} = \frac{\phi(m+1,n) + \phi(m-1,n) - 2\phi(m,n)}{\delta^2} + O(\delta^2), \qquad \text{(A-4)}$$

$$\frac{\partial^2 \phi}{\partial y^2} = \frac{\phi(m,n+1) + \phi(m,n-1) - 2\phi(m,n)}{\delta^2} + O(\delta^2), \qquad \text{(A-5)}$$

$$\frac{\partial^2 \phi}{\partial x \partial y} = \frac{\phi(m+1,n+1) + \phi(m-1,n-1) - \phi(m+1,n-1) - \phi(m-1,n+1)}{4\delta^2} + O(\delta^2), \qquad \text{(A-6)}$$

$$\frac{\partial \phi}{\partial x} = \frac{\phi(m+1,n) - \phi(m-1,n)}{2\delta} + O(\delta^2), \qquad \text{(A-7)}$$

$$\frac{\partial \phi}{\partial y} = \frac{\phi(m,n+1) - \phi(m,n-1)}{2\delta} + O(\delta^2). \qquad (A-8)$$

It is also possible to express $\partial\phi/\partial y$ as an off-center difference correct to order δ^2 as[27]

$$\frac{\partial \phi}{\partial y} = \pm \frac{3\phi(m,n) - 4\phi(m,n\mp 1) + \phi(m,n\mp 2)}{2\delta} + O(\delta^2). \qquad (A-9)$$

In terms of these finite difference approximations, the differential equation (A-1) becomes

$$A \frac{\phi(m+1,n) + \phi(m-1,n) - 2\phi(m,n)}{\delta 2} +$$

$$+ 2B \frac{\phi(m+1,n+1) + \phi(m-1,n-1) - \phi(m+1,n-1) - \phi(m-1,n+1)}{4\delta 2} +$$

$$+ C \frac{\phi(m,n+1) + \phi(m,n-1) - 2\phi(m,n)}{\delta 2} + D \frac{\phi(m+1,n) - \phi(m-1,n)}{2\delta} +$$

$$+ E \frac{\phi(m,n+1) - \phi(m,n-1)}{2\delta} + O(\delta^2) = 0. \qquad (A-10)$$

Rearranging the above, there results for all m,n to which the differential equation (A-1) applies,

$$r(m,n) \equiv \phi(m,n) - \{\alpha_{+,o}\phi(m+1,n) + \alpha_{-,o}\phi(m-1,n) + \alpha_{o,+}\phi(m,n+1) +$$

$$+ \alpha_{o,-}\phi(m,n-1) + \gamma[\phi(m+1,n+1) - \phi(m+1,n-1) - \phi(m-1,n+1) +$$

$$+ \phi(m-1,n-1)]\} = 0, \qquad (A-11)$$

where

$$\alpha_{+,o} = (A + D\delta/2)/2(A + C), \quad \alpha_{-,o} = (A - D\delta/2)/2(A + C),$$

$$\alpha_{o,+} = (C + E\delta/2)/2(A + C), \quad \alpha_{o,-} = (C - E\delta/2)/2(A + C), \tag{A-12}$$

$$\gamma = B/4(A + C),$$

and r(m,n) is the residual at the point m,n. The derivatives appearing in A,B,C as given by Eqs. (4-74) and (4-79) may be calculated according to the finite difference approximations (A-7) and (A-8).

Since the second of the boundary conditions (A-3) is applied on the boundaries y = 0,1, the introduction of exterior points into the mesh may be avoided by using the off-center difference approximation (A-9) to $\partial\phi/\partial y$. Thus, for all m,n on the boundary y = 0,

$$\frac{\partial \phi}{\partial y} = -\frac{3\phi(m,n) - 4\phi(m,n+1) + \phi(m,n+2)}{2\delta} + O(\delta^2). \tag{A-13}$$

For all m,n on the boundary y = 1,

$$\frac{\partial \phi}{\partial y} = \frac{3\phi(m,n) - 4\phi(m,n-1) + \phi(m,n-2)}{2\delta} + O(\delta^2). \tag{A-14}$$

It may be observed that the difference approximations (A-13) and (A-14) do not involve points external to the boundaries y = 0,1. The derivative $\partial\phi/\partial x$ is calculated according to (A-7). Substituting the finite difference forms (A-7), (A-13), or (A-14) into the boundary condition (A-3), there results

For m,n on the boundary y = 0,to which the condition (A-3) applies,

$$r(m,n) \equiv \phi(m,n) - \frac{1}{3}\{4\phi(m,n+1) - \phi(m,n+2) -$$

$$- \eta[\phi(m+1,n) - \phi(m-1,n)]\} = 0. \qquad \text{(A-15)}$$

For m,n on the boundary y=1, to which the condition (A-3) applies,

$$r(m,n) \equiv \phi(m,n) - \frac{1}{3}\{4\phi(m,n-1) - \phi(m,n-2) -$$

$$- \eta[\phi(m+1,n) - \phi(m-1,n)]\} = 0. \qquad \text{(A-16)}$$

A.3 Iterative Methods of Solution

For all cases considered in this work, the difference equations (A-11), (A-15), and (A-16) were solved using iterative relaxation[34,37] according to the algorithm

$$\phi^{(p+1)}(m,n) = \phi^{(p)}(m,n) - \omega r^{(p)}(m,n). \qquad \text{(A-17)}$$

The superscript p denotes the p^{th} iterate and $\omega > 0$ is the relaxation parameter. Every point in the mesh is first set with an initial value. Each point is then corrected according to the algorithm (A-17) in a specified and regular order. The process is continued until the residual r(m,n) at each point has been reduced to a small, predetermined value.

For all cases for which convergence was achieved, the operator L was uniformly elliptic so that

$$B^2 - AC < 0. \qquad \text{(A-18)}$$

in addition, for those cases where the conductivity was specified as a function of space, the A,B,C,D,E were independent of $\partial\phi/\partial x$ and $\partial\phi/\partial y$, so that the operator L was linear. A rigorous guarantee of the convergence of the algorithm (A-17) to the solution of the differential equation (A-1) exists for this case with modest restrictions on the behavior of ϕ and the discrete form of the operator L.[34] In particular, it is required that the mesh size δ be small enough so that $\alpha_{+,o}$, $\alpha_{-,o}$, $\alpha_{o,+}$, $\alpha_{o,-}$ defined by Eqs. (A-12) are each always less than one. These criteria were satisfied by mesh refinement in those regions where the conductivity gradients were large leading to large D,E. These refined mesh regions were joined to the coarse mesh using simple linear interpolation.

A systematic study of convergence rates and optimal relaxation parameters was not performed in the present work; however, a limited amount of experience has been obtained and is now described. For those cases in which the conductivity was specified as a function of space as discussed in chapter 3, a refined mesh was utilized between the lines y=0,.2 and y=.8,1. Typical mesh sizes for the conductivity distributions discussed in chapter 3 were of the order of 50 mesh points in the x direction by 10 mesh points in the y direction in the refined mesh regions; in the core region the mesh size was of the order of 10 by 10 mesh points. For these typical sizes, the number of iterations required to reduce the residuals to less than .01 varied from 20 to 200, depending upon the initial guess. In general, it was found that cases with regions of high conductivity near the electrodes and insulators required more iterations to converge than did those cases with low conductivity regions. Relaxation parameters for these calculations of $1 < \omega < 1.3$

were found to yield satisfactory convergence rates. It was found that $\omega \sim 1.6$ was near optimal for the case when the conductivity was uniform. With a nonuniform conductivity, the optimal ω was found to decrease.

The order in which the points were visited by the relaxation algorithm (A-17) was found to influence the rate of convergence. The most rapid rate of convergence was achieved when the effects of the boundary conditions were integrated into the mesh as rapidly as possible. This was achieved by sweeping upward through the refined mesh adjacent to the boundary y=0. The core mesh was then swept up to the match line y=.8. The refined mesh adjacent to the boundary y=1 was then swept *downward* from the boundary. Typical times for all cases in which the conductivity was specified as a function of space were of the order of one to five minutes on the IMB 7090 for total mesh sizes ranging from 200 to 1400 points.

When a nonequilibrium conductivity is considered, the operator L is quasi-linear and non-symmetric (because of the Hall effect). A rigorous theory of convergence for quasi-linear elliptic operators according to the algorithm (A-17) exists;[35] however, there is no criterion for the convergence of the algorithm (A-17) for nonsymmetric operators. Nevertheless, it was found that convergence could be achieved for all cases provided that L was uniformly elliptic. As an experiment, the Hall parameter was made large enough so that the operator L was no longer uniformly elliptic (c.f. section 4.3). Rapid divergence quickly occurred when the relaxation algorithm (A-17) was used for this case. In some cases (those close to the limit of uniform ellipticity), it was found that under-relaxation ($\omega < 1$) improved the rate of convergence.

The under-relaxation used for such cases involved ω of the order of .2.

Typical mesh sizes of the cases in which a nonequilibrium conductivity occurred as discussed in chapter 5 were 20×20 mesh points. Depending upon the initial guess, the number of iterations required to reduce the residuals to less than .01 varied from 20 to 150. These iterations required between 1 and 4 minutes on the IBM 7090.

A.4 Strong Hall Effects

When the Hall parameter β is large, the large factor $\eta = \pm\beta$ in the difference equations for the boundary conditions (A-14) and (A-15) may be expected to give rise to numerical instabilities; indeed, these difference equations were found to lead to instabilities for Hall parameters greater than two. Stable difference equations for these boundary conditions may be developed in the following way. The derivative $\partial\phi/\partial x$ on the boundary is expressed in finite difference form as an off-center difference similar to (A-9):

$$\frac{\partial\phi}{\partial x} = \pm\frac{3\phi(m,n) - 4\phi(m\mp1,n) + \phi(m\mp2,n)}{2\delta} + O(\delta^2). \qquad \text{(A-19)}$$

On the boundary y=0, the condition (A-3) in terms of the finite difference approximations (A-13) and (A-19) becomes

$$r(m,n) \equiv \phi(m,n) -$$

$$- \frac{\mp\eta[-4\phi(m\mp1,n) - \phi(m\mp2,n)] - 4\phi(m,n+1) + \phi(m,n+2)}{3(-1 \pm \eta)} = 0. \qquad \text{(A-20)}$$

The presence of $(-1 \pm \eta)$ in the denominator of this difference expression has a stabilizing effect for large η [compare with the difference formula (A-15)]. When $\phi = \psi$, i.e., the calculation is in the current representation, $\eta = -\beta$ $\beta > 0$, and the upper sign is selected in Eq. (A-20) so that the denominator $(-1 \pm \eta)$ is always negative and less than -1. Conversely, when $\phi = \Phi'$, i.e., the calculation is in the field representation, $\eta = \beta$, $\beta > 0$, and the lower sign is selected in Eq. (A-20).

On the boundary y=1, the condition (A-3) in terms of the finite difference approximations (A-14) and (A-19) becomes

$$r(m,n) \equiv \phi(m,n) -$$

$$- \frac{\mp \eta[-4\phi(m\mp1,n) + \phi(m\mp2,n)] + 4\phi(m,n-1) - \phi(m,n-2)}{3(1 \pm \eta)} = 0. \qquad \text{(A-21)}$$

The positivity or negativity of η again dictates the choice of sign in Eq. (A-21) so that the denominator $(1 \pm \eta)$ in absolute value is always greater than unity.

The difference approximations (A-20) and (A-21) were used for Hall parameters as high as $\beta = 6$ with no difficulty and no evidence of numerical instability.

A.5 Finite Rate Effects

For those cases where finite rates of ionization and recombination were present as discussed in chapter 7, the governing equations were numerically treated as a system consisting of (A-2) with A=C=1, B=0,

supplemented by the electron continuity and energy equations. From Eqs. (7-5) for β uniform,

$$D = \frac{\partial \ell n\, n_e}{\partial x} + \beta \frac{\partial \ell n\, n_e}{\partial y}, \qquad E = \frac{\partial \ell n\, n_e}{\partial y} - \beta \frac{\partial \ell n\, n_e}{\partial x}. \tag{A-22}$$

The electron energy equation was shown to be

$$T_e = T + \omega_E (\nabla\phi)^2. \tag{A-23}$$

The solution of the electron continuity equation with finite rates [chapter 6; appendices C,D] is

$$n_e = \left\{ \frac{1}{u} \left[F(x) + \frac{e^{-\lambda(x)/u}}{1 - e^{-\lambda(1)/u}} F(1) \right] \right\}^{-\frac{1}{2}}. \tag{A-24}$$

where

$$\lambda(x) \equiv 2 \int_0^x \alpha[T_e(\eta)] n_e^{*2}[T_e(\eta)]\, d\eta,$$

$$F(x) \equiv 2 \int_0^x \alpha[T_e(\eta)] e^{-[\lambda(x) - \lambda(\eta)]}\, d\eta.$$

It should again be noted that the variables appearing in the foregoing equations are assumed to be in the nondimensional form discussed in chapters 5 and 6. In section 4.3 it was shown that this system is para-

bolic; however, ϕ, T_e, and n_e are nonlinearly coupled. The solution of this system is obtained by using the algorithm (A-17). After all $\phi(m,n)$ are operated on according to (A-17), the temperature T_e is calculated at each point in the mesh according to (A-23). The number density n_e and the number density gradients appearing in D,E of Eqs.(A-22) are then calculated from (A-24) by numerically performing the quadrature. The relaxation algorithm (A-17) is then repeated until the cycle converges.

The above method was used in obtaining the finite rate solutions discussed in chapter 7. In all cases where the criterion for stability of the nonsteady equations was obeyed as discussed in section 4.1, convergence was achieved. As an experiment, this stability condition was violated by increasing the Hall parameter, and it was found that the calculation rapidly diverged. It is important to note that this stability condition is a physical stability condition, not a numerical stability condition. Nevertheless, it appeared to control the condition of numerical convergence for the steady equations where a relaxation algorithm was used. It should also be noted that the steady equations become of mixed type when the stability condition is violated as discussed in section 4.3. It was pointed out in appendix A.3 that convergence was also not achieved when the steady equations became of mixed type.

Relaxation parameters of $\omega \sim 1$ were found to give satisfactory results except when conditions were close to the stability limit mentioned above, and the convective effect in Eq. (A-24) was not strong ($u < 5$). Under-relaxation ($\omega \gtrsim .2$) was required to achieve convergence in this case.

A.6 Solution of the Coupled Saha and Electron Energy Equations

In chapter 5 it was shown that in the current representation the electron temperature T_e and electron number density n_e were governed by the electron energy and Saha equations respectively:

$$T_e = T + \omega_J(\nabla\psi)^2/n_e^2, \tag{A-25}$$

$$n_e = \frac{2f^{-1}}{1 + \sqrt{1 + 4/\zeta(T_e)}}, \tag{A-26}$$

where f was the degree of initial ionization and

$$\zeta(T_e) \equiv n_o T_e^{\frac{3}{2}} \exp(-\varepsilon_i/T_e). \tag{A-27}$$

The variables T_e, n_e are transcendentally coupled in these two equations prohibiting an explicit solution for T_e, n_e for a given T, $\nabla\psi$, f, ω_J n_o, and ε_i. Newton-Raphson iteration[38] was therefore used to solve this system. The energy equation (A-25) was expressed as

$$r(T_e,n_e) = T_e - T - \omega_J(\nabla\psi)^2/n_e^2,$$

and the iterative algorithm for the $k^{\underline{th}}$ iterate of T_e, denoted $T_e^{(k)}$, was

$$T_e^{(k+1)} = T_e^{(k)} - \frac{r^{(k)}}{\left(\frac{\partial r}{\partial T_e}\right)^{(k)}}. \tag{A-28}$$

Using the energy equation (A-25), it follows that

$$\frac{\partial r}{\partial T_e} = 1 + (T_e - T) \frac{\partial \ell n\, n_e}{\partial T_e}, \qquad \text{(A-29)}$$

and $\partial \ell n\, n_e / \partial T_e$ is given by Eq. (5-13). From Eqs. (A-29) and (5-13), all terms in the Newton algorithm (A-28) may be expressed in terms of T_e. It was found that using the initial guess $T_e^{(1)} = T$, convergence to $r < .01$ could be achieved in three to four iterations for typical values of the parameters appearing in (A-1) and (A-2) discussed in chapter 5.

APPENDIX B

DISSIPATION AND UNIQUENESS THEOREMS FOR A NONUNIFORM CONDUCTING MEDIUM

B.1 Integral Theorems for a Nonuniform Conducting Medium

Consider potential function Φ' and current $\vec{J}$ defined in a planar domain D with boundary curve C governed by the equations

$$\nabla\cdot\vec{J} = 0, \qquad \vec{J} = -\overleftrightarrow{\sigma}\cdot\nabla\Phi', \tag{B-1}$$

where $\overleftrightarrow{\sigma}$ is defined by Eq. (2-4). In what follows it is assumed that the conductivity tensor $\overleftrightarrow{\sigma}$ may be nonuniform but is a given function of space at each point within D. If the divergence of the product $\Phi'\vec{J}$ is integrated over D, there results

$$\iint_D \nabla\cdot(\Phi'\vec{J})dA = \iint_D (\Phi'\nabla\cdot\vec{J} + \vec{J}\cdot\nabla\Phi')dA. \tag{B-2}$$

Using the divergence theorem[33] and Eq. (B-1), the above result becomes

$$\iint_D \vec{J}\cdot\nabla\Phi' dA = \oint_C \Phi'\vec{J}\cdot\vec{n}\,ds, \tag{B-3}$$

where $\vec{n}$ is the outward drawn unit normal. From (B-1) and the definition of $\overleftrightarrow{\sigma}$, Eq. (B-3) may be expressed as

$$\iint_D \frac{J^2}{\sigma} = \iint_D \sigma_\beta(\nabla\Phi')^2 = -\oint_C \Phi'\vec{J}\cdot\vec{n}\,ds, \tag{B-4}$$

where σ and σ_β are defined following Eq. (2-4). In similar fashion, if Eq. (B-1) is integrated over D and the divergence theorem applied, there

results

$$\iint_D \nabla\cdot\vec{J}\, dA = \oint_C \vec{J}\cdot\vec{n}\, ds = 0. \tag{B-5}$$

The domain D will now be selected as one period of the periodic electrode MHD channel described in section 2.3 (Fig. 2.1). The integrals over the boundary curve C in (B-4) and (B-5) for this domain are

$$\oint_C \Phi'\vec{J}\cdot\vec{n}\, ds = -\Phi'(0,0)\int_{-\frac{a}{2}}^{\frac{a}{2}} J_y(x,0)dx + \int_0^h \Phi'(\ell/2,y)J_x(\ell/2,y)dy + \tag{B-6}$$

$$+ \Phi'(0,h)\int_{-\frac{a}{2}}^{\frac{a}{2}} J_y(x,h)dx - \int_0^h \Phi'(-\ell/2,y)J_x(-\ell/2,y)dy,$$

$$\oint_C \vec{J}\cdot\vec{n}\, ds = -\int_{-\frac{a}{2}}^{\frac{a}{2}} J_y(x,0)dx + \int_0^h J_x(\ell/2,y)dy + \tag{B-7}$$

$$+ \int_{-\frac{a}{2}}^{\frac{a}{2}} J_y(x,h)dx - \int_0^h J_x(-\ell/2,y)dy.$$

In developing (B-6) and (B-7) it has been assumed that Φ' is constant on the conducting surfaces and that $\vec{J}\cdot\vec{n}$ vanishes on insulating surfaces. From the periodicity of $\vec{J}$ over the period ℓ, $J_x(-\ell/2,y) = J_x(\ell/2,y)$ for all y. Equation (B-7) thus implies

$$\int_{-\frac{a}{2}}^{\frac{a}{2}} J_y(x,0)dx = \int_{-\frac{a}{2}}^{\frac{a}{2}} J_y(x,h)dx, \tag{B-8}$$

i.e., the periodicity of total current flow in the axial direction requires that all current leaving the electrode on y = 0 must enter the electrode on y = h. Equation (B-6) thus becomes

$$\oint_C \Phi' \vec{J}\cdot\vec{n}\, ds = - I_x V_x' - I_y V_y', \tag{B-9}$$

where the global currents I_x, I_y, and the voltages V_x', V_y' are defined as (Note that periodicity of $\nabla\Phi'$ makes V_x' independent of y.)

$$\begin{aligned} I_x &\equiv - \int_0^h J_x(\ell/2,y)dy, \\ I_y &\equiv - \int_{-\frac{a}{2}}^{\frac{a}{2}} J_y(x,0)dx, \end{aligned} \tag{B-10}$$

$$V_x' \equiv \Phi'(\ell/2,y) - \Phi'(-\ell/2,y),$$

$$V_y' \equiv \Phi'(0,h) - \Phi'(0,0).$$

B.2 Power Dissipation

Substituting from Eq. (B-9) into Eq. (B-4) there results

$$I_x V_x' + I_y V_y' = \iint_D \sigma_\beta (\nabla\Phi')^2 dA. \tag{B-11}$$

Equation (B-11) may be viewed as a theorem relating to the power dissi-

pation in a nonuniform conducting medium. The local rate of power dissipation per unit volume in a conducting medium described by the conductivity tensor (2-4) may be readily shown to be[39] $-\vec{J}\cdot\nabla\Phi' = \sigma_\beta(\nabla\Phi')^2$ and is an inherently positive quantity. Equation (B-11) thus states that the total power dissipated per unit channel depth is equal to the sum of the products of the axial current and voltage and the transverse current and voltage. In terms of the impedance tensor $\overleftrightarrow{R}$ defined in section 2.3, the power dissipation may be expressed as

$$\iint_D \sigma_\beta(\nabla\Phi')^2 dA = I_x^2 R_{xx} + I_y^2 R_{yy} + I_x I_y (R_{xy} + R_{yx}). \quad \text{(B-12)}$$

The elements of $\overleftrightarrow{R}$ thus represent the internal impedance of the conducting medium. Equation (B-11) will serve as a basis for the uniqueness theorems to be discussed below.

B.3 Uniqueness Theorems

Consider that two solutions Φ_1', Φ_2' exist to the differential equation (B-1) satisfying certain boundary conditions to be discussed below. The difference function $\phi \equiv \Phi_1' - \Phi_2'$ implies the existence of a current difference function $\vec{j}$ defined as $\vec{j} = \vec{J}_1 - \vec{J}_2$ where

$$\vec{J}_1 = -\overleftrightarrow{\sigma}\cdot\nabla\Phi_1', \qquad \vec{J}_2 = -\overleftrightarrow{\sigma}\cdot\nabla\Phi_2'. \quad \text{(B-13)}$$

The function ϕ satisfies the differential equation

$$\nabla\cdot(\overleftrightarrow{\sigma}\cdot\nabla\phi) = 0. \quad \text{(B-14)}$$

In terms of the functions ϕ, $\vec{j}$, the quantities v_x, v_y, i_x, i_y may be

defined as

$$
\begin{aligned}
v_x &\equiv \phi(\ell/2,y) - \phi(-\ell/2,y), \\
v_y &\equiv \phi(0,h) - \phi(0,0), \\
i_x &\equiv -\int_0^h j_x(\ell/2,y)dy, \\
i_y &\equiv -\int_{-\frac{a}{2}}^{\frac{a}{2}} j_y(x,0)dx.
\end{aligned}
\tag{B-15}
$$

As was shown in section B.2, the difference function ϕ, by virtue of satisfying Eq. (B-14), must satisfy the dissipation theorem

$$
\iint_D \sigma_\beta(\nabla\phi)^2 = v_x i_x + v_y i_y. \tag{B-16}
$$

The possible sets of boundary conditions which may be applied to Φ' and which lead to a unique distribution of $\nabla\Phi'$ and $\vec{J}$ within D may now be discussed using Eq. (B-16). If the identical boundary conditions applied to the two possibly different functions Φ_1', Φ_2' are the specification of V_x' and V_y', it follows from the first and second of Eqs. (B-15) that $v_x = v_y = 0$. Since the integrand in Eq. (B-16) is inherently positive, the only ϕ satisfying (B-16) is $\nabla\phi = 0$, which implies $\vec{J} = 0$. Thus, it follows that $\nabla\Phi_1' = \nabla\Phi_2'$ and $\vec{J}_1 = \vec{J}_2$ within D. The specification of V_x' and V_y' thus leads to a unique distribution of field $\nabla\Phi'$ and

and current $\vec{J}$ within D. In similar fashion, it is readily shown that the specification of pairs of the global voltages and currents such as (V_x', I_y), (V_y', I_x), (I_x, I_y) also lead to unique distributions of field and current within D.

APPENDIX C

IONIZATION AND RECOMBINATION RATES IN ALKALI METAL PLASMAS

The frequency of recombination collisions in an ionized gas may be expressed as

$$\nu_r = \alpha n_e^2, \tag{C-1}$$

where α is the recombination coefficient and n_e is the number density of electrons. From the principle of detailed balance, the ionization frequency due to electron-neutral impacts is

$$\nu_i = \nu_r = \alpha n_e^{*2}, \tag{C-2}$$

where $n_e^*(T_e)$ is the equilibrium number density of electrons. For alkali metals such as cesium or potassium, the equilibrium number density is given by

$$n_e^{*2} = (n_{s_o} - n_e^*) \left(\frac{2\pi m_e k T_e}{h^2} \right)^{\frac{3}{2}} \exp(-\varepsilon_i / k T_e).$$

The quantities ν_r and ν_i are thus known in terms of the recombination coefficient α.

For temperatures in the range $kT_e/e \lesssim 0.25$ electron volts, Hinnov and Hirschberg[24] have calculated $\alpha(T_e)$ to be (in units of $cm^6\ sec^{-1}$)

$$\alpha(T_e) = 5.6 \times 10^{-27} \left(\frac{kT_e}{e} \right)^{-\frac{9}{2}}, \tag{C-3}$$

where (kT_e/e) is the electron temperature expressed in electron volts. The three body recombination coefficient ν_r for potassium has been calculated according to the above expressions and is shown as a function of n_e and T_e in Fig. C-1. Also shown are lines of equilibrium number density for various values of the ionizable species number density n_{s_o}.

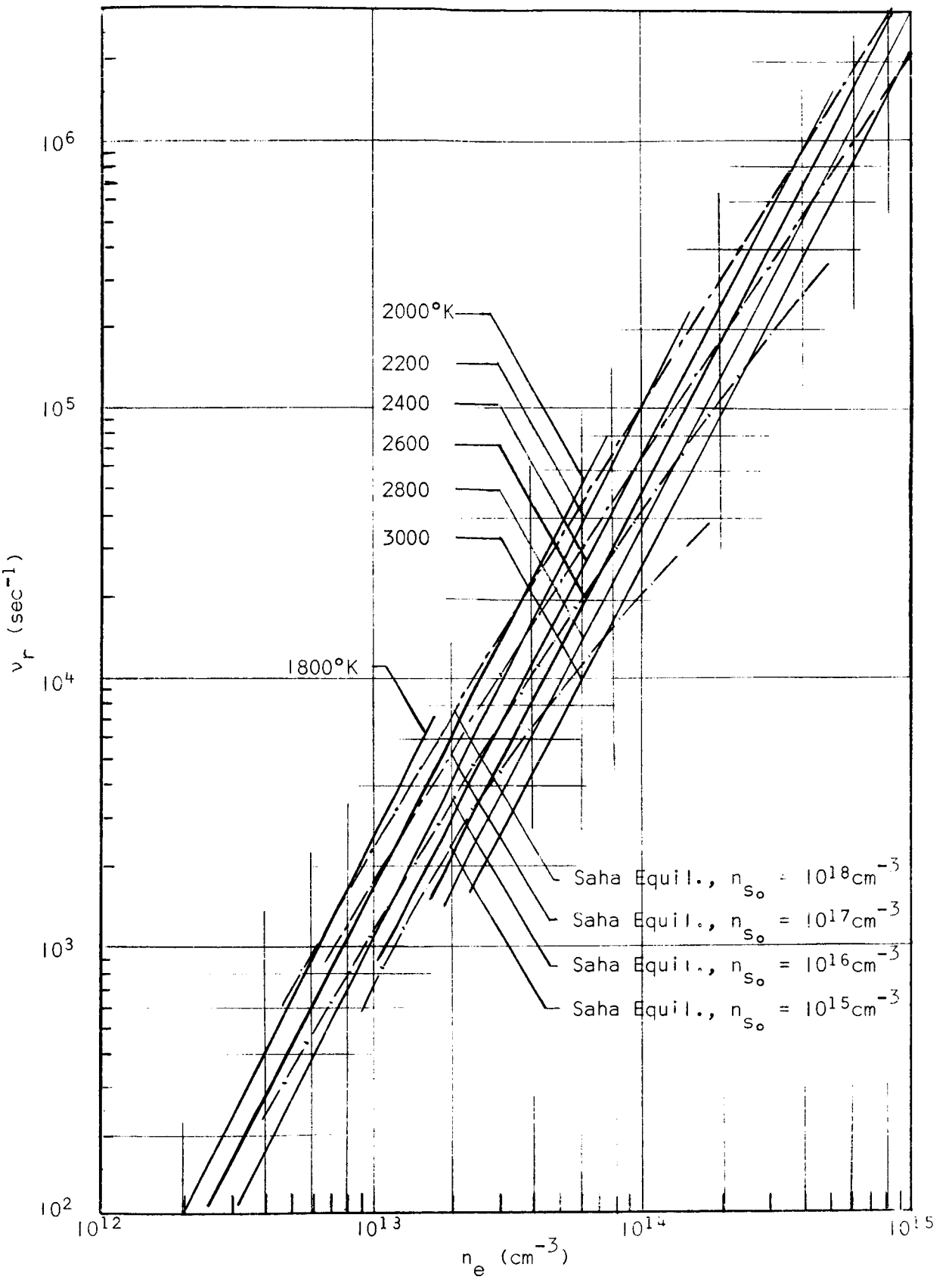

Fig. C-1 Recombination frequency of electrons in potassium

APPENDIX D

SOLUTION OF THE ELECTRON CONTINUITY EQUATION WITH IONIZATION AND RECOMBINATION

D.1 Transformation of the Nonlinear Rate Equation to a Linear Form

The electron continuity equation discussed in chapter 6 was shown to be

$$u \frac{dn_e}{dx} = \nu_i n_e - \alpha n_e^3. \qquad \text{(D-1)}$$

This nonlinear first order differential equation is of the Bernoulli type and may be transformed into a linear equation with the substitution

$$n_e = \zeta^{-\frac{1}{2}}.$$

The result of such a transformation is

$$u \frac{d\zeta}{dx} + 2\nu_i \zeta = 2\alpha, \qquad \text{(D-2)}$$

which is linear in ζ.

D.2 Asymptotic Solutions with Periodic Disturbances

Equation (D-2) may be expressed as

$$\frac{d\zeta}{dx} + \gamma(x)\zeta = f(x). \qquad \text{(D-3)}$$

The solution to (D-3) is readily shown to be

$$\zeta(x) = \left[\zeta(0) + \int_0^x f(\xi) e^{\lambda(\xi)} d\xi\right] e^{-\lambda(x)}, \qquad \text{(D-4)}$$

where

$$\lambda(x) \equiv \int_0^x \gamma(\xi)\, d\xi. \qquad \text{(D-5)}$$

The quantity $\lambda(x)$ represents an effective decay length. If the disturbances which lead to finite rate effects in ζ are periodic and ℓ is the length of the period, the coefficients $\gamma(x)$, $f(x)$ are periodic in ℓ:

$$\begin{aligned} \gamma(x+N\ell) &= \gamma(x), \\ f(x+N\ell) &= f(x), \end{aligned} \qquad \text{(D-6)}$$

where N is an integer. From (D-5) and the periodicity of $\gamma(x)$, it follows that $\lambda(x)$ has the property

$$\lambda(x+N\ell) = N\lambda(\ell) + \lambda(x). \qquad \text{(D-7)}$$

The solution of Eq. (D-4) consists of two parts: an initial distribution $\zeta(0)$ which decays exponentially:

$$\zeta_i = \zeta(0)\, e^{-\lambda(x)}, \qquad \text{(D-8)}$$

and a forcing disturbance

$$\zeta_f = e^{-\lambda(x)} \int_0^x f(\xi)\, e^{\lambda(\xi)} d\xi. \qquad \text{(D-9)}$$

The solution (D-9) is now examined for large values of x for which the initial distribution $\zeta(0)$ has decayed to a very small value. The coordinate change

$$x = N\ell + x'$$

is introduced where x' is measured from the beginning of the $N^{\underline{th}}$ period. Using the property (D-7), the forced part of the solution (D-9) may then be written as

$$\zeta_f(x') = e^{-\lambda(x')}\left\{\int_0^{N\ell} f(\xi)\, e^{\lambda(\xi) - N\lambda(\ell)}d\xi + \right.$$

$$\left. + \int_{N\ell}^{N\ell+x'} f(\xi)\, e^{\lambda(\xi) - N\lambda(\ell)}d\xi\right\}. \qquad \text{(D-10)}$$

Changing variables and using the periodicity property (D-6), the above result becomes

$$\zeta_f(x') = e^{-\lambda(x')}\left\{\int_0^{x'} f(\xi)e^{\lambda(\xi)}d\xi + \sum_{m=1}^{N} e^{-m\lambda(\ell)}\int_0^{\ell} f(\xi)e^{\lambda(\xi)}d\xi\right\}.$$

The sum $\sum_{m=1}^{N} e^{-m\lambda(\ell)}$ may readily be calculated. It is of the form $\sum_{m=1}^{N} z^{-m}$ where $z = e^{-\lambda(\ell)} < 1$. This is a simple geometrical progression. In the limit $N \to \infty$,

$$\sum_{m=1}^{\infty} z^{-m} = \frac{z}{1-z} = \frac{e^{-\lambda(\ell)}}{1 - e^{-\lambda(\ell)}}. \qquad \text{(D-11)}$$

For a large number of periods ($N >> 1$) away from the entrance x=0, there

results

$$\zeta_i \to 0,$$

$$\zeta_f \to F(x') + \frac{e^{-\lambda(x')}}{1 - e^{-\lambda(\ell)}} F(\ell) , \qquad \text{(D-12)}$$

where

$$F(x) \equiv \left(\int_0^x f(\xi)\, e^{\lambda(\xi)} d\xi \right) e^{-\lambda(x)} .$$

It may readily be verified that ζ_f is indeed periodic and that

$$\zeta_f(0) = \zeta_f(\ell) = \frac{F(\ell)}{1 - e^{-\lambda(\ell)}} . \qquad \text{(D-13)}$$

D.3 Application to the Electron Continuity Equation

The general results derived above may now be applied to the electron continuity equation with finite rates of ionization and recombination. In the above notation $\gamma(x) = 2\nu_i/u$ and $f(x) = 2\alpha/u$, where $\nu_i = \alpha n_e^{*2}$. The asymptotic result (D-12) is then (where x is measured from the beginning of a period far away from the channel entrance)

$$n_e^{-2} = F(x) + \frac{e^{-\lambda(x)}}{1 - e^{-\lambda(\ell)}} F(\ell) . \qquad \text{(D-14)}$$

where

$$\lambda(x) = \frac{2}{u} \int_0^x \alpha \, n_e^{*2} \, d\xi, \tag{D-15}$$

$$F(x) = \left(\frac{2}{u} \int_0^x \alpha \, e^{\lambda(\xi)} d\xi \right) e^{-\lambda(x)}. \tag{D-16}$$

In the limit when $u \to 0$, Eq. (D-14) yields the equilibrium result

$$n_e = n_e^*.$$

In the limit when $u \to \infty$, the frozen limit result is obtained:

$$n_e = \sqrt{\langle \alpha n_e^{*2} \rangle / \langle \alpha \rangle}, \tag{D-17}$$

where

$$\langle f(x) \rangle = \frac{1}{\ell} \int_0^\ell f(x) \, dx. \tag{D-18}$$

The number density in the frozen limit is thus the RMS average over the period of the equilibrium number density weighted against the recombination coefficient.

REFERENCES

1. Kerrebrock, J. L., "Magnetohydrodynamic Generators with Nonequilibrium Ionization," AIAA Journal 3, 591-601 (1965).

2. Hurwitz, H., Sutton, G., and Tamor, S., ARS Journal, 1237 (August, 1962).

3. Hoffman, M. A., AIAA Journal 2, 1080 (1963).

4. Zukoski, E. E., Cool, T. A., and Gibson, E. G., "Experiments Concerning Nonequilibrium Conductivity in a Seeded Plasma," AIAA Aerospace Sciences Meeting, New York (January, 1964).

5. Rosa, R. and Klepeis, J., "Experimental Studies of Strong Hall Effects and V×B Induced Ionization," AVCO Research Laboratory Report No. 177 (1964).

6. Velikhov, E. P., "Hall Instability of Current-Carrying-Slightly-Ionized Plasmas," *Magnetoplasmadynamic Electrical Power Generation*, The Institution of Electrical Engineers, London (1963).

7. McCune, J. E., "Wave Growth and Instability in Partially-Ionized Gases," AVCO-Everett Research Report AMP 136 (April, 1964).

8. McCune, J. E., "Nonlinear Effects of Fluctuations on MHD Performance," AVCO-Everett Research Report 205 (January, 1965).

9. Hurwitz, H., Jr., Kilb., R. W., and Sutton, G. W., "Influence of Tensor Conductivity on Current Distribution in an MHD Generator," J. Appl. Phys. 32, 205 (1961).

10. Sutton, G. W., "End Losses in Magnetohydrodynamic Channels with Tensor Electrical Conductivity and Segmented Electrodes," J. Appl. Phys. 34, No. 2 (1963).

11. Fishman, F., "Effect of Electrode Nonuniformities along the Magnetic Field in MHD Generators," AVCO-Everett Research Report 176 (1963).

12. Podolsky, B. and Sherman, F. S., "Influence of Tensor Conductivity on End Currents in Crossed Field MHD Channels with Skewed Electrodes," J. Appl. Phys. 33, No. 4 (1962).

13. Schultz-Grunow, F. and Denzel, D. L., "Evaluation of the Performance Characteristics of a Faraday Generator," *Engineering Developments in Energy Conversion*, ASME, New York (1965).

14. Dzung, L., "The Magnetohydrodynamic Generator with Hall Effect at the Duct Ends," Brown Boveri Review, 49, 6 (1962).

15. Crown, J. C., "Analysis of Magnetohydrodynamic Generators Having Segmented Electrodes and Anisotropic Conductivity," United Aircraft Corporation Report R-1852-2 (1961).

16. Celinski, Z. N. and Fischer, F. W., "Effect of Electrode Size in MHD Generators with Segmented Electrodes," AIAA Journal 4, No. 3 (1966).

17. Witalis, E., "Performance of MHD Generator for Various Electrode-Insulator Length Ratios," private communication from G. W. Sutton (1965).

18. Rosa, R. J., "Hall and Ion-Slip Effects in a Nonuniform Gas," Phys. Fluids 5, 1081-1090 (1962).

19. Kerrebrock, J. L., "Segmented Electrode Losses in MHD Generators with Nonequilibrium Ionization," AVCO-Everett Research Report 178, BSD-TDR-64-35 (April,1964); also *Magnetohydrodynamic Electrical Power Generation*, European Nuclear Energy Agency and Organization for Economic Cooperation, Paris (1964).

20. Kerrebrock, J. L., "Segmented Electrode Losses in MHD Generators with Nonequilibrium Ionization-II," AVCO-Everett Research Report 201 (January,1965).

21. Sherman, A., "Nonequilibrium Ionization in Magnetohydrodynamic Channel Flow with Finite Segmented Electrodes," General Electric Missle and Space Division Report R66SD3 (January, 1966).

22. Kerrebrock, J. L., "Nonequilibrium Ionization Due to Electron Heating, Part I: Theory," AIAA Journal 2, 1072-1080 (1964).

23. Alfven, H. A. and Falthämmar, C. G., *Cosmical Electrodynamics*, Oxford University Press, London, 2nd ed., Chap. 5 (1962).

24. Hinnov, E. and Hirschberg, J. G., "Electron-Ion Recombination in Dense Plasmas," Phys. Rev., 125, p 795-801 (February, 1962).

25. Kruger, C. and Viegas, J. R., Phys. Fluids 7, 11, 1879 (1964).

26. Lyubimov, G. A., "Change of Electrical Potential Near Wall of Channel During Motion of Ionized Gas in Magnetic Field," Zhurnal Prikladnoy Mekhaniki i Teknicheskoy Fiziki, No. 5 (1963).

27. Rogers, J. W., "A Theoretical Investigation of the Inlet Current Distribution in an MHD Channel," S. M. Thesis, Massachusetts Institute of Technology (June, 1964).

28. Fischer, F. W., "Experimentalle Untersuchungen der Stromdichteverteilung in einem Magnetohydrodynamischen Generator mit Segmentierten Elektroden," Institut FÜr Plasmaphysik, Garching bei MÜnchen, IPP 3/41 (July, 1966).

29. Hoffman, M. and Oates, G., "Electrode Current Distribution in MHD Channels," Report PR-4573-1, Center for Space Research, Massachusetts Institute of Technology (January, 1965).

30. Wright, J. K., "A Temperature Instability in Magnetohydrodynamic Flow," Proc. Phys. Soc. 81, 498 (1963).

31. Dethlefson, R. and Kerrebrock, J. L., "Experimental Investigation of Fluctuations in a Nonequilibrium MHD Plasma," Seventh Symposium on Engineering Aspects of Magnetohydrodynamics, Princeton University (April, 1966).

32. Courant, R. and Hilbert, D., *Methods of Mathematical Physics*, Vol. 2, John Wiley and Sons, New York (1961).

33. Kellog, O. D., *Potential Theory*, Dover Publications Reprint, New York (1958).

34. Forsythe, G. E., and Wassow, W. R., *Finite Difference Methods for Partial Differential Equations*, John Wiley and Sons, N.Y. (1960).

35. Schechter, S., "Iteration Methods for Nonlinear Problems," Trans. Amer. Math. Soc., 104, 1 (July, 1962).

36. Garabedian, P., *Partial Differential Equations*, John Wiley and Sons, New York, (1964).

37. Ames, W. F., *Nonlinear Partial Differential Equations in Engineering*, Academic Press, New York (1965).

38. Morrey, C. B. JR., "Nonlinear Methods" in *Modern Mathematics for the Engineer*, E. F. Beckenbach (ed.), McGraw Hill, New York (1956).

39. Jackson, J. D., *Classical Electrodynamics*, John Wiley and Sons, New York (1961).

40. Kruger, C. H., and Mitchner, M., "Kinetic Theory of Two Temperature Plasmas," SU-IPR Report No. 94, Stanford University Institute For Plasma Research (August, 1966).